CATALYTIC CONVERSION OF CELLULOSE INTO NANOCELLULOSE IN IONIC LIQUID

TAN XIAO YUN

INSTITUTE OF GRADUATE STUDIES
UNIVERSITY OF MALAYA
KUALA LUMPUR

2016

CATALYTIC CONVERSION OF CELLULOSE INTO NANOCELLULOSE IN IONIC LIQUID

TAN XIAO YUN

DISSERTATION SUBMITTED IN FULFILMENT OF THE REQUIREMENTS FOR THE DEGREE OF MASTER OF PHILOSOPHY

INSTITUTE OF GRADUATE STUDIES
UNIVERSITY OF MALAYA
KUALA LUMPUR

2016

UNIVERSITY OF MALAYA

ORIGINAL LITERARY WORK DECLARATION

Name of Candidate: TAN XIAO YUN

Matric No: HGA 130017

Name of Degree: Master of Philosophy

Title of Project Paper/Research Report/Dissertation/Thesis ("this Work"):

Catalytic Conversion of Cellulose into Nanocellulose in Ionic Liquid

Field of Study: Chemistry (Catalysis)

I do solemnly and sincerely declare that:

(1) I am the sole author/writer of this Work;
(2) This Work is original;
(3) Any use of any work in which copyright exists was done by way of fair dealing and for permitted purposes and any excerpt or extract from, or reference to or reproduction of any copyright work has been disclosed expressly and sufficiently and the title of the Work and its authorship have been acknowledged in this Work;
(4) I do not have any actual knowledge nor do I ought reasonably to know that the making of this work constitutes an infringement of any copyright work;
(5) I hereby assign all and every rights in the copyright to this Work to the University of Malaya ("UM"), who henceforth shall be owner of the copyright in this Work and that any reproduction or use in any form or by any means whatsoever is prohibited without the written consent of UM having been first had and obtained;
(6) I am fully aware that if in the course of making this Work I have infringed any copyright whether intentionally or otherwise, I may be subject to legal action or any other action as may be determined by UM.

Candidate's Signature Date:

Subscribed and solemnly declared before,

Witness's Signature Date:

Name:

Designation:

ABSTRACT

Nanocellulose have emerged as a promising material and have attracted considerable attention owing to their promising properties such as high surface area, high strength and stiffness as well as biodegradability. In the present study, 1-butyl-3-methylimidazolium hydrogen sulfate ($BmimHSO_4$) and 1-butyl-3-methylimidazolium acetate (BmimOAc) ionic liquids were utilized to function as catalyst and solvent to convert cellulose into nanocellulose. Despite having the same cations, $BmimHSO_4$ with higher acidity is suggested to induce hydrolytic cleavage of glycosidic bonds. On contrary, higher electronegativity of BmimOAc much prone to cause solvolysis of cellulose. Comprehensive investigations on different synthesis parameters including reaction temperature, time, concentration (mass loading of MCC) and sonication treatments were conducted in order to control the specific architecture and properties of nanocellulose.

Improved crystallinity of nanocellulose with the preservation of crystalline cellulose *I* structure has been successfully acquired with acidic $BmimHSO_4$ through hydrolysis. Hydrolytic reaction of $BmimHSO_4$ performed at a temperature of 90 ºC for 1.5 hours has contributed to the formation of highly crystalline nanocellulose (CrI 92.2 %) with smaller diameter (~15 nm). Increasing the temperature and time of the hydrolytic reaction predominantly increased the crystallinity of nanocellulose and produced smaller size of nanocellulose. However, the crystallinity decreased gradually with further increased in the temperature and time beyond the optimum conditions. Besides that, the cellulose concentration (in wt%) also has significant impact on the crystallinity as well as size of nanocellulose. Interestingly, the size of nanocellulose increased proportionally with increasing cellulose concentration.

On the other hand, transformation of crystal structure from cellulose *I* into cellulose *II* took place in nanocellulose obtained from solvolysis reaction with BmimOAc.

Nanocellulose with a crystallinity of 78.8 % was acquired at 80 °C for 1 hour of solvolysis and cellulose was found to swell in BmimOAc. It is noteworthy that crystallinity of nanocellulose decreased relatively with increasing temperature and time of dissolution. Meanwhile, cellulose concentration also significantly influenced the crystallinity and size of nanocellulose. With increasing cellulose concentration, the crystallinity dropped gradually and size increased proportionally.

In addition, ultrasonication treatment is essentially important to improve the crystallinity and yield smaller size nanocellulose with improved colloidal stability. Suspension of nanocellulose prepared with $BmimHSO_4$ and BmimOAc are considered rather stable with their higher absolute zeta potential values of -37.5 mV and -22.3 mV, respectively. Morphological observations demonstrated that rod-like nanocrystalline cellulose was obtained after hydrolysis with $BmimHSO_4$ whereas spherical cellulose nanoparticles were acquired through solvolysis with BmimOAc. Hydrolytic reaction imparted lower thermal stability for nanocrystalline cellulose due to the presence of sulfate groups from $BmimHSO_4$. While cellulose nanoparticles with enhanced thermal stability were acquired after the solvolysis reaction.

In the present study, ionic liquids were function as both the catalyst and solvent to prepare nanocellulose. The synthesis route with ionic liquids is an environmental friendly approach because neither undesirable nor toxic products will be produced. Meanwhile, it is an economical feasible process because of the high retrieval of ionic liquids (recovery yield of about 90 %) and they are recyclable as well as reusable.

ABSTRAK

Nanoselulosa merupakan suatu bahan yang menjanjikan dan juga menarik perhatian oleh kerana ciri-cirinya yang istimewa seperti memiliki permukaan yang luas, kekuatan dan kekukuhan serta kemampuan untuk biopemerosotan. Dalam kajian ini, *1-butyl-3-methylimidazolium hydrogen sulfate (BmimHSO$_4$)* dan *1-butyl-3-methylimidazolium acetate (BmimOAc)* cecair ionik telah digunakan sebagai pemangkin dan pelarut untuk menghasilkan nanoselulosa daripada selulosa. Walaupun mempunyai kation yang sama, keasidan *BmimHSO$_4$* dicadangkan menyumbang kepada hidrolisis. Sementara itu, *BmimOAc* dengan keelektronegatifan yang tinggi lebih cenderung dalam proses solvolisis untuk menghasilkan nanoselulosa. Kajian yang komprehensif dalam parameter sintesis yang berlainan seperti suhu, masa, kepekatan (jisim tambahan MCC) dan rawatan sonikasi telah dijalankan untuk mengawal sifat-sifat tertentu nanoselulosa.

Peningkatan hablur dengan pengekalan struktur hablur selulosa *I* dalam nanoselulosa telah berjaya dihasilkan dengan menggunakan *BmimHSO$_4$*. Berbanding dengan MCC, hidrolisis pada suhu 90 ºC dalam masa 1.5 jam telah menyumbang kepada penghasilan nanoselulosa dengan sifat hablur yang tinggi (CrI 92.2) serta berdiameter kecil (~15 nm). Nanoselulosa dengan sifat hablur yang tinggi serta saiz yang lebih kecil dapat dihasilkan dengan meningkatkan suhu dan masa reaksi hidrolitik. Walau bagaimanapun, pemerosotan hablur nanoselulosa telah berlaku dengan meningkatkan lagi suhu dan masa melebihi daripada keadaan optimum. Selain itu, kepekatan selulosa (dalam wt%) juga menpunyai kesan yang agak besar dalam mempengaruhi hablur dan saiz nanoselulosa. Dalam hal ini, saiz nanoselulosa telah bertambah berikutan dengan penambahan kepekatan selulosa.

Manakala itu, transformasi struktur hablur dari selulosa *I* kepada *II* telah berlaku dalam nanoselulosa diperolehi daripada reaksi solvolisis dengan *BmimOAc*. Nanoselulosa

dengan 78.8 hablur telah berjaya diperolehkan menerui solvolisis pada suhu 80 ºC dalam masa 1 jam. Selulosa didapati mengembang dalam *BmimOAc*. Pengurangan hablur dalam nanoselulosa telah diperhatikan sewaktu dalam usaha meningkatkan suhu dan masa untuk pencairan. Sementara itu, kepekatan selulosa juga didapati mempengaruhi hablur dan saiz nanoselulosa. Hablur nanoselulosa telah merosot manakala saiz nanoselulosa mengalami pertingkatan berikutan dengan penambahan kepekatan selulosa.

Selain itu, rawatan ultrasonikasi adalah penting untuk mengukuhkan hablur dan menghasilkan nanoselulosa yang bersaiz kecil dengan kestabilan koloid. Larutan nanoselulosa yang diperolehi dengan *BmimHSO₄* dan *BmimOAc* adalah dianggap agak stabil dengan mempunyai nilai mutlak *zeta potential* yang tinggi, iaitu -37.5 mV dan -22.3 mV masing-masing. Pemerhatian morfologi menunjukkan hablur nanoselulosa dalam bentuk seperti rod telah berjaya dihasilkan menerui hidrolisis dengan $BmimHSO_4$ manakala zarah nanoselulosa berbentuk bulat didapatkan melalui proses solvolisis dengan BmimOAc. Hablur nanoselulosa mempunyai kestabilan haba yang rendah disebabkan penambahan kumpulan sulfat menerusi proses hidrolisis. Sedangkan itu, zarah nanoselulosa yang dihasilkan dalam proses solvolisis memiliki kestabilan haba.

Dalam kajian ini, cecair ionik berfungsi sebagai pemangkin dan pelarut untuk menghasilkan nanoselulosa. Penghasilan nanoselulosa dengan menggunakan cecair ionik merupakan suatu kaedah yang mesra alam kerana tiada bahan-bahan buangan berbahaya dan toksik dijanakan dalam proses ini. Sementara itu, kaedah ini berfaedah dari segi ekonomi disebabkan kadar pemulihan cecair ionik yang agak tinggi (sebanyak 90 %) dan ia dapat dikitar serta boleh digunakan semula.

ACKNOWLEDGEMENTS

First and foremost, I would like to express my sincere gratitude to my supervisors, Prof. Dr. Sharifah Bee Abd Hamid and Dr. Lai Chin Wei for spending their precious time to provide me with excellent guidance, motivation as well as invaluable suggestion throughout my research journey.

In addition, I would like to convey grateful appreciation to all the research assistant and friends in NANOCAT. The success of my research would not been made possible without their support and kind assistance. Besides that, I would like to thank Ministry of Higher Education Malaysia for funding my master program which provided me with the opportunity to inevitably broaden my perspectives and knowledge.

Last but not least, deepest gratitude is convey to my family and friends who give me unconditional support and encouragement throughout the time in completing this research. Special thanks dedicated to my friends who inspired me and lent me a hand whenever I faced difficulties throughout the master study.

Thank you.

TABLE OF CONTENTS

LIST OF FIGURES

LIST OF TABLES

LIST OF SYMBOLS AND ABBREVIATIONS

α	:	Alpha
Å	:	Angstrom
β	:	Beta
cm	:	Centimeter
g	:	Gram
GPa	:	Gigapascal
h	:	Hour
kg	:	Kilogram
kJ	:	Kilojoule
kV	:	Kilovolt
kWh	:	Kilowatt hour
m	:	Meter
mA	:	Milliampere
mg	:	Milligram
min	:	Minutes
mL	:	Milliliter
mPa	:	Millipascal
MPa	:	Megapascal
nm	:	Nanometer
N	:	Normality
rpm	:	Rotation per minute
s	:	Second
µm	:	Micrometer
wt%	:	Weight percentage

°C	:	Degree Celsius
θ	:	Diffraction angle
λ	:	Wavelength
AFM	:	Atomic force microscope
AGU	:	Anhydroglucose
[Amim]Cl	:	1-allyl-3-methylimidazolium chloride
BF_4^-	:	Tetrafluoroborate anion
$[Bmim]^+$	:	1-butyl-3-methylimidazolium cation
[Bmim]Br	:	1-butyl-3-methylimidazolium bromide
BmimCl	:	1-butyl-3-methylimidazolium chloride
$BmimHSO_4$	:	1-butyl-3-methylimidazolium hydrogen sulfate
BmimOAc	:	1-butyl-3-methylimidazolium acetate
[Bmim]SCN	:	1-butyl-3-methylimidazolium sulfocyanate
BNC	:	Bacterial nanocellulose
CNC	:	Cellulose nanocrystals
CNF	:	Cellulose nanofiber or nanofibrils
CNPs	:	Cellulose *II* nanoparticles
CNW	:	Cellulose nanowhiskers
CrI	:	Crystallinity index
CTAB	:	Cetyl trimethylammonium bromide
$[C_6mim]Cl$	:	1-hexyl-3-methylimidazolium chloride
$[C_8mim]Cl$	:	1-octyl-3-methylimidazolium chloride
DI	:	Deionized
DLS	:	Dynamic-light scattering
DMAc	:	N,N-dimethylacetamide
DMF	:	N,N-dimethylformamide

DMI	:	1,3-dimethyl-2-imidazolidinone
DMSO	:	Dimethyl sulfoxide
DTG	:	Differential thermogravimetric
EDA	:	Electron donor-electron acceptor
EFB	:	Empty fruit bunches
ELS	:	Electrophoretic light scattering
EmimOAc	:	1-ethyl-3-methylimidazolium acetate
FESEM	:	Field emission scanning electron microscope
FTIR	:	Fourier transform infrared spectroscopy
$[H^+]$	:	Proton
$[H_3O]^+$	:	Hydronium ion
HMF	:	Hydroxymethylfurfural
HPC	:	Hydroxypropylated cellulose
HRTEM	:	High resolution transmission electron microscope
$[HSO_4]^-$	:	Hydrogen sulfate anion
IL	:	Ionic liquid
ILs	:	Ionic liquids
LD_{50}	:	Median lethal dose
MCC	:	Microcrystalline cellulose
MFC	:	Microfibrillated cellulose
NCC	:	Nanocrystalline cellulose
NFC	:	Nanofibrillated cellulose
NMMO	:	N-methylmorpholine oxide
$[OAc]^-$	:	Acetate anion
OECD	:	Organization for Economic Co-operation and Development
OH	:	Hydroxyl group

PDI	:	Polydispersity index
PLA	:	Polylactic acid
PSD	:	Particle size distribution
RTILs	:	Room temperature ionic liquids
SO_3H	:	Sulfonic acid
$[SO_4]^{2-}$	:	Sulfate
T_0	:	Onset decomposition temperature
TBAF	:	Tetrabutylammonium fluoride
TEMPO	:	2,2,6,6-tetramethylpiperidinyl-1-oxyl
TGA	:	Thermogravimetric analysis
T_{max}	:	Maximum thermal decomposition temperature
TSILs	:	Task-specific ionic liquids
XRD	:	X-ray diffraction

LIST OF APPENDICES

CHAPTER 1: INTRODUCTION

1.1 Introduction

In recent decades, modern society is habituated to a high degree of mobility, fast communication and daily comfort, all of which require considerable energy input. People nowadays are getting increasing awareness on the issues regarding energy crisis. Indeed, our modern world is heavily dependent on fossil fuels (85% of the world energy consumption), mainly goes to commercial and industrial uses. Thus, one of the steps taken by many countries to aid the earth and minimizing environmental problems is applying renewable and sustainable development for energy resources. It seems that cellulose which obtained from the biomass residues would be a great potential of renewable and sustainable energy resources as a promising alternative to fossil-derived products. The utilization of biomass materials is suggested able to decrease the dependence away from the non-renewable fossil-fuels. In urbanization world, renewable and sustainable development for energy resources is a strategic goal of modern society reflecting contemporary demand for economic, social, political and environmental development. Therefore, the finding of alternative clean energy source is crucial in leading a high quality of life, which is in harmony with nature.

Recently, enormous interest has been focused on biomass as a potential alternative resource for fuels and petrochemicals due to the depletion of fossil fuels and global warming issues (Mehmood et al., 2015). In this case, biomass resources such as lignocellulosic feedstock that derived from the commodity crops and residues from industries and forestry have prompted the prospect of biomass as a promising substitute for fossil fuel to secure the future supply of a clean and sustainable energy. Therefore, establishment of new methods and technologies are required for the beneficial utilization of biomass (Kilpeläinen et al., 2007).

It is a well-known fact that biomass is sustainable and abundance in availability. According to the literatures, there is more than 150 million tons of biomass are being generated annually as the side-product from industrial and agricultural wastes globally (Ang, Ngoh, Chua, & Lee, 2012; Tadesse & Luque, 2011; Zhao et al., 2007). The sources of biomass are generally from wood chips, agricultural residues, domestic waste, effluent sludge and animal wastes. These inedible crop residues are usually cost effective due to abundance and available in high quantity (Ang et al., 2012; Lee, Hamid, & Zain, 2014).

In general, biomass composed of three major components, such as cellulose, hemicellulose and lignin. Particularly, cellulose is the most abundant biopolymer, which consists of about half to one-third (30-50%) of the total biomass constituents. In fact, cellulose is an almost inexhaustible source of material and became the most abundant renewable resource available in nature as well as present in all living organisms. As a matter of fact, biomass is an increasingly important material for the requirement of environmental friendly, biocompatible as well as biodegradable products in the current hunt for greener technologies materials (Zhang, Li, Yu, & Hsieh, 2010).

Cellulose is a polysaccharide under the carbohydrate groups. It is the most abundant biopolymer available on earth, which can be derived from plant or animal origins. Cellulose is biocompatible, biodegradable and non-toxic, so that it can be used in biomedical and drug delivery applications. For instance, it can be used as antimicrobial agents or drug carriers. This proves the biocompatibility of cellulose in which it functions as the chelating agent to bind with other biomolecules such as proteins, cells and metal ions to perform targeted applications. In terms of degradation, cellulose is readily biodegraded by organisms that utilize cellulase enzymes (Puls, Wilson & Hölter, 2011). For instance, cellulose composites in the packaging materials will enable them to slowly

degradable in the environment. Therefore, it is sensible to judge the biocompatibility as well as biodegradability of cellulose due to its biomolecular structure.

Nowadays, cellulose has been widely applied as the source of energy and for the building materials, including textiles, paper and clothing, in the form of wood as well as the plant fibers. The aforementioned cellulose utilization was benign from its hierarchical structure to provide sufficient strength and stiffness to support the materials. Furthermore, cellulose played an important role in material engineering system as strength supporting for the composite materials. However, several obvious hindrances to the widespread use of cellulose as reinforcements in polymers are its incompatibility with hydrophobic polymer matrix, tendency of aggregation during processing and prone to swell in water. In addition, the mechanical properties can be influenced by the type of cellulose, parts of a plant as well as different plants (Brinchi, Cotana, Fortunati, & Kenny, 2013).

On the other hand, high durability property of cellulose has emerged as the leading candidate as efficient building blocks, especially the elementary unit of nanocellulose. In this context, nanocellulose is the cellulose structure that exists in nanometer scale, precisely range from 1 to 100 nm for at least one of its dimensions. It is the basic reinforcement unit that constitutes for the strength and stiffness to structure of plants and trees. Besides, nanocellulose has an exceptional mechanical performance, such that its outstanding axial Young's modulus is approximate to the one derived from theoretical chemistry. Nanocellulose is also comparable stronger than that of Kevlar and steel as well as within the range of other reinforcement materials (Brinchi et al., 2013).

The Young's modulus of nanocellulose with a density of 1.6 g cm^{-3} is approximate 167.5 GPa. It is comparably stronger than Kevlar with Young's modulus of 60-125 GPa (density around 1.45 g cm^{-3}) and potentially stronger than steel (200-220 GPa, density around 8 g cm^{-3}) (Lemaitre et al., 2009). Indeed, the specific Young's modulus, which is

the ratio between the Young's modulus and the density, of nanocellulose is around 65 J g^{-1} for microfibrils and 85 J g^{-1} for nanocrystals whereas it is around 25 J g^{-1} for steel (Dufresne, 2013). This signifies that nanocellulose is about 8 times stronger than that of steel, in terms of the ratio between strength and weight. Therefore, crystalline nanocellulose has interesting mechanical properties for use in material applications.

Apart from that, nanocellulose also has many unique characteristics such as lightweight, low density, high surface area, high aspect ratio and even modifiable surface properties due to the reactive OH functional groups. Furthermore, evaluation of its biodegradable properties in aqueous environment has been conducted according to the OECD standard. In fact, biodegradation rate of nanocellulose is much faster than that of their macroscopic counterpart, whereas other type of carbon-based nanomaterials such as fullerenes and carbon nanotubes are not providing any biodegradation property (Brinchi et al., 2013). The main reason of fast biodegradation rate is attributed to its natural structure which derived from and constitute for the macroscopic cellulose.

The processing of cellulose into nanocellulose for better utilization and exploration its new functional properties still remains as a great challenge. The reasons might be attributed to the non-thermal plastic behavior and insolubility of cellulose in water as well as most common organic solvents (Kilpeläinen et al., 2007). Moreover, hydrolysis of cellulose molecules is difficult as their molecules are not readily hydrolyzed under ambient conditions. Usually, harsh condition such as highly acidic or alkaline conditions or the use of high pressure systems is required for transforming cellulose into nanocellulose.

Generally, cellulose are recalcitrant to chemical treatments because their molecules are embedded within the complex structure of lignocellulosic matrix in order to protect them from chemical and biological attacks (Karatzos, Edye, & Doherty, 2012). Therefore,

well-designed natural structure of cellulose is still matter of debate in dissolving the cellulose without any chemical modification or derivatization. The reasons might be attributed to the rigidity of long-chain as well as strong inter- and intramolecular hydrogen bonding that constitute for the stiff cellulose structure such that it is impermeable to most of the molecules. Hence, development and identification of new efficient approach and solvent systems prompted the need for prospect utilization and application of cellulose (Zhang et al., 2010). Many scientists and researchers believed that improvement of hydrophilicity with excellent biocompatibility as well as their biodegradability properties would broaden the interest of nanocellulose as a promising smart and green material in the field of composite, packaging as well as biomedical applications.

In this research studies, nanocellulose was synthesized from cellulose precursor by using ionic liquids (ILs) function as both the catalyst and solvent. Ionic liquid (IL) is suggested to perform dual functions in the present study: (1) catalyzed the hydrolysis by cleavage of glycosidic linkage and meanwhile, (2) as a reaction medium for the solvolysis or dissolution of cellulose to disrupt the hydrogen bonding. The selected ILs in this study were 1-butyl-3-methylimidazolium hydrogen sulfate [BmimHSO$_4$] (acidity) and 1-butyl-3-methylimidazolium acetate [BmimOAc] (high electronegativity).

As a matter of fact, both imidazolium-based ILs could be provided good interaction with cellulose by disrupting the hydrogen bonds due to the coordination effect of anion groups of ILs with the hydroxyl groups of cellulose (Yuan et al., 2015). Thus, this research was conducted to investigate the influence of synthesis parameters such as reaction temperature, time, concentration in term of mass loading of microcrystalline cellulose (MCC) and different sonication treatments in the preparation of nanocellulose. The crystallinity, morphology and thermal properties of nanocellulose by controlling aforementioned processing parameters will be investigated in detail. The low complexity

of process, less time consuming and improved properties of nanocellulose produced are strongly augmented by using ILs as catalyst and solvent, thus making the project attractive and profitable.

Preparation of nanocellulose is of significant importance to expand the potential applications in vast industries as the stiff structure of cellulose hindered its exploitations. This approach is believed to be an environmental friendly route because ILs are known as green solvent for cellulose processing as they are recyclable and reusable. The high crystallinity and enhanced thermal properties of nanocellulose produced are of great interest as it can be further composites with other materials and used in reinforcement purposes.

1.2 Problem Statement

In general, processing and derivatization of cellulose are rather difficult due to the complex structure of biopolymeric network and presence of numerous noncovalent interactions between cellulose molecules. Besides that, partially crystalline, highly ordered structure as well as the stiff molecules results from the closely-packed chains via extended network of inter- and intramolecular hydrogen bonds and rigid linkages lead to insolubility of cellulose in water and other common organic solvents (Kokol, Božič, Vogrinčič, & Mathew, 2015; Xu, Wang, & Wang, 2010). In this case, these constitutes a serious problem for cellulose dissolution and activity as well as obstruct the application of cellulose. A number of methods such as acid hydrolysis, steam explosion, mechanical process, TEMPO-mediated oxidation, thermal hydrolysis and pyrolysis have been used to breakdown the cellulose molecule into nanocellulose. However, these methods not only destroy the pristine structure of cellulose but also added impurities such as halide and metal ions into the final products and are difficult controllable processes as there are propensity of over degradation of cellulose (Tang, Huang, Ou, Chen, & Chen, 2011).

To date, numerous solvent systems have been identified such as N-methylmorpholine oxide (NMMO), N,N-dimethylacetamide/ lithium chloride (DMAc/LiCl), N,N-dimethylformamide/nitrous tetroxide (DMF/N_2O_4), dimethyl sulfoxide/tetrabutylammonium fluoride (DMSO/TBAF), 1,3-dimethyl-2-imidazolidinone/ lithium chloride (DMI/LiCl) and some molten salt hydrates such as $LiClO_4 \cdot 3H_2O$, $LiSCN \cdot 2H_2O$ and other aqueous metal complexes are able to dissolve cellulose effectively (Tian, Han, Lu, Zhang, & Yuan, 2014; Xu, Zhang, Zhao, & Wang, 2013). Those methods and solvents systems proposed are worthy to mention several shortcomings might be occurred including toxicity, high cost, volatility, generation of poisonous gas, difficulty in solvent recovery and process instability (Lan, Liu, Yue, Sun, & Kennedy, 2011). In addition, multistep treatment and complicated separation process are usually required, followed by prolonged reaction time up to several hours to days.

One of the most common methods adopted in the manufacture of nanocellulose is acid hydrolysis. Acid hydrolysis is by far the most popular method for nanocellulose production known for its effectiveness, since last decades. However, this method is not recommended because it usually requires relatively harsh conditions such as extreme acidic condition and often using hazardous chemicals such as concentrated acids and alkaline and hence, is not environmental friendly. Furthermore, acid hydrolysis might be contributed to serious environmental threats due to the acid recovery and reuse issues once discharged into the effluent streams. For a commercial scale production, large quantity of acid is used and prolonged usage of acid will cause the corrosion of reactor and other equipment which are expensive and cumbersome (Harmsen et al., 2010; Lee, Hamid & Zain, 2014; Sun & Cheng, 2002).

In the limelight of this issue, the demand for the implementation of “green” processes for cellulose processing is getting more considerable attentions, with increasing

governmental regulations in the industries. The use of ILs for cellulose processing is suggested to be a green technology with their non-toxic and non-harsh characters under mild conditions because ILs are able to recyclable and reusable, thereby effectively reduced solvent consumption. ILs are essentially green solvents for cellulose attributed to their 2-3 lower magnitude orders of acidity than the conventional concentrated mineral acids. ILs can be employed as substitution to the traditional volatile organic solvents and conventional acids in the production of nanocellulose. ILs are capable to solubilize cellulose by causing the disruption to the hydrogen bonding network of cellulose. Besides that, atmospheric solvent loss and flammability hazard can be minimized via the application of ILs because they have low vapour pressure and better thermal stability. Moreover, they are ease of recovering and the ability to recycle and reusable contribute to the lower operating cost of the catalytic process. In overall, the substitution of acids by ILs can act as an environmentally friendly approach to synthesis the nanocellulose.

Development of new materials and green processes are driven by the goals to achieve green chemistry, sustainability and eco-efficiency. To date, environmental concerns have gained considerable attention and cannot be neglected. Therefore, the establishment of recycle-based and sustainable communities is becoming increasingly important. A strong driving force is initiated toward the exploitations of nanocellulose as a promising renewable, sustainable and biodegradable material into the synthetic development of environmental friendly and biocompatible products (Lin et al., 2014).

1.3 Objectives of Research

The objectives of this study are listed as follow:

- To develop methodology for the development of nanocellulose aided by ionic liquid by controlling synthesis parameters (temperature, time, mass loading of MCC and ultrasonication conditions).

- To characterize the nanocellulose obtained for its morphology, physical, chemical and thermal properties for better understanding in method development.

1.4 Scope of Study

There are three main sections within the present research study. First stage of study is about the preparation of nanocrystalline cellulose (NCC) by using 1-butyl-3-methylimidazolium hydrogen sulfate ($BmimHSO_4$) to catalyze the hydrolysis of β-glycosidic linkage. On the other hand, second stage of study is about the preparation of cellulose *II* nanoparticles (CNPs) in 1-butyl-3-methylimidazolium acetate (BmimOAc) through dissolution and regeneration approaches. The synthesis procedures of nanocellulose were carried out at different reaction temperatures, times, concentrations and subjected to different sonication treatments. The resultant nanocellulose that regenerated from IL was then further isolated by using repeated centrifugations and washing steps to remove the residual IL. Nanocellulose was allowed to freeze dry prior performing characterizations.

In the last stage of research study, multiple characterization techniques were used to characterize the resultant nanocellulose in terms of morphological, physical, chemical, structural and thermal properties. The phase structure and crystallinity of nanocellulose were characterized by X-ray diffraction (XRD) and chemical functional groups was investigated by Fourier Transform Infrared Spectroscopy (FTIR). In addition, the size and surface charges of nanocellulose were examined by Zeta Sizer. Moreover, Field Emission Scanning Electron Microscope (FESEM), Atomic Force Microscope (AFM) and High Resolution Transmission Electron Microscope (HRTEM) were used to illustrate the morphology, size and shape of the resultant nanocellulose samples. Other than that, thermal decomposition behavior of nanocellulose was determined by Thermogravimetric

Analysis (TGA). The basic principle and details of each characterization techniques will be discussed in Chapter 3-Research Methodology.

1.5 Outline of thesis

This thesis is organized into five chapters consecutively. Chapter 1 provides a brief introduction of this research study, problem statement, objectives, scope of study and thesis overview. Chapter 2 presents the structure of cellulose, different types of nanocellulose, properties and applications of nanocellulose as well as methods of production of nanocellulose. Moreover, literature review on ILs such as properties, applications, dissolution of cellulose in ILs are also included in Chapter 2. Chapter 3 describes the specification of raw materials and chemicals used, experimental methods and each of the characterization techniques adopted in this research. Chapter 4 presents the results obtained from the characterizations and subsequent data analysis. Discussion and explanation based on the results are included in this chapter. Lastly, Chapter 5 summarizes the conclusion of the study as well as several suggestions and recommendations for the future work.

CHAPTER 2: LITERATURE REVIEW

2.1 Introduction

Nowadays, public concern about the environment, climate change and limited fossil fuel resources have given rise to the urgent need of fostering development in the area of renewable energies, which are inexhaustible and non-polluting. Cellulose is one of the most promising prospects for efficient renewable resources due to its high abundance and availability in nature. Recent studies have indicated that "nano" sized cellulose has emerged as the excellent candidate to composite with other materials because of its superior mechanical properties and biocompatibility. In order to further improve the shortcomings of cellulose, considerable effort has to be exerted to increase the utilization of cellulose by applying ILs as catalyst and dissolution solvent. Lately, interesting and unique features of "nanocellulose" have gained much attention and became favorite research matter among various groups of scientists.

The relationship between cellulose and ILs was still a matter of debate and remains unclear. It was noted that the properties of this "nanocellulose" primarily depend on the nature of the preparation method and the role of optimum ILs incorporated into the cellulose. Therefore, the development of an efficient nanocellulose synthesis technique remains to be determined. In the subsequent section, the introduction of cellulose and nanocellulose as well as methods and ILs that commonly used by researchers with regards to the nanocellulose will be reviewed in detail.

2.2 Cellulose

As early as 1838, cellulose was first isolated from plant matter and being discovered by Anselme Payen on his research on ligneous matter. He reported that ligneous matter was considered a single substance, which contained two chemically distinct materials. One of these, the French chemist declared that it had the same chemical composition as

starch, but differed in structure and properties. Prior to its polymeric structure being identified and recognized, cellulose has been utilized as a precursor for chemical modification. In this context, the wood cell wall polymers were chemically modified due to the abundant number of hydroxyl groups. It is this hydroxyl groups contribute to the site for reactivity in the polymers and most reaction schemes have been based on the reaction of hydroxyl groups for hydroxyl substitutions. Because the properties of wood result from the chemistry of the cell wall components, the basic properties of a wood can be changed by modifying the basic chemistry of the cell wall polymers. A major step came in 1920 with the discovery of the polymeric structure of cellulose determined by Hermann Staudinger (Klemm, Schmauder, & Heinze, 2005).

Nowadays, cellulose remains as the most abundant natural biopolymers on earth with a remarkable annual production expected to be over 7.5×10^{10} tons (Habibi, Lucia, & Rojas, 2010). It is one of the important polysaccharide because it is available widely in higher plants (such as trees and wood), in annual crops (such as wheat straw, corn and rice husks), in several aquatic animals (such as tunicates) and a lesser degree found in simpler microorganisms including algae, bacteria, fungi, amoeba and invertebrates (Klemm et al., 2011). In fact, cellulose is a major component that can be extracted from these sources in which it comprising about 40 to 50 % of the total biomass components. Therefore, it is a potential inexhaustible source of renewable bioenergy to replace the dependence on fossil-based resources.

The cellulose obtained from higher plant, crops and aquatic animals such as tunicates consist mainly of I_β. Whereas cellulose produced by algae is rich in I_α form. However, higher cellulose content with great strength, closeness of texture and durability can be acquired from higher plants. Moreover, the cellulose fibers are long and exhibit strengthen properties to provide sufficient support to the higher plants. On contrary, lower

plants such as crops contained lower cellulose content and the fibers are much shorter and smaller with limited tensile strength as compared to the higher plants.

Regardless of the source of cellulose, it is a linear polysaccharide consisting of D-glucopyranose units linked together via β-glycosidic linkages at position C1 and C4 of the repeating glucose units. It is a well-known fact that cellobiose is the basic repeating unit of cellulose and is a dimer of glucose (Habibi et al., 2010). Each repeating unit of cellulose exhibits three hydroxyl groups. The structure of cellulose is illustrated as in Figure 2.1. The presence of hydroxyl groups on C2, C3 and C6 of repeating unit in one chain can form hydrogen bonding with hydroxyl groups within the chain or with neighboring cellulose chains. In particular, intrachain hydrogen bonding between C3 hydroxyl group and adjacent in-ring C5 oxygen as well as between C2 and adjoining C6 hydroxyl groups essentially stabilized the glycosidic linkages. On the other hand, different cellulose chains are interconnected via hydrogen bonds between C6 and C3 hydroxyl groups on the adjoining chains to form microfibril structure. In fact, all of these hydroxyl groups are responsible for hydrogen bonding, which are vital in governing the crystal packing as well as the physical properties of cellulose (Habibi et al., 2010; John & Thomas, 2008). The intermolecular and intramolecular hydrogen bonding of cellulose are demonstrated in Figure 2.2.

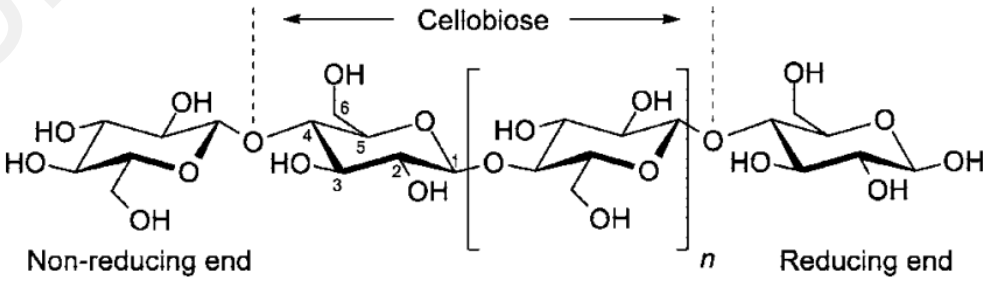

Figure 2.1: Structure of cellulose polymer chain (Pinkert, Marsh, Pang, & Staiger, 2009).

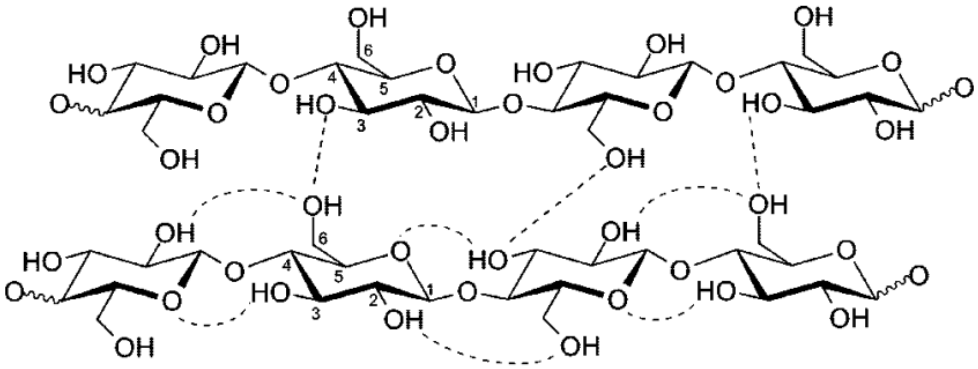

Figure 2.2: Intermolecular and intramolecular hydrogen bonding in cellulose (Pinkert et al., 2009).

Cellulose is a hydrogen bond cross-linked polymer. The presence of several hydroxyl groups on one chain formed the hydrogen bonding with the adjoining oxygen to constitute for a very stable and rigid molecule. Due to the intricate network of hydrogen bonding between cellulose chains and its rigid linkages, this makes it to be insoluble in water and other common organic solvents. In addition, the ordered structure with extensive network of inter and intramolecular hydrogen bonding constitute to the stable structure that providing the necessity strength and stiffness for supporting the plant.

Cellulose does not exist as an isolated individual molecule in nature due to its cross-linked hydrogen bonds network structure. Indeed, it is found as assemblies of individual cellulose chain-forming fibres due to the intricate network of hydrogen bonding between the cellulose polymer chains. Stacked sheets of cellulose chains are integrated into elementary fibrils. These are further aggregated into larger microfibrils units (5-50 nm in diameter and several microns in length), which subsequently assembled into collectively fibres (Habibi et al., 2010; Moon, Martini, Nairn, Simonsen, & Youngblood, 2011).

Native cellulose consists of crystalline regions associated with amorphous parts within a single cellulose chain (Brinchi et al., 2013; Klemm et al., 2005). Crystalline cellulose is consists of highly ordered structure that tightly packed and stabilized by strong and complex network of intra and intermolecular hydrogen bonds (Habibi et al., 2010).

Crystalline cellulose are strong and inaccessible structural elements. As against, amorphous cellulose consists of disordered structure with chain segments that having the length as short as the order of one cellobiose unit. Amorphous regions are weak and accessible places of the fibrils which held by van der Waals forces (Ioelovich, 2016). They are distinct from crystalline domains such that small molecules can easily penetrate into the disordered region and access to the inner cellulose molecules. Expectedly, amorphous cellulose is more chemically reactive and much prone to hydrolysis than the corresponding crystalline parts reasonably due to the difference in their structural arrangement (Moon et al., 2011; Pengfei, Kobayashi, & Fukuoka, 2011).

In addition, both inter- and intramolecular interactions and the molecular orientations within the crystalline regions played a crucial role in differentiate the polymorphs or allomorphs of cellulose. Cellulose exists in different crystal polymorphs in terms of unit cell dimensions and hydrogen bonding patterns. Native cellulose generally consists of cellulose I and it exists in two suballomorphs of cellulose Iα and Iβ. The existence of cellulose I allomorphs is dependent on the origin of cellulose where Iα is widespread in algae and bacterial cellulose, whereas Iβ is predominantly found in higher plants (Habibi et al., 2010).

Cellulose I can be converted to other polymorphs such as cellulose II or III because it is thermodynamically metastable. Cellulose II is the most stable structure because the transformation of cellulose I to II is suggested to be irreversible (Pengfei et al., 2011). This implies the difference in the hydrogen bonding patterns which give rise to different crystalline structure. Cellulose II is more stable as the cellulose chains are stacking alternatively in antiparallel modes between different hydrogen bonding planes. In contrast, the parallel arrangement of cellulose chains aligned in the same direction caused cellulose I to be less stable. Cellulose III and IV can be produced by treated with various

chemicals such as liquid ammonia or aqueous sodium hydroxide (Moon et al., 2011; Pengfei et al., 2011). The thermodynamic characteristics of various cellulose allomorphs is summarized in Table 2.1. Based on the obtained thermodynamic characteristics reported in Table 2.1, the stability of various crystalline forms of cellulose and amorphous cellulose was estimated. The thermodynamic stability of the cellulose allomorphs decrease in the order of cellulose II > cellulose IV > cellulose I> cellulose III > amorphous cellulose (Ioelovich, 2016).

Table 2.1: Thermodynamic characteristics of various cellulose allomorphs (Ioelovich, 2016).

Allomorph	Standard enthalpy of formation, $-\Delta_f H°$ (kJ/mol)	Gibbs free energy of formation, $-\Delta_f G°$ (kJ/mol)	Enthalpy of melting, $\Delta H°_m$ (kJ/mol)
Cellulose I	979.6	676.4	37.2
Cellulose II	986.9	683.7	44.5
Cellulose III	973.2	670.0	30.8
Cellulose IV	980.4	677.2	38.0
Amorphous cellulose	942.4	642.6	0

However, drawbacks of cellulose generally is related to insolubility in water and most organic solvents due to its hierarchical networks of inter and intramolecular hydrogen bonding as well as van der Waals forces (Tolonen et al., 2015). Besides that, the semicrystalline and tightly packed cellulose structures also contribute to recalcitrance of cellulose to chemical treatments. Thus, this provides a great challenge toward the exploitation and utilization of cellulose in the development of environmental friendly material (Moon et al., 2011). Since the first discovery and isolation of cellulose by Anselme Payen in 1838, extensive studies on its physical and chemical aspects have been conducted to expand the niche regarding its promising structural features, biosynthesis and assembly as well as various processing techniques indeed (Habibi et al., 2010). Nowadays, the breakthrough on “nanocellulose” has triggered the subsequent interests in

research by scientists and researchers from all over the world on nanocellulose and made it as an important component in many practical applications.

2.3 Nanocellulose

2.3.1 Types of Nanocellulose

In general, nanocellulose is defined as cellulosic materials with at least one of its dimension (length, width or diameter) within nanometer scale. Basically, nanocellulose can be categorized into three main types accordingly with respect to its dimension, preparation methods and functions, which in turn depend primarily on the sources and processing conditions. Nevertheless, the nomenclature for nanocellulose has not yet standardize and this presents ambiguities in the naming of cellulose particles with dimensions in nanometer range (Klemm et al., 2011).

Nanocellulose can be divided into nanofibrillated cellulose (NFC), nanocrystalline cellulose (NCC) and bacterial nanocellulose (BNC). NFC and NCC usually are obtained via top-down methods such as chemical, enzymatic or physical methodologies for isolation and extraction from higher plants, crops, forest or agricultural residues. In contrast, BNC is synthesized from glucose by a family of bacteria (Gluconoacetobacter xylinius) through bottom-up approach (Klemm et al., 2011). The summary on the types of nanocellulose and respective details are tabulated in Table 2.2. Figure 2.3 illustrated the microstructure images of NFC, NCC and BNC that obtained from respective sources, viewed under electron microscope.

Table 2.2: Types of nanocellulose (Klemm et al., 2011).

Type of nanocellulose	Synonyms	Typical source	Formation process	Average size
Nanofibrillated cellulose (NFC)	Microfibrillated cellulose, cellulose nanofibers, nanofibrils, microfibrils,	Wood, sugar beet, potato tuber, hemp, flax	Delamination of wood pulp by mechanical pressure before and/or after chemical or enzymatic treatment	Diameter: 5-60 nm Length: several micrometres
Nanocrystalline cellulose (NCC)	Cellulose nanocrystals, crystallites, whiskers, nanowhiskers, rod-like cellulose microcrystals	Wood, cotton, hemp, flax, wheat straw, rice straw, mulberry bark, ramie, Avicel, MCC, tunicin, algae, bacterial cellulose	Acid hydrolysis	Diameter: 5-70 nm Length: 100-250 nm (from plant); 100 nm to several micrometres (from cellulose of tunicates, algae, bacteria)
Bacterial nanocellulose (BNC)	Bacterial cellulose, microbial cellulose, biocellulose	Low molecular weight sugars and alcohols	Bacterial synthesis	Diameter: 20-100 nm Different types of nanofiber networks

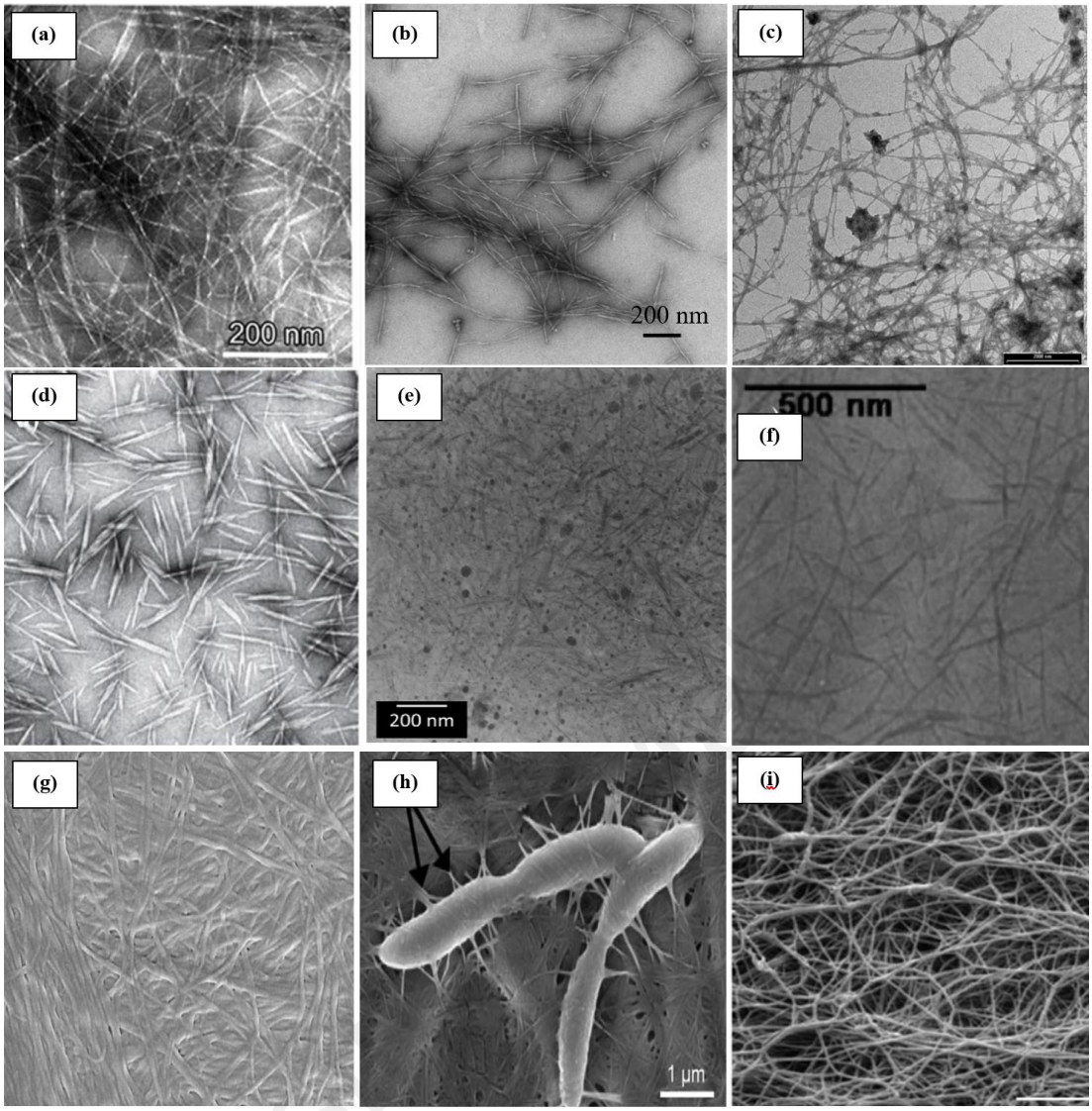

Figure 2.3: Microstructure images of NFC, NCC and BNC where (a) cellulose nanofibers from wood pulp (Chen et al., 2015), (b) cellulose nanofibrils from Kraft pulp (Qing et al., 2013), (c) cellulose nanofibers from banana peel (Tibolla, Pelissari & Menegalli, 2014), (d) cellulose nanocrystals from ramie (Dufresne & Belgacem, 2013), (e) cellulose nanowhiskers from jute fibers (Cao et al., 2012), (f) cellulose nanocrystals from sugar-beet pulp (Azizi, Alloin & Dufresne, 2005), (g) bacterial nanocellulose (de Olyveira et al., 2011), (h) bacterial nanocellulose from *Gluconacetobacter* bacteria (Klemm et al., 2011) and (i) nanofibers of bacterial nanocellulose from Gluconacetobacter strains (Klemm et al., 2011).

Nanofibrillated cellulose (NFC) is in synonyms with microfibrillated cellulose (MFC), cellulose nanofiber or nanofibrils (CNF). NFC is the smallest structural unit of plant fiber in which it usually presents in long and thin structure. Indeed, high aspect ratio of NFC is expected because of its small width of about 4-20 nm and length of up to several micrometers. In addition, alternating crystalline and amorphous domains in NFC contribute to its flexibility (Brinchi et al., 2013). NFC is generally produced by

delamination of wood pulp due to mechanical pressure before and/or after chemical or enzymatic treatment. However, very high consumption energy of over 25,000 kWh per ton is required for defibrillation of NFC due to intensive mechanical treatment which makes the production method not energy efficient (Brinchi et al., 2013; Khalil et al., 2014; Klemm et al., 2011).

It is important to note the differences between NFC and NCC of comparable dimensions. Nanocrystalline cellulose (NCC), usually denoted as cellulose nanocrystals (CNC), cellulose nanowhiskers (CNW), whiskers or rod-like cellulose microcrystals. In fact, NCC typically exhibits as elongated crystallite in rigid rod-like shape. It is usually obtained through acid hydrolysis of cellulose sources to extract the crystalline regions remained intact in NCC. In contrast to NFC, NCC has very limited flexibility because the amorphous regions are removed. NCC has relatively lower aspect ratio with 5-70 nm wide and 50-500 nm in length. The particles are 100 % cellulose and highly crystalline (Moon et al., 2011). Nevertheless, the dimensions of NCC are not uniform due to random cleaving of cellulose chains during hydrolysis process (Habibi et al., 2010; Leung, Lam, Chong, Hrapovic, & Luong, 2013).

Factors such as cellulosic source, preparation technique and conditions are mainly influencing the dimensions, morphologies as well as degree of crystallinity of NCC (Habibi et al., 2010). Cellulose can be obtained from different sources whether it is from higher plants, crops, bacteria or algae and aquatic animals. The cellulose that obtained from a particular source may inherent specific intrinsic properties such as morphology and crystallinity. For example, cellulose that obtained from higher plants usually exhibit long and thin fibers with higher crystallinity. On the other hand, the preparation technique and condition employed also significantly affected the dimensions, morphology and crystallinity of NCC. For instance, NFC is often produced after defibrillation process of

mechanical treatments such as homogenizing whereas NCC is usually obtained after acid hydrolysis process (Brinchi et al., 2013). Besides that, duration of hydrolysis also affects the dimensions of crystals, whereby a shorter crystal is produced upon hydrolyzed at a longer time. Despite that, larger dimension NCC is derived from tunicate and bacterial cellulose as compared to those from the higher plants. This is reasonably due to highly crystalline structure of tunicate and bacterial cellulose that results in cleavage of lower fractions of amorphous regions (Klemm et al., 2011).

There is another type of nanocellulose known as bacterial nanocellulose (BNC). Terminology such as bacteria cellulose, microbial cellulose or biocellulose are refer to BNC. In particular, it is derived from aerobic bacteria of genus *Gluconacetobacter*, which is a kind of acetic acid bacteria that can be found widespread in nature on the occurrence of fermentation of sugars and plant carbohydrates. BNC is actually derived through the bottom-up approach. It is formed through a more natural way as BNC is bio-fabricated from low molecular weight carbon precursor such as glucose and assembled into a polymer nanomaterial. BNC is formed as exopolysaccharide at the interface to the air and exists in stable hydrogel form. It is consists of network of nanofiber with diameter range 20-100 nm enclosed by high proportion of water. On contrary to NC, BNC has very high purity and high molecular weight with highly crystalline and mechanically stable structure. In addition, BNC is capable to have a controllable shape and structure of the nanofiber during biosynthesis with fermentation technology. Thus, this creates an exciting alternative to fabricate cellulose through bottom-up approach (Klemm et al., 2011).

Thus, optimum content of cellulose and possible formation of nanocellulose are important issues to address in order to form an ideal nanoscale cellulose with desired properties.

2.3.2 Advantageous properties of nanocellulose

Nanocellulose is a novel biomaterial to base a new biopolymer composites industry due to its promising and surpass physical and chemical properties. Indeed, it can utilized in myriad of potential applications attributed to its nanoscale dimension. As mentioned previously, nanocellulose has many advantageous properties such as low density (1.6 g/cm^3) (Moon et al., 2011), large surface area (150–250 m^2/g), high aspect ratio (70) (Lam, Male, Chong, Leung, & Luong, 2012) and modifiable surface properties. Besides that, the surface of nanocellulose can be functionalized to tailor particle surface chemistry due to presence of many hydroxyl groups on the surface. For instance, surface functionalization enables self-assembly, modification to alter hydrophilicity, to control dispersion within other matrix polymers, to enable anchoring of metallic nanoparticles on stabilized matrix or to prepare for targeted applications (Lam et al., 2012; Leung et al., 2013).

Besides that, nanocellulose exhibits extraordinary mechanical properties such that its axial Young's modulus is as high as 167.5 GPa which is close to the value derived theoretically and potentially stronger than steel and comparable to Kevlar, within the range of other reinforcement materials. Elastic modulus of nanocellulose from cotton and tunicate could reach up to 105 and 143 GPa, respectively. Meanwhile, the tensile strength of nanocellulose is estimated to be 0.8-10 GPa (Moon et al., 2011). As one of the strongest and stiffest biomaterial, it contains only a small number of defects. Therefore, nanocellulose can be used as reinforcement material in composite to provide superior mechanical performance.

The surpass characteristic of nanocellulose not only in their physical and chemical properties, but also in thermal properties. Nanocellulose exhibits very low coefficient of thermal expansion. It is a well-known fact that nanocellulose has inherent renewability,

sustainability as well as biodegradability and biocompatibility. Furthermore, biodegradability of nanocellulose has been evaluated according to OECD standard 301B (Organization for Economic Co-operation and Development) at where cellulose nanoparticles were degraded in aqueous environment much faster than that its corresponding macroscopic structure (Brinchi et al., 2013; Kümmerer et al., 2011). On the other hand, other carbon-based nanomaterials such as fullerenes and carbon nanotubes are non-biodegradable at all. Therefore, nanocellulose can be applied as environmental friendly material such as biodegradable plastic to replace the dependence on petrochemical-based products.

Nanocellulose behaves differently at the nanometer level as compared to its bulk counterparts, presumably can be explained by the laws of atomic physics (Brinchi et al., 2013; Moon et al., 2011). Indeed, nanocellulose is the fundamental building blocks for macroscopic cellulose. Therefore, in the present work, nanocellulose is fabricated with the aim to provide an environmental friendly materials as an alternative to plastics materials, in addition to its excellent physical, chemical as well as thermal properties.

2.3.3 Potential applications of nanocellulose

Nanocellulose has gained tremendous attentions during the past decades owing to its nanoscale dimension and many others promising physical as well chemical properties. A broad range of applications of nanocellulose exist and summarized as below:

2.3.3.1 Improvement of nanocomposite mechanical properties

Nanocellulose can be used as filler in nanocomposites applications widely to improve the mechanical properties. Since its introduction over the past decades, the applications of nanocellulose as reinforcement materials have been increased exponentially due to its outstanding strength and high stiffness.

Nanocellulose has been incorporated into a wide range of polymeric matrices, including synthetic and natural (such as starch or polylactide). For instance, incorporation of NCC as reinforcing fillers in poly(styrene-co-butyl acrylate) based nanocomposites had introduced in 1995 to enhance their mechanical properties (Angles & Dufresne, 2000, 2001; Brinchi et al., 2013). After that, much more attentions have been devoted to the development of fully bio-based or "green" nanocomposites in which both polymeric matrix and fillers are consist of bio-based and hence, constitute for a biodegradable system (Khalil, Bhat, & Yusra, 2012). In this case, nanocellulose was incorporated into starch-based polymers to reinforce the composites (Cao et al., 2008; Cao et al., 2008). The mechanical properties of plasticized starch (PS) and PS/NCC nanocomposites that obtained from the tensile test are showed in Table 2.3. The improvement in tensile strength, Young's modulus and elongation to break were apparently implied that the composites can be better alternative to plastics as they are more environmentally benign materials and are biodegradable (Brinchi et al., 2013). Instead of using synthetic fibers, cellulosic fibers were widely utilized as fillers for reinforcement purpose to keep our environment safe mainly due to the lower cost, low density, high strength and stiffness as well as biodegradability and inherent renewability of nanocellulose itself (Khalil et al., 2014).

Table 2.3: Mechanical properties of PS (Plasticized starch) and PS/NCC nanocomposites obtained from tensile test (Cao, Chen, Chang, Muir & Falk, 2008).

Samples	Tensile strength, σ (MPa)	Young's module, E (MPa)	Elongation at break, ε_B (%)
PS	3.9 ± 0.3	31.9 ± 5.1	68.2 ± 3.1
PS/NCC (5 %)	6.4 ± 0.2	82.6 ± 5.3	44.3 ± 5.2
PS/NCC (10 %)	7.6 ± 0.3	180.4 ± 13.2	35.9 ± 4.3
PS/NCC (15 %)	8.2 ± 0.4	255.3 ± 12.1	26.8 ± 5.5
PS/NCC (20 %)	8.9 ± 0.3	311.9 ± 20.5	14.1 ± 4.2
PS/NCC (25 %)	10.5 ± 0.5	447.5 ± 14.3	9.4 ± 1.6
PS/NCC (30 %)	11.9 ± 0.8	498.2 ± 23.4	7.2 ± 1.8

In contrast to micro-size composites, nanoscale composites are more advantageous because they exhibit lower defects for reinforcement. More recently, extensive applications of NFC have showed to improve the tensile performance of phenolic resin, hydroxypropylated cellulose (HPC), amylopectin, polyurethane and melamine formaldehyde composites (Khalil et al., 2014). The reinforced tensile strength and modulus of nanocomposites are attributed to the percolation of NFC that formed a rigid network of cellulose nanofibrils that entangled themselves within the polymer matrix of nanocomposites. Therefore, high mechanical properties of nanocomposites could be expected than that of the neat polymer in its elastomeric state. Besides that, incorporation of NFC with polylactic acid (PLA) has increased the storage and tensile modulus of elasticity of the composite materials based on dynamic mechanical analyser (DMA). As mentioned previously, the stiffness and high Young's modulus of nanocellulose (167.5 GPa) can significantly reinforced the tensile strength of the composite materials (Khalil et al., 2014; Lee, Aitomäki, Berglund, Oksman, & Bismarck, 2014). Since then, several attempts have been made to explore the mechanical performance of hybrid system of nanocellulose with a variety of polymers and particles.

2.3.3.2 Improved barrier properties of nanocomposites

According to recent literatures, nanocellulose can be acted as a potential packaging material in light of its superior mechanical performance because it is safe and biodegradable (Leung et al., 2013). As a matter of fact, packaging appeared as the largest industry for plastic materials consumption and this situation also responsible for main sources of problems regarding waste disposal (Brinchi et al., 2013). In general, food packaging materials are usually derived from petrochemical based polymers which are non-degradable and this poses a serious threat to the environment. In recent years, safe and environemtally friendly bio-based materials have getting increasing demand to use as food packaging materials. Therefore, this driven the discovery of nanocellulose as

desirable bio-based nanocomposites is required due to its inherent abundance and renewability. Besides that, problems with waste disposal and pollution can be reduced consecutively because of the biodegradable property of nanocellulose.

In addition to mechanical strength, packaging materials for food are particularly required barrier for oxygen molecules, moisture migration, flavour as well as aroma control (Khalil et al., 2014). For instance, incorporation of nanocellulose into xylan/sorbitol films to form biodegradable barrier membranes have been significantly reduced the water transmission and oxygen permeability as compared to ethylene vinyl alcohol that commonly used in barrier plastics. The main reason might be attributed to the highly crystalline structure and establishment of integated matrix (dense percolating network) through the formation of intricate and rigid network of hydrogen bonding with polymer matrix to improve the barrier properties of nanocellulose film. The extensive network of cross-linking thereby, hindered the mobility and diffusivity of the water vapor and gas molecules. As a matter of fact, nanocellulose film or membranes practically composed of good barrier properties because interactions between the particles and polymer molecules are strong enough by integrating smaller size particles with the surrounding polymer material (Belbekhouche et al., 2011; Minelli et al., 2010; Rojas, Bedoya, & Ciro, 2015). Thereby, the mobility of chain segments and penetrant diffusivity of water vapour and oxygen molecules are significantly reduced (Dufresne, 2013).

2.3.3.3 Biomedical applications

Nowadays, nanocellulose has a wide variety of applications in biomedical fields arises from its safety and efficacy. By far, toxicity tests have been proved that nanocellulose is non-toxic to human cell and it also does not cause any serious environmental concerns. Furthermore, nanocellulose has been demonstrated that utility for enzyme immobilization, biosensors as well as bioimaging applications. In fact, NCC is a potential

carrier inside cells due to its nanoscale dimension, benign nature composition as well as its modifiable and hydrophilic surface which enable the binding of various cell markers, protein molecules or receptors for targeted applications. It has been labelled with fluorescent moiety fluorescin-5-isothiocyanate in fluorescence bioassay which used as an indicator for in vivo localization and quantification of nanoparticles within a cell (Brinchi et al., 2013). Due to the benign nature, high available surface area, smoothness and reduced porosity, CNF have been reported to be a potential substrates for biosensors. These biosensors are typically prepared by binding peptides or proteins to the support matrix. Activated CNF substrates have been shown to bind to bovine serum albumin (BSA), providing for diagnostics.

Besides that, nanocellulose can be used as substrate or supporting matrix for enzyme immobilization arises from its large surface area and nonporous structure. For instance, immobilized peroxidase on NCC through activation with cyanogen bromide has been improved the removal of chlorinated phenolic compounds in aqueous solutions. The immobilization provides enzyme deactivation effects by precipitated the products induced by conjugating the amino groups. NCC and gold nanoparticles formed a nanocomposite which serves as a matrix for enzyme immobilization, in particular cyclodextrin glycosyl transferase (CGTase) and alcohol oxidase that immobilized on NCC (Lam et al., 2012).

In addition, nanocellulose appeared as a potential detection and biosensing system due to its benign characteristic. The hydroxyl groups on nanocellulose can be further modified and conjugated with different biological moieties and to bind with other molecules such as peptides or proteins to the support matrix for targeted applications. For instance, cellulose can integrated with DNA molecules via bifunctional oxirane 1,4-butanediol diglycidyl ether to form DNA/cellulose hybrid. Consequently, purification of

complimentary mRNA from total poly(A)-enriched RNA can be conducted by the hybrids by affinity chromatography.

Apart from that, NCC were act as surface for the synthesis of metal nanoparticles through a reduction method. Due to their chiral characteristics and structuring ability, NCC can be used to promote the alignment of inorganic particles. In this context, the metal nanoparticles were reduced on the surface of NCC with the use of cationic surfactants CTAB in order to achieve a controllable dimensions of the nanoparticles. Moreover, electrical detection of DNA hybridization can be probed by metal nanoparticle/NCC nanocomposites to identify the complementary target DNA sequence when Ag/carboxylated NCC nanocomposites or Ag-Pd/carboxylated NCC materials are used as labels (Lam et al., 2012). Nanocellulose-based biosensors can be used to detect human neutrophil elastase by peptide conjugation. Non-porous cellulosic films can be provided for diagnostics by conjugation of NFC substrates with bovine serum albumin (BSA). On the other hand, bacterial nanocellulose already exists in applications regarding medical devices and tissue engineering such as wound dressing, implants including cardio-vascular graft, as well as scaffolds for tissue replacement (Brinchi et al., 2013; Salas, Nypelö, Rodriguez-Abreu, Carrillo, & Rojas, 2014). These required for the properties of high crystallinity and purity of cellulose nanofibrils excreted by Gluconacterobacter xylinum bacteria which are apparently low cytotoxicity and genotoxicity.

2.3.3.4 Drug delivery

Apart from that, nanocellulose has been proposed for suitably targeted drug delivery arises from its exceptional physical properties such as nanoscale dimension, high surface area and modifiable surface properties. The hydroxyl groups on the surface of nanocellulose can be tailored for functionalization to enable modification and grafting.

Besides that, nanocellulose show no cytotoxicity which makes it suitable for internalization within cells. Chemically modified nanocellulose offers as targeted drug delivery excipient for both hydrophilic ionisable water soluble antibiotics and hydrophobic anticancer drugs. Likewise, the surface of NCC was coated with CTAB in order to bind significant quantities of hydrophobic anticancer drugs such as paclitaxel, etoposide and docetaxel, so as to release the drugs in a controlled manner over a period of several days (Brinchi et al., 2013; Jackson et al., 2011). Moreover, ionisable drugs tetracycline and doxorubicin are integrated with commercial softwood NCC to release the drugs rapidly (Lam et al., 2012). Additionally, NCC was proposed as a carrier in targeted delivery of therapeutics in which the delivery of folic acid for targeting mammalian brain cancer tumors can be beneficial from the shape of NCC (Salas et al., 2014).

2.3.3.5 Nanopaper for flexible electronics

Other than that, nanostructure cellulose can be utilized to form cellulose nanopaper. Cellulose nanopaper refers to a network constructed by intertwining nanofibrils predominantly of high aspect ratio with random surface orientation. In this manner, nanopaper can be beneficial from its high strength and transparency with low coefficient of thermal expansion as well as less defects characteristics. It then can be processed to use as a template for electronic materials (Khalil et al., 2014). As such, minimal porosity and densely packing within the solid film enhanced the conductivity of nanocellulose film. With the benign character of nanocellulose such as lightweight and good chemical and thermal stability, it became the promising candidate for developing flexible electronic devices.

Recently, CNF showed promising applications to work as precursor of carbon nanofibers which can be used as anode material in sodium-ion batteries (Luo et al., 2013). Moreover, it was shown that carbon fibers derived from CNF exhibit superior

reversibility, the rate capability required for fast charging and excellent cycling capacity (Nyström et al., 2010). Similarly, CNF-based supercapacitors have been prepared in combination with various electroconductive materials such as graphene, carbon nanotube or indium tin oxide (Gao et al., 2013; Legnani et al., 2008). CNF-based electroactive composites was showed to be conductive, electroactive and suitable for energy storage and electrochemically controlled separation. The above-mentioned described the advances of nanocellulose in flexible electronics and also highlighted the applications of nanocellulose as a supporting or active materials for flexible electronic devices (Li et al., 2013). Thus, nanocellulose can be served as an efficient supercapacitor to enable the formation of conductive composite when conjugated with conductive materials (Salas et al., 2014).

2.4 Potential techniques for synthesizing nanocellulose

It is a well-known fact that depolymerisation of cellulose into nanocellulose is generally difficult under mild conditions attributed to the stiff structure and extensive network of inter and intramolecular hydrogen bonding in cellulose (Yuan et al., 2015). The crystallites domains having three-dimensional order are strong and inaccessible structural elements. The ordered structure and stiffness of chains within the crystalline regions are attributed to the intricate and extensive network of hydrogen bonding which constitutes for its recalcitrant to the hydrolysis (Ioelovich, 2016). Practically, recalcitrance of crystalline cellulose to hydrolysis caused the hydrolysis process often required harsh conditions such as the use of highly concentrated acids, intensive mechanical treatments, high temperature and pressure systems are required to cleave the strong bonds in order to open its structure to expose the reactive groups (Lee, Hamid, & Zain, 2014). These appeared as major obstacle for its further exploitation.

Lately, there are a number of existing methods for the production of nanocellulose, either from its raw materials such as wood pulp, wheat straw, sugar-cane bagasse or other modal compounds including microcrystalline cellulose (MCC) and filter papers (Ahmadi, Madadlou, & Sabouri, 2015; Li et al., 2012; Palme, Theliander, & Brelid, 2016; Satyamurthy & Vigneshwaran, 2013). In fact, these methods employed could be divided into chemical reactions (acid hydrolysis, oxidation), mechanical (high pressure homogenization, grinding, microfluidization, cyrocrushing) and biological treatment (enzymatic hydrolysis). Generally, numerous studies have been proved that top-down approaches were successfully applied and subjected to destruct and disintegrate the cellulosic fibres into nanostructure by controlling their dimensions and crystallinity structure accordingly (Khalil et al., 2014; Lee, Hamid & Zain, 2014; Qing et al., 2013). In the following section, the most commonly employed techniques are briefly reviewed.

2.4.1 Acid hydrolysis

Among various preparation techniques available as mentioned, acid hydrolysis has been commonly used technique for the preparation of NCC or cellulose nanocrystals (CNCs). Mineral acids such as sulfuric, hydrochloric and phosphoric acids are usually used for hydrolysis process (Habibi et al., 2010). Typically, amorphous regions of cellulose are preferentially hydrolyzed during hydrolysis because they have higher accessibility to hydronium ions generated by the acids and more susceptible to hydrolytic cleavage (Lee et al., 2014). As a consequence, individual crystallites were liberated after the hydrolysis process for synthesizing high crystalline structure of NCC or CNCs (Palme et al., 2016).

In summary, it was found that there are some important parameters should be taken into consideration during hydrolysis including reaction temperature, time, agitation, acid to cellulose ratio, types and concentration of acids. These factors played an important role

in controlling the dimension and properties of synthesized nanocellulose. In fact, typical hydrolysis reaction was quenched by dilution of excess water and followed by washing with repeated centrifugations. Additional steps such as dialysis against water were required in order to remove free acid molecules from the suspension. Lastly, a mechanical treatment, typically sonication is applied to disperse the NCC homogenously for size uniformity (Klemm et al., 2011).

Nevertheless, the types of acid used for the hydrolysis will influenced the surface properties of resulting NCC. For instance, improved colloidal stability of NCC suspension has been acquired with sulfuric acid hydrolysis due to the effect of anionic stabilization via electrostatic repulsion of negatively charged sulfate groups. The esterification of surface hydroxyl groups of cellulose eventually caused the grafting of anionic sulfate ester groups which resulted in improving the dispersion of NCC in water. However, thermal stability of NCC was compromised due to the presence of sulfate groups (Dufresne, 2013). On the other hand, NCC suspension formed by hydrochloric acid hydrolysis has limited dispersion and likely flocculate, which explained its poor colloidal stability.

Typically, the sulfuric acid hydrolysis for synthesizing nanocellulose were performed at a concentration of about 64-70 wt%, with temperature range from room temperature up to 70 °C and varied the reaction time from 30 minutes to overnight depending on the temperature employed. In contrary, hydrochloric acid hydrolysis usually were conducted at reflux temperature with acid concentration of 2.5-4 N at varied time of reaction, depending on the cellulosic sources. It was found that smaller dimension (less than 10 nm width) NCC was acquired at higher temperature of 72 °C and prolonged hydrolysis up to 2 hours with 63.5 wt% sulfuric acid (Elazzouzi-Hafraoui et al., 2007; Habibi et al., 2010). In general, the higher the temperature and the longer the time of reaction will resulted in

the production of nanocellulose with significantly lower crystallinity as well as lower yield. This is because the progressive and uncontrollable hydrolysis conditions caused the removal of both amorphous and crystalline domains of cellulose which consequently lower the cellulose content of the materials.

Despite its effectiveness in preparation of NCC, acid hydrolysis still remains a crucial drawback that is excessive usage of concentrated acids. In this case, massive concentrated acids waste will be produced after the hydrolysis process, thus, proper waste management and disposal is required. Generally, hazardous concentrated acid waste usually is high toxicity that will eventually cause severe environmental issues. In addition of that, concentrated acids created serious corrosion to synthesis equipment and reactor. This drawbacks make the production cost of acid hydrolysis process relatively expensive due to the extra efforts and money is required in order to establish a high corrosion resistant reactor. The other drawback of this method is the wastage of solution after the hydrolysis process. The acid waste is difficult to regenerate and recover after the hydrolysis, manifesting that the process is economically infeasible.

Low yield of NCC is another drawback when applying the acid hydrolysis method in the production of nanocellulose. This is reasonably due to uncontrollable hydrolysis under harsh condition (concentrated acid and high temperature system) would lead to over degradation of cellulose into reducing sugars and other undesirable side products (Brinchi et al., 2013; Lee at al., 2014). Therefore, intensive care and strictly controlled of acid hydrolysis processing conditions are demanding to generate desirable NCC.

2.4.2 Oxidation synthesis

Oxidation synthesis or TEMPO-mediated oxidation is a most prominent and well-established process to form nanocellulose using 2,2,6,6- tetramethylpiperidinyl-1-oxyl (TEMPO) radicals. During the process, C6 hydroxyls of cellulose acted as the primary

alcohol groups and are selectively oxidized to carboxylate. Subsequently, presence of significance numbers of carboxylate and aldehyde groups triggered from regioselective oxidation imposed a higher density of negatively charged groups on the surface of cellulose chains. This condition could generates sufficient interfibrillar repulsion between the fibrils for effective fibrillation to overcome the adhesion between the cellulose fibrils (Masruchin et al., 2015; Rattaz, Mishra, Chabot, & Daneault, 2011). In fact, TEMPO-mediated oxidation could be modified the surface properties of nanocellulose toward carboxylated to prevent the establishment of strong interfibrillar hydrogen bonds (Qing et al., 2013; Rattaz, Mishra, Chabot, & Daneault, 2011; Saito, Kimura, Nishiyama, & Isogai, 2007). Thereby, the interfibrillar repulsion forces generated via TEMPO-mediated oxidation facilitated the isolation of nanofibers by inducing defibrillation and disintegration of cellulose microfibrils.

Many literatures reported that TEMPO-mediated oxidation actually retained the crystallinity and fibrous morphology of nanocellulose (Khalil et al., 2014; Rattaz et al., 2011). In this case, the oxidation reaction happens only at the surface of cellulose fibrils instead of penetrate into the crystallites interior. Besides that, the oxidation process could give rise to the individual very small width fibrils (3-5 nm) with intact crystallinity (Johnson, Zink-Sharp, & Glasser, 2011). The reasons might be attributed to establish repulsion between the negatively charged cellulose fibrils resulted in effective defibrillation of fibrils to isolate the individual nanofibers. In addition, oxidation synthesis is a highly selective catalytic process which contributed to the high rate of reaction and yield of nanofibers (Rattaz et al., 2011).

Despite the prospective effectiveness of TEMPO oxidation, there are some shortcomings with respect to environmental concerns caused by TEMPO radicals and high production cost. In addition, it must be taken into account that TEMPO radicals are

relatively expensive and toxic (Brinchi et al., 2013). Furthermore, the oxidation process was typically carried out under alkaline condition of pH > 12 and the process must be accompanied by the use of halide-based reagents such as sodium hypochlorite (NaClO) and sodium bromide (NaBr) as the co-oxidizing agents (Khalil et al., 2014). This situation caused a serious impact to our environmental due to highly basic condition and detrimental effect of halide-based reagents to our aquatic ecosystem. Although the process has been introduced since 14 years ago, however, it is still not yet commercialization in operation up to today due to the above mentioned concerns (Rattaz et al., 2011).

2.4.3 Steam explosion

Steam explosion is also widely employed due to its capability in separating nanofibers directly from lignocellulosic biomass (Cherian et al., 2008). The process typically requires high pressure steaming followed by fast decompression to depolymerize and defibrillate the cellulose microfibrils with the ultimate goal to produce nanofibers or NFC. Before the process is carried out, biomass sample is first milled into smaller components. Then, the dry material is saturated with steam at elevated temperature and pressure for a particular reaction time. The pressure adopted for steam explosion is typically range 14-16 bar, with a temperature range of 200-270 °C for a relatively short time (20 s to 20 min) (Brinchi et al., 2013). The pressure in digester is then released immediately by opening the steam to allow the material to expose to normal atmospheric pressure. Consequently, flash evaporation of water will be happen due to sudden dropped of pressure generates a thermo-mechanical force on the cellulosic material, which caused cellulose to rupture (Cherian et al., 2010). Indeed, the lignocellulosic structure is broken down arises from the explosion.

Steam explosion method has been used extensively as preferential biomass pretreatments over the past two decades because the resulting cellulosic material is more susceptible to enzymatic hydrolysis (Brodeur et al., 2011; Kumar et al., 2009). In summary, non-cellulosic components such as hemicellulose and lignin can be decomposed and converted into low molecular weight compounds by applying this steam explosion. For instance, most of the water soluble contents of hemicellulose can be removed by water extraction method. Meanwhile, lignin also can be extracted by other chemical treatment. The removal of lignin and hemicellulose leave the cellulose moieties intact under optimal conditions (Brinchi et al., 2013). Nanofibrils can be further separated from the bundles of cellulose microfibrils and liberated as individual entities to increase their aspect ratio and surface area for subsequent enzymatic hydrolysis reaction or reinforced the nanocomposites in applications (Cherian et al., 2010).

Nevertheless, the types of biomass feedstock will have a profound influence on the effectiveness of steam explosion. The method practically has higher ability for hardwood than softwood (Hamelinck, Van Hooijdonk, & Faaij, 2005). This method is benign to produce nanofibers by defibrillation. However, the demand for significantly high pressure and temperature system makes this process not economically feasible. Moreover, strictly monitoring of pressure and temperature is essential to prevent extensive destruction to the crystalline structure of cellulose. The advantages and disadvantages of steam explosion method for the processing of lignocellulosic biomass are given in Table 2.4.

Table 2.4: Advantages and disadvantages of steam explosion method for the processing of lignocellulosic biomass (Brodeur et al., 2011).

Method	Advantages	Disadvantages
Steam explosion	Cost effective	Partial hemicellulose degradation
	Lignin transformation and hemicellulose solubilization	Acid catalyst needed to make process efficient with high lignin content material
	High yield of glucose and hemicellulose in two-step process	Toxic compound generation

2.4.4 Mechanical treatments

In general, NFC can be obtained through defibrillation of cellulose as the intensive mechanical treatments effectively diminished the cellulose fibers into nanofibers. Among various preparation techniques available as mentioned earlier, mechanical treatments been commonly used technique for the preparation of NFC by applying high-pressure homogenization, refining, microfluidization, grinding and cryocrushing (Khalil et al., 2014; Qing et al., 2013). These mechanical approaches can be operated solely or in combination of several intensive mechanical forces for effective disintegration of fibers into nanofibers. Indeed, these process caused irreversible changes in the resultant nanofibers (Nakagaito & Yano, 2004).

Typically, high-pressure homogenization is one of the most promising prospects for mechanical treatment to form NFC. Within this process, high velocity cellulose slurry is passed across a vessel with a very small nozzle to generate a high pressure stream. High velocity and pressure as well as impact and shear forces on fluid generate shear rates in the stream that decrease the size of fibers to nanoscale (Frone et al., 2011). During the high temperature and pressurized treatment, the carbohydrate linkage within cellulose fractions was subjected to break down and rendered the release of shorter cellulose chains with lower degree of polymerization in the nanofibers (Brodeur et al., 2011). With homogenization, uniform size NFC with smaller diameter (2-5 nm) is usually formed and this method accounted for its high efficiency and simplicity without the use of any organic solvents (Jonoobi, Niska, Harun, & Misra, 2009; Khalil et al., 2014).

Despite its efficiency, a crucial problem associated with clogging is likely to occur during homogenization process due to smaller diameter size of orifice (Jonoobi et al., 2009). Hence, the fibers required to be diminished before subjected to homogenization

stage in order to prevent the clogging issue. Nevertheless, the homogenization process is encouraged to apply with other mechanical treatments to further improve its effectiveness. The number of passes or cycles and applied pressure are strongly dependent on the nature of biomass sample. It was reported that the number of cycles is varied from 10-15 cycles with pressure 30-50 MPa (Habibi, Mahrouz, & Vignon, 2009). Similar to homogenization, microfluidization also involves an integrated pressurized system within the chamber to generate impact and shear forces on cellulosic fibers for defibrillation due to interaction between colliding streams and channel walls (Ferrer, Filpponen, Rodríguez, Laine, & Rojas, 2012; Qua, Hornsby, Sharma, & Lyons, 2011).

Apart from that, refining is another potential method to defibrillate nanofibers. In this case, refining involves a combination of mechanical shearing as well as frictional forces in the fibrillation process. Production of NFC is usually beneficial upon the breakage of hydrogen bonding by mechanical forces and meanwhile, the abrasive actions generate frictional forces on the surface of fibers for repulsion. Generally, softwood is much easier to refine than hardwood ascribed to variation of cellulose content. Stelte and Sanadi (2009) have applied refining and homogenization at 50 MPa on hardwood and softwood pulps to fibrillate the nanofibers. They revealed the diameter of obtained nanofibers was around 10-25 nm for both pulps. However, excessive refining and homogenization lead to decrease in the failure strain and strength of softwood nanocellulose fibers. Furthermore, they reported that refining process was more efficient and faster for softwood compared to hardwood pulp as the structure of softwood was broken after 25 passes while hardwood fibers were remained intact after 75 cycles. This is reasonably attributed to the internal and external fibrillation phenomenon of cellulose in hardwoods and softwoods (Stelte & Sanadi, 2009). Internal fibrillation took place as a result of hydrogen bonds breakage due to mechanical actions, while external fibrillation occurred

on the surface of fibers by abrasive actions (Khalil et al., 2014). Thus, the effectiveness of refining process is determined by the number of cycles passing through the refiner.

A report in 2011 by Karande and co-workers suggested that the increase in the number of passes or cycles through refining or grinding were practically decreased the size, crystallinity, degree of polymerization as well as decreased the failure strain and strength of the nanofibers. The reason might be attributed to breaking of hydrogen bonding within the crystalline domains of cellulose after intensive mechanical actions. Besides that, combination of frictional and shear forces provide defibrillation effects on the surface of cellulose fibers by abrasive action (Karande, Bharimalla, Hadge, Mhaske, & Vigneshwaran, 2011; Khalil et al., 2014). The results showed that there is a distinct dependency of the number of cycles of refining on crystallinity, physical and mechanical properties of nanofibers.

In addition, defibrillation of nanofibers can be achieved by cryocrushing. In this process, crushing action generates a high impact force on the immediate frozen cellulosic fibers. It is suggested that pressure exerted by crushing of ice crystals is the main reason for the collapse of cellulosic structure. As a result, individual nanofibers were liberated from the bundles of microfibrils as separate entities (Siró & Plackett, 2010). Defibrillation process of cellulosic fibers involves combination of intensive mechanical shearing forces as well as frictional forces. These fibers are diminished due to the breakdown of hydrogen bonds and cell wall structures by impact shear forces and individualization of microfibrils to nanoscale fibers by repulsion of surface fibers attributed to the frictional forces generated through the abrasive actions (Siró & Plackett, 2010).

In summary, the aforementioned mechanical approaches have their own distinct features over others. The research finding indirectly showed the importance role of the homogenization and microfluidization adopted with high pressure system to generate

higher shear and impact to produce homogenous size distribution of smaller width NFC (Spence, Venditti, Rojas, Pawlak, & Hubbe, 2011). On the other hand, refining and grinding effectively caused defibrillation through abrasive actions in which the heat is generated as frictional forces for the fibrillar repulsion (Siró & Plackett, 2010). Therefore, different mechanical treatments have different shear mechanisms and varied intensity of shear forces, which results in different effects on the characterization of NFC (size, crystallinity and degree of polymerization) (Qing et al., 2013).

In overall, the above discussed mechanical treatments contribute to several drawbacks. The most critical issue is primarily associated with high consumption of energy for production of NFC from mechanical defibrillation process (Dufresne, 2013). Besides that, dramatic reduction of yield and aggregation and entanglement of nanofibers are apparent for this process. Moreover, monitoring as well as higher number of cycles which often consists of several paths through the disintegration device are practically essential for production of NFC. In addition, clogging of fiber suspensions within the reaction chamber is often occurred for high pressure homogenization and microfluidization (Qing et al., 2013). These problems present serious obstacle which hindered the successful commercialization for production of nanocellulose.

Nevertheless, combination of several potential mechanical treatments with chemical or enzymatic routes will be ideal for nanocellulose production (Khalil et al., 2014; Lee et al., 2014). The defibrillation of cellulose fibers through mechanical treatments required intensive energy and high power consumption. Chemical or enzymatic pretreatments are often took place before mechanical fibrillation (Chauhan & Chakrabarti, 2012). It is worth noting that appropriate pretreatments of cellulosic fibers could promote the accessibility of hydroxyl groups, increase the inner surface, alter the crystallinity, and break the cellulose hydrogen bonds and therefore, boost the reactivity of the fibers towards

subsequent mechanical fibrillation (Khalil et al., 2014; Szczęsna-Antczak, Kazimierczak & Antczak, 2012). The synergistic effect can be benign from the efficiency and effectiveness of the combined methods which will compromise for the energy demand for effective isolation of smaller and uniform size nanocellulose (Khalil et al., 2014; Lee et al., 2014).

2.4.5 Enzymatic hydrolysis

Based on the literatures, biological treatment such as enzymatic hydrolysis has been shown its effectiveness in preparation of NFC (Duran, Lemes, Duran, Freer, & Baeza, 2011). Contrary to acid hydrolysis, it is much more benign from the environment point of view. Therefore, cellulase enzyme has been widely used for the pretreatment of biomass materials as well as hydrolysis of cellulose due to its high selectivity and mild reaction condition. It is a well-known fact that the enzyme is capable of modify and degrade the hemicellulose and lignin components, with the retention of cellulose domains. In the meantime, restrictive and selective hydrolysis of specified component in the cellulosic fibers also induced by the enzyme cellulase (Janardhan & Sain, 2007).

In general, enzymatic hydrolysis of cellulose is a multistep catalytic process in which the cellulase enzyme is initially adsorbed onto the cellulose surface. The cellulose is subsequently breakdown via synergistic action of multiple components of cellulase. The reason attributed to a single enzyme component is not possible to degrade the fiber due to the presence of different organic compounds within the complex structure of cellulose. Lastly, desorption of cellulase from the cellulose residue render its release into the supernatant (Kuo & Lee, 2009). It is believed that the synergistic action of endoglucanases and exoglucanases/cellobiohydrolases are responsible for the enzymatic hydrolysis of cellulose. Initial cleavage of internal bonds (non-covalent interaction) within the disordered structure was done by endoglucanases because they tend to attack

the amorphous regions. Afterwards, exoglucanases/cellobiohydrolases attack on the exposed glycosdic end of cellulose chains generated by endoglucanases to release shorter cellulose chains. Subsequently, this ease the further breakdown of glycosidic linkages of shorter chains by cellobiases/betaglucosidases into formation of nanocellulose where defibrillation presumably occurred (Lee et al., 2014).

Enzymatic hydrolysis is usually carried out in combination with mechanical shearing or acid hydrolysis in order to improve its efficiency (Brinchi et al., 2013). For instance, bleached softwood pulp has been treated at combined mild enzymatic hydrolysis with homogenization and refining to prepare NFC (Pääkkö et al., 2007). During the mechanical treatment, the NFC were defibrillated through the combination of mechanical shearing forces and frictional forces to break down the tight packing arrangement within the cellulose crystalline domains. By doing so, this can increased the exposed surface area of cellulose polymer chains that are accessible for adsorption by cellulose enzyme for further hydrolysis. Nevertheless, the rate of cellulose hydrolysis is determined by the accessibility of cellulase to bind with adsorption sites on crystalline cellulose, which is a rate limiting step (Kuo & Lee, 2009). The rate of enzymatic hydrolysis is typically dependent on the structural features or organization and cellulase accessibility for the adsorption sites, which in turn dependent on the purity of cellulose (Igarashi et al., 2011).

The rate of enzymatic hydrolysis is relatively slow. Studies have demonstrated that significant enzymatic activity was noticeable only after 5 days of incubation. This confirmed the mild enzymatic hydrolysis that usually carried out over a period of 7 to 14 days of incubation. The size of nanocellulose is reduced as the time progressed due to the continued hydrolysis catalyzed by the enzymes. Also, Satyamurthy and Vigneshwaran have reported on the steady reduction in the degree of polymerization of nanocellulose with the progress of hydrolysis over the period of 15 days. Despite that, there was a

significant increase in the crystallinity of the nanocellulose to 81 % as compared to 69 % crystallinity of MCC. The increase in crystallinity is reasonably attributed to preferential hydrolysis of the amorphous regions of MCC by cellulase enzymes (Satyamurthy & Vigneshwaran, 2013).

The hydrolysis induced by enzyme cellulase give rise to the potentially higher yield, higher aspect ratio of NFC and higher selectivity under milder synthesis conditions than chemical route (Siddiqui, Mills, Gardner, & Bousfield, 2011). This process is beneficial in terms of lower energy costs and more environmental benign. However, such technique is impeded by the drawbacks of economical aspect associated with costly cellulase enzyme and technical with respect to long processing time is usually required for cellulose degradation (rate limiting step). These issues remain its primary obstacle from commercialization of nanocellulose synthesis, although it offers a numbers of potential benefits (Lee et al., 2014).

2.5 Ionic Liquids

Design and development of nanostructure cellulose has gained significant scientific interest and become the most studied material as it exhibits promising physical, mechanical and functional properties. An obvious hindrance to the widespread use of cellulose is its compact and semi-crystalline structure which caused it to recalcitrant to hydrolysis and has low solubility in water (George & Sabapathi, 2015; Kalia et al., 2011). Therefore, considerable efforts have been exerted to form nanocellulose via green route by following our governmental regulations and policies. Thus, utilization of ionic liquids (ILs) in nanocellulose synthesis stage is essential that lead to the higher efficiency of hydrolysis and dissolution (solvolysis) process in forming nano-sized cellulose (Dong, Holm, & Lassi, 2015). In the subsequent section, the introduction regarding to the ILs, advantageous properties as well as ILs for cellulose processing will be reviewed in detail.

2.5.1 Introduction to Ionic Liquids (ILs)

In this section, the brief introduction of ILs are reviewed. It is a well-known fact that ILs are molten salts with relatively low melting temperature (<100 °C) and typically exist in liquid form at low temperature (below or around 100 °C) (Liu, Sale, Holmes, Simmons, & Singh, 2009; Pinkert et al., 2009). They comprise entirely of cations and anions at where all of the ions are poorly coordinated. In fact, the cations of ILs consist of bulky, unsymmetrical organic ions with a delocalised charge whereas the anions of ILs can varied from halide ions to linear or branch organic ions. It can be understood that the bulkiness of ions, low internal symmetrical structure between cations and anions with charge delocalization as well as the poor coordination of the ions are responsible for the lower melting temperature of ILs (Pinkert et al., 2009).

Contrary to ILs, most salts or ionic compounds have high melting points because the electrostatic interactions that hold the compounds together are very strong. A good example to be presented is that sodium chloride (NaCl) with high melting point of 801 °C and it exists as solid at room temperature. The strong coulomb attraction between cations and anions give rise to the formation of strong and stable crystal lattice structure. However, this phenomenon is not favorable for ILs due to the sufficiently distortion to the ordered ions structure that required for lower melting temperature of ILs.

In 1914, ILs were firstly introduced by Walden. The innovation by Walden produced the first viable IL was ethylammonium nitrate, featuring a melting point of 12 °C, which has been revolutionized the ILs industry (Walden, 1914). Then, ILs with alkyl-substituted imidazolium and pyridinium based cations were introduced in 1970s and 1980s (Herrmann, 2015). However, numerous researches on ILs potential utilization was only extensively studied and reported over the past few decades.

Recent studies have indicated that ILs can act as promising solvents, which can benefit from their remarkable physiochemical properties including high thermal and chemical stability, negligible vapour pressure, non-flammability, wide electrochemical window, low volatility, large liquid range and high solvency power to dissolve various inorganic and organic substances (Wang, Gurau, & Rogers, 2012). ILs have gained much attention and became favourite research matter among various groups of scientists due to their above-mentioned interesting and unique features. As a matter of principle, ILs have been known as promising "green" solvents as an alternative source to replace conventional volatile organic solvents (Hu et al., 2013). ILs have myriad of potential applications including electrochemistry, catalysis, organic synthesis, polymer chemistry as well as extraction (Liu et al., 2010; Pinkert et al., 2009).

The cations of ILs are often featuring an aromatic or cyclic structure and long alkyl chain. Common cations are alkylimidazolium, alkylpyridinium and quaternary ammonium based. Whereas the anions of ILs can be varied from chloride, formate, acetate, bromide, tetrafluoroborate, hexafluorophosphate or methanesulfonate (Gericke, Fardim, & Heinze, 2012). Some common examples of cations and anions for ILs with their molecular structures are presented in Figure 2.4. In fact, various combinations of cations and anions will contribute to the variety types of ILs. As such, task-specific ILs (TSILs) are arises for particular applications with desirable properties. Also, room-temperature ILs (RTILs) are liquid ILs which have melting temperature below room temperature.

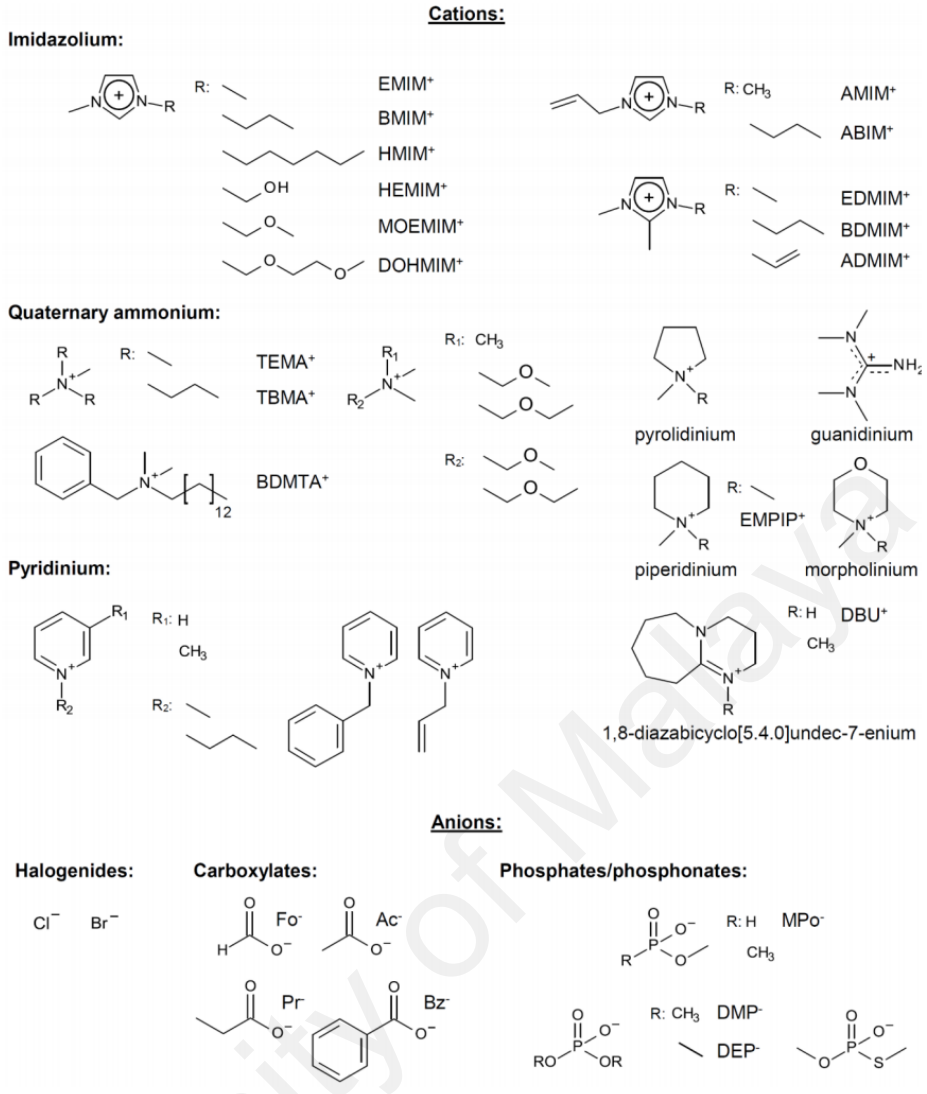

Figure 2.4: Examples of cations and anions for ILs with their molecular structures and abbreviations (Gericke et al., 2012).

2.5.2 Ionic liquids for cellulose dissolution

ILs have been investigated to act as a powerful solvent for cellulose dissolution and hydrolysis owing to their excellent solvency properties and process benefits. In 2002, Swatloski and his co-workers were the pioneer to discover that cellulose could be dissolved in high concentrations (up to 10 wt% cellulose) by heating (at around 100 °C) without derivatization using 1-butyl-3-methylimidazolium chloride ([Bmim]Cl) and the regenerated cellulose was less crystalline (Swatloski, Spear, Holbrey, & Rogers, 2002). Indeed, this experimental work presented a breakthrough for innovative new approaches about the cellulose dissolution which led to a development of a novel cellulose solvent.

Since then, utilization of ILs for biomass processing has been growing exponentially and ILs were discovered to be effective in cellulose dissolution, as a reaction medium for functionalization and chemical reactions, to form cellulose composite materials and to produce cellulose films, fibers or beads. Besides that, ILs were capable to dissolve raw biomass materials such as wood, shrimp shell, empty fruit bunches (EFB), rice husks and many others (Wang et al., 2012).

In 2002, Swatloski and co-workers postulated that the dissolution of cellulose in [Bmim]Cl was mainly attributed to the interaction between anions of IL with cellulose (Swatloski et al., 2002). In particular, the solvation of cellulose might be attributed to the coordination of chloride ions with the hydroxyl protons of cellulose. Then, the poorly coordinated chloride ions were disintegrated themselves from [Bmim]Cl upon heat treatment stage. Subsequently, the free chloride ions can interact with the hydroxyl groups of cellulose by causing disruption to the hydrogen bonding within and between adjoining cellulose polymer chains. The dissolution of cellulose in IL is believed due to the hydrogen bonding interaction between chloride anions and hydroxyl protons of cellulose (Wang et al., 2012).

In order to prove the hypothesis and gain insight into cellulose dissolution by ILs, Zhang and coworkers performed dissolution of cellobiose (the repeating unit of cellulose) in 1-ethyl-3-methylimidazolium acetate ([Emim]OAc) for 45-60 minutes at around 100 °C. It has been noted that formation of hydrogen bonding between acetate anions ($[OAc]^-$) and hydroxyls of cellobiose contributed to the solvation. In this case, acetate anions favored the formation of hydrogen bonding with hydroxyl protons of cellobiose (Zhang et al., 2010). The authors have been concluded that formation of hydrogen bonding between anions of ILs and hydroxyl protons of cellulose are responsible for dissolution of cellulose. As a consequence, the intermolecular hydrogen bonds between cellulose

chains are weakened and disrupted. In the meantime, an electron donor-electron acceptor (EDA) complex (solvate complex) was formed between hydroxyl oxygen and proton of cellulose with the charged species of ILs. The dissolution of cellulose is attributed to the formation of new bonds primarily between C6 and C3 hydroxyl groups of neighbored cellulose chains. Thus, new intermolecular hydrogen bonds are established between ILs and cellulose. The cellulose dissolution in IL is facilitated as cellulose is swelled due to the separation of hydroxyl groups of different cellulose chains (Novoselov, Sashina, Petrenko, & Zaborsky, 2007; Pinkert et al., 2009). In overall, cellulose dissolution in IL can be explained due to the interaction between anions of IL with the hydroxyl groups of cellulose, though the IL cations might have a minor role (Wang et al., 2012). The proposed simple dissolution mechanism of cellulose in ILs is depicted in Figure 2.5.

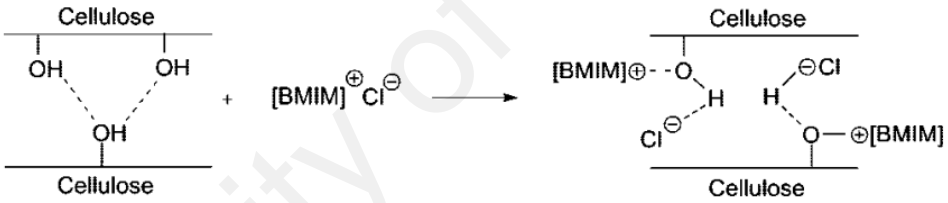

Figure 2.5: Proposed dissolution mechanism of cellulose in [Bmim]Cl (Pinkert et al., 2009).

Both of the cation and anion of ILs play an important role in the dissolution of cellulose. However, anions are essentially vital for cellulose dissolution in which anions were dominating the hydrogen bonding capability with hydroxyl groups of cellulose (da Costa Lopes et al., 2013; Pinkert et al., 2009; Wang et al., 2012). Thus, hydrogen bonding acceptor ability (basicity) of anions of IL are presumably to have an important role in dominating the solubility of cellulose. In general, anions with good hydrogen bond acceptors are more effective to dissolve cellulose. Examples are chloride, formate, acetate, phosphate and phosphonate anions. The solubility of cellulose in ILs is dependent on the hydrogen bond accepting ability of the anions. For instance, the solubility of cellulose in ILs is likely to increase proportionately with increasing hydrogen bond

accepting ability of the anions (Itoh, 2014). The higher the hydrogen bond basicity or accepting ability, the higher the ability of that particular anion of ILs to dissolve cellulose. Anions with higher hydrogen bond basicity are necessity for cellulose dissolution because the high basicity can practically weakens the inter and intramolecular hydrogen bonding of cellulose. In addition, ILs containing non-coordinating or symmetry anions such as BF_4^- and PF_6^- cannot solubilize the cellulose (Pinkert et al., 2009; Wang et al., 2012). Therefore, careful selection of potential anions to dissolve the cellulose is a challenging task.

ILs with aromatic imidazolium and pyridinium cations are more effective to dissolve cellulose when associated with a strong hydrogen bond basicity anions. Imidazolium and pyridinium based cations are commonly used for cellulose dissolution because of their aromatic nature and the ability to screen the solvate anion/cellulose polymer (EDA) complexes. The aromatic rings structure contributes to lower relative interaction strengths (lower symmetry) between the cations and anions due to reduction of electrostatic strength. Moreover, the lower internal symmetry character essentially promotes charge delocalization within the aromatic rings to make them more polarizable (Fernandes et al., 2011). As such, anions are easier to form hydrogen bonds with cellulose (Wang et al., 2012).

Apart from that, the length of alkyl chain substituents in the cations also influenced the solubility of cellulose. Cellulose has lower solubility for longer alkyl chain length of ILs cations. For example, [Bmim]Cl is more efficient to dissolve cellulose as compared to 1-hexyl-3-methylimidazolium chloride, ($[C_6mim]Cl$) and 1-octyl-3-methylimidazolium chloride, ($[C_8mim]Cl$). ILs containing longer alkyl chain length cations tend to have lower solvation power to dissolve cellulose because of reduced effective anion concentration or the hydrophobic interactions between cations which

likely reduce their ability to shield the solvate anion/cellulose complexes. Thus, cellulose dissolution is lowered with the reduced effective anion concentration of ILs (Swatloski et al., 2002; Wang et al., 2012). Alkyl groups in the cations of ILs are indirectly affected the viscosity and dissolution of cellulose. The greater the number of alkyl chain length, the more viscous the ILs and therefore, the reduced solubility of cellulose in ILs.

On the other hand, 1-alkyl-3-methylimidazolium-based ILs with even-numbered alkyl chains, particularly below six carbon units exhibit higher capacities to solubilize cellulose compared to odd-numbered alkyl chains. For instance, it is reported that cellulose is practically unable to dissolve in [C_3mim]Cl and [C_5mim]Cl. While, ILs with even numbered alkyl chain substituent cations such as [Bmim]Cl and [C_6mim]Cl are far more effective for cellulose dissolution. This phenomenon is attributed to odd-even effect which contributes to additional polarity in the heteroatomic substituents on the imidazolium ring and is more apparent for small alkyl chains (Pinkert et al., 2009; Wang et al., 2012; Zhang, 2013).

Therefore, small and even-numbered alkyl chain substituent cations ILs that paired with stronger hydrogen bond basicity anions are preferable in solvation of cellulose. The roles of cations seems like to assist in solvating and separate the cellulose polymer chains by interfere with hydrogen bonding of cellulose (Wang et al., 2012; Zhang, 2013). In addition, cations also function to shield the solvate anion/cellulose polymer (EDA) complexes in moieties.

Interestingly, ILs containing halide anions, especially anions, are particularly effective for solvation of cellulose. It has been reported that cellulose has a solubility of 10 wt% by conventional heating in [Bmim]Cl while with a greater solubility of up to 25 wt% achieved by microwave heating (Rinaldi & Dwiatmoko, 2012). On the other hand, although bromide anions ([Bmim]Br) and sulfocyanate anions ([Bmim]SCN)

alkyimidazolium based ILs are capable of dissolving cellulose, but their solubility is less than half of [Bmim]Cl. Recent studies showed that different ILs including 3-methyl-N-butylpyridinium chloride, 1-butyl-3-methylimidazolium chloride ([Bmim]Cl) and 1-allyl-3-methylimidazolium chloride ([Amim]Cl) were capable to solubilize cellulose of up to 39, 25 and 14.5 % wt% respectively (Dadi, Schall, & Varanasi, 2007; Isik, Sardon, & Mecerreyes, 2014). The greater capability of chloride anions based ILs to dissolve a high amount of cellulose are attributed to their high chloride concentration in ILs to disrupt and extensively break down the hydrogen bonding in cellulose, without caused derivatization (Cao et al., 2009).

Despite their effectiveness for dissolution of cellulose, ILs with chloride anions possess several drawbacks. One of the main problem is relatively high viscosity of chloride anions-based ILs which brought difficulties during dissolution process (Isik et al., 2014). In general, dissolution of cellulose is strongly affected by viscosity of ILs. High viscosity ILs practically unfavorable for dissolution and mass transfer due to probable inefficiency mixing process (Gericke et al., 2012). [Bmim]Cl is known to exhibit high viscosity of 11,000 MPa and melting point at 65 °C. The relatively high melting point and viscosity of [Bmim]Cl caused dissolution of cellulose occurred at relatively higher temperature (often above 80 ◦C). Besides that, [Bmim]Cl is somewhat toxic and exhibits high corrosive character. Its toxicity has been evaluated in which its median lethal dose (LD_{50}) is range from 50 mg kg^{-1} to 300 mg kg^{-1} and it is toxic to mice at maternally toxic dosages (Wang et al., 2012). Therefore, the uncertain toxicity and potential hazardousness of this IL that will be brought into ecosystems and zoology after ineluctable release into the environment as well as corrosiveness are seriously limit their practical applications in cellulose processing and derivatization in the industrial scale (Itoh, 2014). The combination of cations and anions of ILs should be screened with careful selections and their properties should be investigated such that the potential

toxicity and hazardousness can be minimized for the targeted applications as well as utilizations. In the light of these issues, it is of great interest to develop halide-free ILs with greater capability for solvation of cellulose and with low viscosity and melting point (Cao et al., 2009). Table 2.5 summarizes the applications of different ILs for the dissolution of cellulose.

Table 2.5: Application of Ionic Liquids (ILs) for cellulose dissolution (Chowdhury et al., 2014).

Ionic liquids (ILs)	Abbreviation	Cellulose Substrate	Reaction Condition		Solubility (wt%)
			Temperature (°C)	Time	
1-allyl-2,3-dimethylimidazolium bromide	[Ammim][Br]	Pulp	80	-	12
1-allyl-3-methylimidazolium chloride	[Amim][Cl]	Avicel Cellulose pulp Cotton pulp	90 80 100-130	- - 40-240 min	5 14.5 5-14.5
1-butyl-3-methylimidazolium chloride	[Bmim][Cl]	Avicel Cellulose pulp	90 100	- -	5 10
1-butyl-3-methylimidazolium bromide	[Bmim][Br]	Cellulose Avicel	Microwave 100	- 1	5-7 2-3
1-butyl-3-methylimidazolium iodide	[Bmim][I]	Avicel	100	1	1-2
1-butyl-3-methylimidazolium tetrafluroborate	[Bmim][BF_4]	Pulp cellulose	Microwave	-	Insoluble
1-butyl-2,3-dimethylimidazolium dicyanamide	[Bmim][DCA]	Avicel	110	-	1
Tetrabutylphosphonium formate	[Bu_4P][HCOO]	Avicel	110	-	6
1-ethyl-3-methylimidazolium chloride	[Emim][Cl]	Avicel Avicel	100 90	1 -	10-14 5
1-ethyl-3-methylimidazolium bromide	[Emim][Br]	Avicel	100	1	1-2

Table 2.5, continued.

1-ethyl-3-methylimidazolium acetate	[Emim][OAc]	Avicel	100	35 min	10
1-ethyl-3-methylimidazolium dimethylphosphate	[Emim][$(MeO)_2PO_2$]	Microcrystalline cellulose	65	30 min	10
1-hexyl-3-methylimidazolium chloride	[Hexmim][Cl]	Pulp cellulose Avicel	100 100	- 1	5 6-7
1-octyl-3-methylimidazolium chloride	[Omim][Cl]	Avicel	100	-	4.5
1-propyl-3-methylimidazolium chloride	[Prmim][Cl]	Avicel	100	-	>1
1-propyl-3-methylimidazolium bromide	[Prmim][Br]	Avicel	100	1	1-2
1-pentyl-3-methylimidazolium chloride	[Pemim][Cl]	Avicel	100	-	1.5
1-butyl-3-methylimidazolium hexaflurophosphate	[Bmim][PF_6]	Pulp cellulose	Microwave	-	Insoluble

2.5.3 Acidic Ionic Liquid for Hydrolysis and Dissolution of Cellulose

In recent years, researchers are getting considerable attention on the development of chemical processes and the utilization of reactants that are more sustainability and eco-efficiency towards achieving green chemistry, with the implementation of government regulations and policies. Therefore, ILs provide a new and versatile platform for cellulose processing and derivatization because cellulose can be easily regenerated from ILs without liberation of any hazardous waste products. In addition, ILs are capable of recycling and reusable.

After the discovery of halide anion based alkylimidazolium ILs to be effective for cellulose dissolution, much attentions have been paid on the utilization of ILs for

hydrolysis of cellulose. It is suggested that the incorporation of an acidic functional groups into structure of IL would contributes to a more efficient hydrolysis process. Imidazolium Brönsted acidic ILs, which combine the advantageous properties of mineral acid and ILs, are reported to be effective for dissolution and hydrolysis of cellulose. Therefore, Brönsted acidic ILs were capable to function as both the solvent and catalyst for cellulose processing under mild reaction temperatures and at ambient atmospheric pressure (Amarasekara & Owereh, 2009; Liu, Xiao, Xia, & Ma, 2013).

Over the past few years, acidic ILs have been adopted as solvent and catalyst for conversion of cellulose into valuable chemicals. First application of acidic ILs including 1-(1-propylsulfonic)-3-methylimidazolium chloride and 1-(1-butylsulfonic)-3-methylimidazolium chloride has been reported by Owereh and Amarasekara for dissolution and hydrolysis of cellulose to yield glucose and total reducing sugar (Amarasekara & Owereh, 2009). Since then, acidic ILs incorporated with SO_3H functional groups have been widely used as a catalyst for the conversion of cellulose into fructose, HMF and furfural (Tao, Song, & Chou, 2011a, 2011b). Moreover, SO_3H functionalized ILs have been used to increase the rate of cellulose hydrolysis because acidic ILs exhibit higher catalytic activity (Liu et al., 2013). In short, the hydrolysis of cellulose is facilitated due to the fracture of glycosidic bonds induced by the acidic ILs (Amarasekara & Owereh, 2009).

In the present study, 1-butyl-3-methylimidazolium hydrogen sulfate ([Bmim]HSO_4) is adopted to catalyze the hydrolysis of cellulose in order to produce nanocrystalline cellulose (NCC). In this context, [Bmim]HSO_4 is expected to perform dual functions of catalysing and dissolution of cellulose. In addition, [Bmim]HSO_4 also serves as a medium for dissolution or swelling and hydrolytic reaction of cellulose. Cellulose can be regenerated from IL with ease and subsequent recycling of IL is also possible. In addition,

no extra efforts are required for neutralization and separation of the acid catalyst and no hazardous waste will be generated because the IL can be recovered, recycled and reused conveniently. The structure of $[Bmim]HSO_4$ is depicted in Figure 2.6. Alkylimidazolium cations with butyl side chains are selected to compromise for the solubility of cellulose. This is because shorter alkyl chain length cations have higher effective anion concentration and higher solvation power which can beneficial for the dissolution of cellulose.

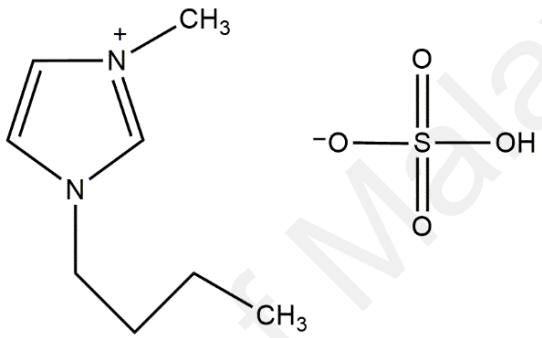

Figure 2.6: Chemical structure of $[Bmim]HSO_4$ (Mao, Osorio-Madrazo, & Laborie, 2013).

$[Bmim]HSO_4$ has an intrinsic acidic character whose acidity is due to hydrogen of $[HSO_4]^-$ that has a pK_a value around 2 in water. The Hammett acidity measurements revealed that $[Bmim]HSO_4$ has H_0 values of 1.97 which reflects that a higher concentration of $[HSO_4]^-$ is available per unit volume of IL. It is expected that acidity of $[Bmim]HSO_4$ was improve at elevated temperatures and thus can protonate and cause hydrolytic cleavage of β-glycosidic bonds within cellulose (To, 2012). On one hand, acidic $[Bmim]HSO_4$ initially swelled the cellulose to increase the interlayer spacing between stacked sheets of cellulose polymer chains and destroy the hydrogen bonding (Tian et al., 2014). Subsequently, the hydrolytic cleavage of β-glycosidic bonds between the cellulose molecules was triggered by the presence of small amounts of water as impurities to further induce dissociation of acidic proton from $[HSO_4]^-$. Therefore, the β-

glycosidic bonds dissolved in [Bmim]HSO_4 can be easily attacked by hydronium ions which facilitated the hydrolysis of cellulose (Mao et al., 2013).

Acidic [Bmim]HSO_4 offers a promising approach for the synthesis of nanocellulose from cellulose by performing cellulose dissolution with remarkable catalytic activity. [Bmim]HSO_4 showed apparent hydrolytic activity attributed to its stronger acidity (due to proton from $[HSO_4]^-$). On the contrary, [Bmim]Cl exhibits lower catalytic capability because it has limited acidity (Tian et al., 2014). Despite that, the highly viscous [Bmim]Cl has a negative impact on the catalytic activity in which the mobility of ions are restricted.

In summary, the structure, acidity and viscosity of ILs are important factors to influence the catalytic capability of ILs. In particular, acidity and viscosity of ILs are significantly affected the catalytic activity of ILs. The stronger acidity (active acid sites) with low viscosity acidic ILs are well-suited and more effective for catalysing hydrolysis of cellulose to accelerate the fracture of glycosidic linkages to produce more NCC (Liu et al., 2013). The inherent acidic characteristic of acidic ILs which have dual functions of swelling and catalyzing, makes them as a viable alternative approach in the production of nanocellulose (Tian et al., 2014). Therefore, this approach could be developed into a green, economical and efficient cellulose hydrolysis protocol for the production of nanocellulose with the recycling of Brönsted acidic ILs after the reaction.

2.5.4 Acetate based Ionic Liquid for Cellulose Dissolution

A promising cellulose solvents ideal for dissolution should have most of the following characteristics: (i) able to dissolve a high amount of cellulose at low temperature, (ii) chemically and thermally stable, (iii) non-toxic and non-volatile, (iv) low melting point and viscosity, (v) easy cellulose regeneration, (vi) no decomposition of cellulose, (vii) high recovery of solvents and recyclable, and lastly (viii) cost effective process (Wang et

al., 2012). Therefore, a new IL was discovered based on the aforementioned features especially the requirements for lower melting points and viscosity with sufficient polarity to dissolve cellulose effectively.

Acetate based ILs are the most efficient solvent for dissolution of cellulose. 1-ethyl-3-methylimidazolium acetate ([Emim]OAc) has been demonstrated to dissolve cellulose up to 16 wt% by heating whereas a cellulose concentration of as high as 25 wt% can be achieved by microwave heating (Isik et al., 2014). Therefore, acetate based imidazolium ILs showed the potential to dissolve a higher amount of cellulose under mild conditions and useful for effective cellulose dissolution. The structure of [Bmim]OAc is provided in Figure 2.7.

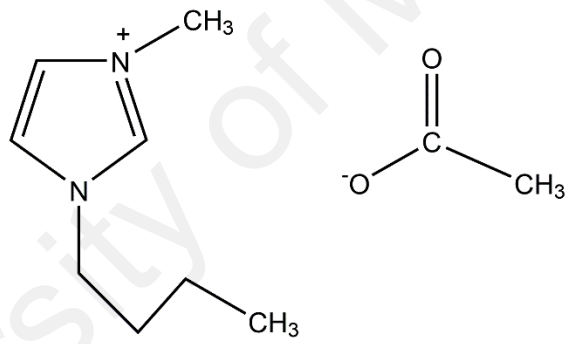

Figure 2.7: Chemical structure of [Bmim]OAc (Wang et al., 2012; Zhang, 2013).

Acetate based imidazolium ILs such as [Emim]OAc and 1-butyl-3-methylimidazolium acetate ([Bmim]OAc) are promising solvents for cellulose dissolution. [Bmim]OAc has a lower melting point (< -20 °C), lower viscosity exist at liquid state (646 mPa at room temperature) and less toxic and corrosive character than [Bmim]Cl (Cao et al., 2009). In contrast, [Bmim]Cl is noteworthy to exist in solid state at room temperature with a significantly higher viscosity of 11,000 mPa. Besides that, the higher melting point of [Bmim]Cl (66 °C) typically required higher temperature (100 °C) for cellulose dissolution (Olivier-Bourbigou, Magna, & Morvan, 2010). These aspects make acetate

based ILs to become interesting solvent for processing and homogeneous derivatization of cellulose due to their capability to enhanced cellulose dissolution.

Important properties of ILs, particularly their polar character (based on Kamlet-Taft parameter), basicity of anions of ILs and their ability to generate hydrogen bonding significantly dictate their functional roles in dissolution capability. Based on Kamlet-Taft parameter, [Bmim]OAc (β =1.09) has better efficiency in dissolution than [Bmim]Cl (β =0.83) because they have stronger hydrogen bond basicity. In general, the weakening of the hydrogen bonding network of cellulose polymer chains is achieved by ILs with stronger hydrogen bond basicity (Olivier-Bourbigou et al., 2010). Acetate anions display higher dissolution capacity for cellulose because they have enhanced basicity as compared to chloride ILs. Therefore, acetate anions are more efficiently to disrupt the hydrogen bonding within the crystalline domains of cellulose by coordination with hydroxyl groups of cellulose through hydrogen bonding (da Costa Lopes, João, Morais, Bogel-Łukasik, & Bogel-Łukasik, 2013). The hydrogen bonding between cellulose chains is weakened by acetate anions and resulted in the solvation of cellulose in ILs. Table 2.6 summarizes the comparison of main properties of [Bmim]Cl and [Bmim]OAc relevant to cellulose dissolution.

Table 2.6: Comparison of main properties of ILs relevant to dissolution.

Ionic liquid	Melting point (°C)	Viscosity (mPa at 25 °C)	Solvato-chromic parameter (β, hydrogen bond basicity)	Dissolved cellulose (wt %)
[Bmim]Cl	66	11,000	0.83-0.87	10 wt% by conventional heating; 25 wt% by microwave heating
[Bmim]OAc	<-20	646	1.09	16 wt% by conventional heating; 25 wt% by microwave heating

In this work, [Bmim]OAc is selected as the solvent for dissolution or solvolysis of cellulose mainly due to its lower viscosity and melting point These features will enable the dissolution much more favorable to conduct at lower temperature. Besides that, it is suggested that a higher concentration of cellulose is able to dissolve well in [Bmim]OAc because of its high dissolution capability and excellent solvency power for cellulose (Olivier-Bourbigou et al., 2010). Nevertheless, [Bmim]OAc has less acidity in character than [Bmim]HSO_4 and this can explained why the hydrolysis reaction did not proceed extensively in [Bmim]OAc (To, 2012). In fact, it has higher nucleophilicity and stronger hydrogen bond basicity which makes it tends to accept hydrogen bonding for solvation of cellulose.

On the other hand, [Bmim] cations are selected as the compromise to cost effective and solubility of cellulose. It has been suggested that solubilization temperature of cellulose are relevant to the length of alkyl side chains of imidazolium cations and viscosity of ILs. Since viscosity of ILs are generally increases for longer alkyl side chains, so do the increase in solubilization temperature (Itoh, 2014; Ohno & Fukaya, 2009). Therefore, shorter alkyl side chains (butyl) imidazolium cations have decreased viscosity of ILs which favoured for the dissolution of cellulose at lower temperature.

In short, [Bmim]OAc shows promise in the production of nanocellulose through solvolysis or dissolution approach. With its excellent solvency power, it shows its potential functional roles as solvents and catalysts for the efficient process of cellulose dissolution.

2.5.5 Regeneration of Cellulose from Ionic Liquid Suspension

Regeneration of cellulose from cellulose/ILs mixture is possible by adding anti-solvents to precipitate the cellulose. Typically, the ILs used to dissolve cellulose is water soluble. The choices of anti-solvents are plenty such as water, ethanol, methanol, acetone,

acetonitrile and isopropanol (Wang et al., 2012). Nevertheless, water and ethanol are most commonly used anti-solvents to precipitate the dissolved cellulose (Olivier-Bourbigou et al., 2010). The usage of water as anti-solvent presents inexpensive and environmentally benign approach because water is safe and do not pose any hazards. The criteria to be an effective anti-solvent required that it is a polar solvent with the ability to form hydrogen bond with anions of ILs more strongly than cellulose and solvate the charged species of ILs (Wang et al., 2012).

Most ILs are recognized for their hygroscopic properties in which they have strong absorbability for water. For instance, [Amim]Cl and [Bmim]Cl are completely miscible with water in any ratio. Hence, the regenerated cellulose materials are easily obtained by coagulations due to competitive hydrogen bonding between cellulose and water molecules with ILs. In the regeneration process, ILs tend to form hydrogen bonding with water molecules as O-H bonding has higher electronegativity than the C-H type hydrogen bond (Han, Zhou, French, Han, & Wu, 2013). Despite that, the ions of ILs are extracted into the aqueous phase through hydrogen bonding, dipolar and Coulombic forces in the regeneration steps. Subsequently, the ions of ILs are surround by water molecules to form hydrodynamic shells to shield the direct interactions of ILs ions with cellulose. Consequently, the hydrogen bonds between cellulose and ILs are weakened while the inter and intramolecular hydrogen bonds between cellulose chains are rebuilt and reconnect. Therefore, this results in the precipitation of cellulose (Zavrel et al., 2008). The regenerated cellulose can be isolated due to separation by centrifugation or filtration process.

The regenerated cellulose can be obtained in various forms such as cellulose membranes, fibres, films, beads and monoliths, depending on the processing conditions. For instance, rapid mixing of water into ILs solution results in the precipitation of

cellulose as powdery flocs. Thin cellulose films can be obtained by casting the cellulose/IL solution onto a glass plate and then coagulated in water. A transparent cellulose film can be obtained after subsequent removal of IL and drying. On the other hand, cellulose fibres or rods can be prepared by extrusion of cellulose/IL solution into an anti-solvent or wet spinning or dry jet-wet spinning process and subsequent coagulated with water (Cao et al., 2009; Wang et al., 2012; Zavrel et al., 2008). The process involved in regeneration of cellulose fibers is presented in Figure 2.8.

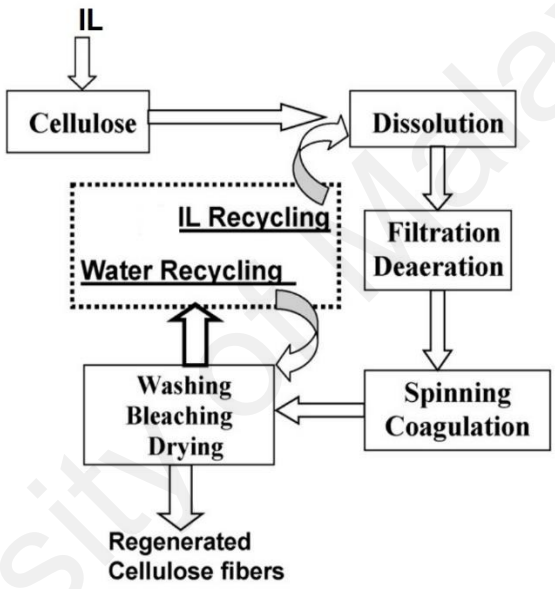

Figure 2.8: Process involved in regeneration of cellulose fibers (Cao et al., 2009).

After the regeneration process, the regenerated nanocellulose may experience significant change to its macroscopic morphology and degree of crystallinity. Contrary to native cellulose, the regenerated nanocellulose typically exhibit lower degree of crystallinity and structural transformation into a more disordered form after dissolution in ILs (Wang et al., 2012). For instance, crystallinity reduction is apparent for cellulose that reconstituted from dissolution in [Amim]Cl and [Bmim]Cl, as compared to native cellulose. In addition, the resultant regenerated cellulose is mostly amorphous (Olivier-Bourbigou et al., 2010).

Apart from that, the yield of regenerated cellulose is affected by the types of anti-solvents used. Water is most widely used as anti-solvents for cellulose regeneration because the regeneration yield for water is higher than that in methanol, ethanol and acetone. This is because water indeed, is a polar protic solvent and its easiness and strength of the hydrogen bond formation between water and cellulose. Besides that, mixture of anti-solvents such as ethanol and acetone results in the precipitation of cellulose with porous appearance and enhanced dispersion in the solvents without formation of gel (da Costa Lopes et al., 2013). On top of that, the anti-solvents selected must be easily separated and removed from ILs. This can ensure that both components can be recycled and reused from the environmentally benign standpoint and also a cost effective way from the economical point of view.

2.5.6 Recovery of Ionic Liquids

Generally, ILs can be recovered after the regeneration of cellulose due to their characteristic low vapor pressure and non-volatility. ILs can be removed from the cellulose suspension through multiple washing with centrifugation steps. After the repeated centrifugations, the ILs solution are isolated from the cellulose suspension as the cellulose is precipitated as the sediment. Numerous methods have been investigated for recovery of ILs, for example distillation, solvent extraction, adsorption, salting-out process and membrane based methods such as nanofiltration and reverse osmosis. The summary of each methods to recover ILs is provided in Table 2.7. The selection of appropriate recovery process is actually depends on the characteristics of systems/processes.

Table 2.7: Summary of methods used for recovery and recycling of ILs (Mai, Ahn, & Koo, 2014).

Methods	Remarks	Advantages	Disadvantages
Distillation	Volatile compounds/impurities are distilled while ILs are remained as residual	Simple, rapid and robust method	Energy consuming
Solvent extraction	Organic solvent/water are used to extract various compounds from ILs, thus allowing recovery and reuse of ILs	Simple, no complex equipment, controlled recovery, selectivity and flexibility	Emulsion formation, not efficient, loss of compounds, complicated, laborious, pre-concentration step required
Adsorption	Various adsorbents are used to adsorb ILs from dilute stream. A desorption step with solvent are carried out to recover ILs	Robust, relatively easy to operate	Require equilibrium adsorption and desorption data; desorption solvent
Salting-out process	Electrolytes or salts are introduced into ILs suspension solution to form aqueous bi-phases system (ABS) including ILs rich phase and water-rich phase	Simple, effective; using less expensive inorganic salts	Environmental problems of high inorganic salt in salt-rich phase
Membrane based process			
Nanofiltration	Two operation modes where ILs is permeated or retained	Simple, less energy and solvents demand	Relatively low flux and recovery yield
Reverse osmosis	Pressure driven process	Low energy requirement; compact and less space requirement; modular design	Require pretreatment of mixture; limited by osmotic pressure

Table 2.7 summarizes the methods used for the recovery and recycling of ILs. The advantages and disadvantages of each method are briefly discussed. Due to low vapor pressure, distillation technique is always being the first choice adopted to recover and recycle ILs. ILs with relatively high purity (> 90 %) and high recovery rate (> 95 %) can

be recovered via this method. Despite that, the extraction process yield about 89 % of recover ILs. However, this method is associated with the emulsion formation, loss of compounds, required laborious and pre-concentration steps which make the process complicated and not efficient. Although 92 % of recovery rate can be achieved with adsorption process, the requirement of adsorption/desorption data and additional desorption solvents contribute to the sophisticated of the method. In addition, in the continuous adsorption/desorption or chromatography method, the requirement of complex chromatography equipment and pre-concentration step would make the methods costly and laboriously. Besides that, salting-out methods are concerning with environmental problems due to the presence of high inorganic salt which makes the method become economical unfeasible, though its high recovery rate of about 96 %. Apart from that, membrane-based process such as nanofiltration and reverse osmosis process give rise to the relatively lower recovery rate of 14 % and 20 %, respectively.

Distillation is the most simple and conventional method employed for the recovery of ILs in which the thermally stable ILs are retained through the removal of compounds with low boiling point. Distillation of volatile compounds can be performed with vacuum evaporation, molecular as well as column distillation. In the studies regarding to cellulose processing, regenerated cellulose is firstly removed from ILs suspension by filtration. Then, residual ILs in the filtrate is recovered by evaporation under reduced pressure and distillation with subsequent drying in the vacuum conditions for 24 hours in order to eliminate water (Mai et al., 2014). ILs can be recovered with high purity and recycled by this method (Cao et al., 2009). Distillation method is considered to benefits from the difference in boiling points between water (100 °C) and ILs (> 200 °C). Interestingly, ILs have high recovery rate (> 95 %) and purity (> 90 %) (Cao et al., 2009; Swatloski et al., 2002). The recovered ILs can be reused as the recycled ILs exhibit similar capability to dissolve cellulose which reflects their durability in use.

On top of that, efficient recycling of ILs is key for cost effective process in industrial application. Environmental concerns regarding to disposal issues such as toxicity and biodegradation can be resolved to minimize with the recovery and recycling of ILs (Cao et al., 2009). Therefore, application of ILs in the industry can be apparently promoted by taking all the advantageous features of ILs especially recyclable and reusable.

CHAPTER 3: MATERIALS AND METHODOLOGY

3.1 Introduction and Overview

Chapter 3 covers the explanation and discussion of three important sections. The first section provides information about the raw material selection and chemicals that were used in this study. The second section elaborates on the experimental procedure to form nanocellulose by considering the effect of reaction temperature, time, concentration and sonication treatments. These studies aim to determine the optimum processing parameters to obtain desired small size and high crystallinity nanocellulose. The last section in this chapter outlines the characterization of the nanocellulose using various techniques, such as XRD, Zeta sizer, FTIR, FESEM, AFM, HRTEM as well as TGA analysis.

3.2 Raw Materials and Chemicals selections

Table 3.1 provides the general information and properties of raw materials and chemicals used in this research to produce nanocellulose.

Table 3.1: List of raw materials and chemicals used for the synthesis of nanocellulose.

Material	Function	Manufacturer	Properties
Microcrystalline cellulose (MCC)	Cellulose precursor/reactant	Sigma Aldrich	Chemical formula: $(C_6H_{10}O_5)_n$ Source: Cotton linters
$BmimHSO_4$	Catalyst/solvent	Sigma Aldrich	Chemical formula: $C_8H_{16}N_2O_4S$ Purity: ≥ 95%
BmimOAc	Catalyst/solvent	Sigma Aldrich	Chemical formula: $C_{10}H_{18}N_2O_2$ Purity: ≥ 95%
DI water	Anti-solvent/washing solvent	-	Resistivity: 18.2 MΩ.cm pH: 6.8-7.2

3.2.1 Microcrystalline cellulose (MCC)

Microcrystalline cellulose in the form of microcrystalline powder obtained from cotton linters source has repeating unit of $(C_6H_{10}O_5)_n$ and density of 0.6 g/cm^3, was purchased

from Sigma-Aldrich. The CAS number is 9004-34-6. MCC is the starting raw materials used in the present research study.

3.2.2 1-butyl-3-methylimidazolium hydrogen sulfate ($BmimHSO_4$)

1-butyl-3-methylimidazolium hydrogen sulfate, ≥ 95% with a chemical formula of $C_8H_{16}N_2O_4S$, has molecular weight of 236.29 g/mol and a density of 1.277 g/cm^3, was purchased from Sigma Aldrich. The CAS number is 262297-13-2.

3.2.3 1-butyl-3-methylimidazolium acetate (BmimOAc)

1-butyl-3-methylimidazolium acetate, ≥ 95% with a chemical formula of $C_{10}H_{18}N_2O_2$, molecular weight = 198.26 g/mol, and exhibits a density of 1.055 g/cm^3, was purchased from Sigma Aldrich. The CAS number is 284049-75-8.

3.2.4 Deionized water (DI water)

DI water was used throughout the research study as the washing solvent to remove IL after subsequent washing and centrifugation steps. It is also functions to dilute the IL in the IL/cellulose suspension by quenched the reaction.

3.3 Methodology of Experiment

3.3.1 Synthesis of nanocellulose by $BmimHSO_4$

In this stage, nanocellulose was primarily synthesized through IL-mediated hydrolysis method. Microcrystalline cellulose (MCC) powder with different loading amounts was added into $BmimHSO_4$ and heated up to 70, 80, 90, 100 and 110 ºC respectively. The mixture was then heating for different time varied from 0.5 h, 1.0 h, 1.5 h, 2.0 h and 2.5 h with continuous mechanical stirring at a speed of 400 rpm. The mass loading of MCC was varied as 5 wt%, 10 wt%, 15 wt%, 20 wt% and 25 wt%. Several important synthesis parameters including temperature, time and mass loading of MCC were studied and optimized in order to produce smaller dimension nanocellulose with desired properties.

Nanocellulose can be precipitated from the mixture by adding DI water as anti-solvent. The hydrolysis reaction was then quenched by addition of 20 mL cold DI water into the mixture. Powdery flock were formed upon addition of water into the IL/cellulose mixture. The mixture was allowed to stir for 5 minutes and then subjected to different sonication treatments at room temperature. The sonication was carried out with high-intensity ultrasonic probe (Hielscher Ultrasonic, UIP/1000hd) or low-intensity ultrasonic bath (Thermoline, Thermo-6D) respectively. The suspension was subsequently washed with DI water using repeated centrifugation at 7,500 rpm for 15 minutes interval until a stable pH 5 suspension was achieved. The sediment was dried by using a freeze dryer (Labconco, FreeZone 4.5 L Benchtop) for 2 days and kept in refrigerator at -4 ºC before performing further characterization.

3.3.2 Synthesis of nanocellulose by BmimOAc

Preparation of nanocellulose by using BmimOAc was achieved via solvolysis or dissolution approach. The synthesis procedures were similar to the methodology in the previous section (Section 3.3.1) by using $BmimHSO_4$ except for the IL used in the current stage is BmimOAc.

Microcrystalline cellulose (MCC) powder at different mass loading amount was added into BmimOAc in a round bottom flask and heated up to 70, 80, 90, 100 and 110 ºC respectively. The mixture was heated for different times varied from 0.5 h, 1.0 h, 1.5 h, 2.0 h and 2.5 h, respectively in the oil-bath with continuous mechanical stirring at a speed of 400 rpm. The mass loading of MCC was varied accordingly to 5 wt%, 10 wt%, 15 wt%, 20 wt% and 25 wt%. It is well-established that the properties and dimensional features of nanocellulose can be controlled by variety of parameters, such as reaction temperature, time and mass loading of MCC. It was observed that MCC started to dissolve completely as the color of the mixture turned into amber and yield a transparent solution.

The dissolution was then quenched by rapid mixing of 20 mL cold DI water into the mixture to precipitate the nanocellulose. Formation of gel-like off-white flocs were observed upon rapid mixing of water with IL/cellulose mixture. The mixture was stirred for 5 minutes before subjected to sonication treatment at room temperature. The mixture was sonicated by using high-intensity ultrasonic probe (Hielscher Ultrasonic, UIP/1000hd) or low-intensity ultrasonic bath (Thermoline, Thermo-6D) respectively. In the present study, DI water was used to wash the resulting suspension with repeated centrifugations at 7,500 rpm for 15 minutes interval in order to remove residual IL until a stable pH 5 suspension was achieved. The sediment was freeze dried in Labconco, FreeZone 4.5 L Benchtop freeze dryer for 2 days to yield white nanocellulose fine powder. The nanocellulose was kept in refrigerator at -4 ºC prior performing characterizations. The overview of nanocellulose synthesis methodology is illustrated in Figure 3.1.

3.3.3 Recovery of Ionic Liquid

The supernatant that decanted from first two washing was collected for recovery of ILs (recovered BmimHSO$_4$ and BmimOAc) via distillation method. The ILs solution were first concentrated under vacuum by evaporating the water in a rotary evaporator, where the temperature of the water bath is 80 °C and subjected for 20 minutes. Subsequently, the recovered ILs were dried in a vacuum freeze-dryer for 24 hours under the temperature of -40 °C. The recovered ILs were characterized by FTIR to determine any changes to the chemical groups. The recovery yield of ILs is given on Equation 3.1.

$$\text{Recovery yield (\%)} = \frac{Mass\ of\ recover\ IL}{Original\ mass\ of\ IL} \times 100\% \qquad \text{(Equation 3.1)}$$

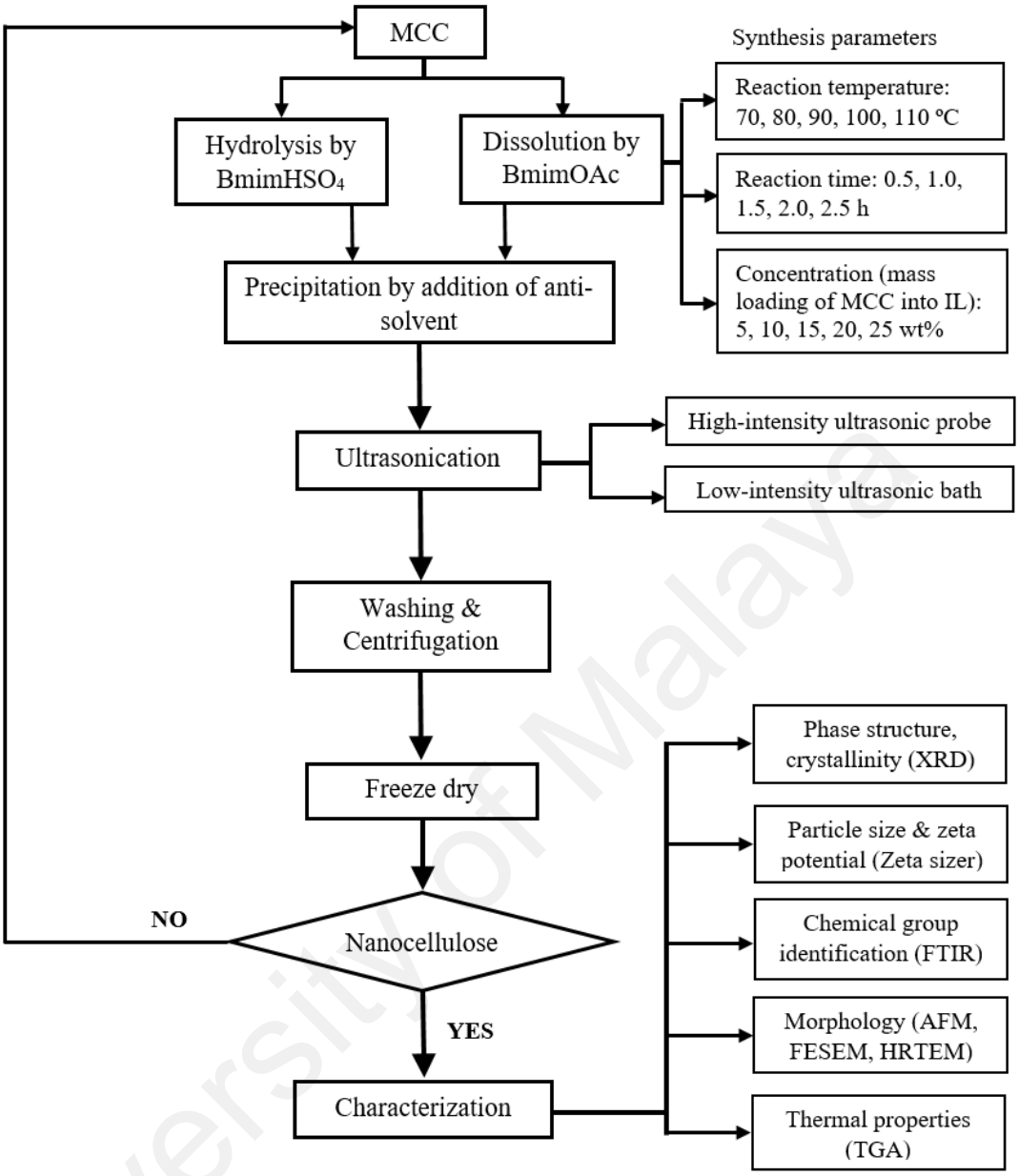

Figure 3.1: Overview flow chart for nanocellulose synthesis methodology.

3.4 Characterization Techniques

All the synthesized nanocellulose samples were characterized accordingly. The structural, morphological, size, chemical and thermal properties of synthesized nanocellulose and pristine MCC were examined and investigated using various characterization techniques. The structural and crystallinity of nanocellulose were characterized by X-ray Diffractometer (XRD). Zeta Sizer was used to measure the hydrodynamic particles size and zeta-potential of the nanocellulose. While Fourier Transform Infrared Spectroscopy (FTIR) was used to identify chemical functional groups

and track any chemical changes. The morphology was characterized using Atomic Force Microscope (AFM), Field Emission Scanning Electron Microscopy (FESEM) and High-resolution Transmission Electron Microscope (HRTEM). Thermogravimetric analysis (TGA) was used to characterize the thermal properties of nanocellulose. In this section, basic principles and information regarding the parameters set for the characterization techniques were discussed briefly.

3.4.1 X-ray diffraction (XRD)

The crystallographic phase structure and crystallinity index of nanocellulose were investigated by X-ray diffraction (XRD) analysis. The fundamental principle of XRD is based on constructive interference of monochromatic X-rays radiation that directed toward a crystalline material. The interaction of the incident rays with the sample produces diffraction patterns or constructive interference. This conditions required to satisfy Bragg's Law ($n\lambda=2d \sin\theta$) where it provides the lattice spacing (or d-spacing) of a crystalline material by relates the wavelength of electromagnetic radiation to the angles of diffraction rays. By exposing the material to radiation that scan at a range of 2θ angles, the diffracted X-rays are detected and all possible diffraction directions of lattice should be attained due to the random orientation of the crystalline material. The diffraction peaks and patterns can be indexed to provide information regarding the phase structure of the material. Typically, identification and evaluation of phase structure of sample is achieved by comparison of obtained XRD diffraction patterns with standard reference patterns from International Centre for Diffraction Data (ICDD) database.

XRD patterns of pristine MCC and nanocellulose were analysed by Bruker D8 Advance X-ray Diffractometer equipped with Ni-filtered monochromatic Cu Kα radiation (λ= 1.5418 Å). The operating voltage was 40 kV and the current was 40 mA. The

intensities were carried out in the range of 5 to 60º with a step size of 0.02º and a rate of 1º min^{-1}.

The crystallinity index (CrI) of each sample was determined by referring to diffraction intensity of crystalline and amorphous regions by using Segal's method (Equation 3.2).

$$\mathrm{CrI} = \frac{I_{200} - I_{am}}{I_{200}} \quad \text{(Equation 3.2)}$$

where I_{200} is the maximum intensity of (200) lattice diffraction, representing the crystalline component whereas I_{am} is the intensity of the baseline at $2\theta = 18º$, representing the amorphous part of cellulose.

The crystallite size of each sample perpendicular to (200) planes, *D* (nm), was calculated by using Debye Scherrer's equation (Equation 3.3).

$$D = \frac{K\lambda}{\beta \cos\theta} \quad \text{(Equation 3.3)}$$

where D is the mean diameter of ordered domains, K is the correction factor (0.94), λ is the wavelength of X-ray radiation (0.154 nm), β is the corrected angular width in radians at half maximum intensity of the (200) peak and θ is the Bragg angle.

3.4.2 Zeta sizer

Particle size distribution and zeta potential of samples were analyzed by Malvern Zetasizer Nano ZS. Particle size distribution is determined based on principle of dynamic light scattering (DLS). A laser beam caused illumination of the sample and subsequently the resultant fluctuations of the scattered light at a known scattering angle were detected by a fast photon detector. The Brownian motion of particles was measured by DLS and the mean diameter of particles was calculated via the Stokes-Einstein equation (Equation 3.4). The particle size that measured is the diameter of the spherical particles diffused

instantaneously as particles being measured. On the other hand, the zeta potential of cellulosic samples was measured by principle of electrophoretic light scattering (ELS). The electrophoretic mobility of each nanocellulose suspension was identified using Huckel approximation for the zeta potential.

$$D = \frac{k_B T}{6 \pi \eta r} \quad \text{(Equation 3.4)}$$

where D is the diffusion constant, k_B is Boltzmann's constant, T is the absolute temperature, η is the dynamic viscosity and r is the radius of the spherical particle.

In the present study, number-based particle size distribution (PSD), polydispersity index (PDI) and zeta potential of nanocellulose were determined. Nanocellulose suspensions were prepared at concentration of 0.05 wt% in DI water and subject to sonication for 30 minutes prior to measurement in order to ensure well dispersibility of the particles in DI water. The measurement was carried out at temperature of 25 ° C with detection angle of 173°. Water was used as dispersant in this study. The measurements were carried out in triplicate for each sample and the average values were reported.

3.4.3 Fourier transform infrared spectroscopy (FTIR)

FTIR spectroscopy is a powerful characterization technique to provide information on the chemical composition of the sample by identifies the functional group present within molecules. It is based on the principle that absorption of light energy by most molecules in the infrared region of electromagnetic spectrum is corresponds specifically to the bonds present in the molecules. Each bond has characteristic vibration frequency to indicate the presence of particular chemical bonds and functional groups specific to the molecules. The infrared spectrum is displayed as the intensity of light transmitted through the sample measured against the wavenumber. FTIR is particularly indispensable for identification of organic molecular structure and compounds.

The changes in chemical structure were analysed by Fourier transform infrared spectroscopy (FTIR). The FTIR spectra for cellulosic sample were recorded on a FTIR spectrometer (Bruker-IFS 66) in the transmittance mode over the range of 4000 to 400 cm^{-1} with a resolution of 4 cm^{-1}. The samples were prepared using KBr disk method in which the weight ratio of samples to KBr was 1:100. About 2 mg of the dried cellulosic samples were ground into powder by a fiber microtome, and then blended with KBr powder before pressing into ultra-thin pellets. The pellets were then placed in FTIR specimen holder for analysis and IR radiation was passed through it. The intensity of transmittance due to IR radiation was collected as FTIR spectrum.

3.4.4 Field emission scanning electron microscopy (FESEM)

Field emission scanning electron microscopy (FESEM) is a non-destructive technique that commonly used to visualize morphology and topography details on the surface of a sample. The working principle of FESEM is relies on the liberation of electrons from a field emission source and electrons are passed through a vacuum column under a high electrical field gradient to focus on the surface of specimen. Deflection of primary electrons by electronic lenses focused them to generate a narrow scan beam that bombards the specimen. Consequently, the angle and velocity of secondary electrons attributed to the interactions with specimen provide the information relate to the surface structure of sample which then generates signals to be detected as sample image. The signals are processed to produce SE or BSE images due to generation of electron beams including secondary electrons (SE), backscattered electrons (BSE) and X-rays that scanned across the surface of sample. FESEM is particularly useful to provide a great depth of field to visualize the surface structure of a sample.

In this research, the surface morphology of nanocellulose was examined by FESEM (JEOL JSM 7600-F) operated at an accelerating voltage of 5 kV and magnifications of 2,

15 and 50 kX were typically used for characterization. Prior to imaging, the freeze-dried nanocellulose was mounted onto metal stubs with double sided electrically conductive carbon tape and sputter coated with gold to prevent surface charging when exposed to the electron beam.

3.4.5 Atomic force microscope (AFM)

In atomic force microscopy (AFM), a cantilever with a very sharp tip is equipped to scan across the surface of the sample. It is able to measure microscopic surface morphology and topography as well as to construct a 3-D image of the surface. When the tip scans over a surface, interatomic forces between the tip and the surface induce the displacement of the tip and deflection of cantilever towards the surface. As the cantilever is lower to the surface which makes the tip makes contact with it, the repulsive force caused the deflection of cantilever away from the surface. A laser beam is used to detect orientation of cantilever by allowed it to transmit to and reflect from the cantilever. A position-sensitive photo diode (PSPD) detector is used to track the changes on the reflected laser beam and deflection of the cantilever. Thus, AFM can provides a topographical image of the sample surface by scanning the cantilever over a region of interest. AFM is a less intrusive surface morphological and topographical microscopic technique where it produces quantitative and 3-D images with high resolution range from a few microns to below 10 Angstroms.

The morphology of nanocellulose was visualized by AFM (Bruker Multimode 8) using silicon cantilevers. A 0.005 wt% concentration of nanocellulose suspension in water was prepared and allowed to sonicate for 10 minutes in order to ensure uniform dispersion of nanocellulose. Before observation, a drop of the diluted nanocellulose suspension was deposited on a freshly cleaved mica and allowed to dry for overnight at ambient condition. The mica substrate was then glued onto a metal disk and attached to a magnetic sample

holder placed on the top of the scanner tube. The images were scanned with contact mode in air at ambient conditions using silicon probes. The cantilever has a tip radius of 5 nm, spring constant of 42 N/m and resonance frequency of 320 kHz. The scan rate for images was 0.5 Hz and images resolution was 512 x 512 pixels. No image processing except flattening was made. The morphology and size of nanocellulose were examined by NanoScope Analysis 1.5 software provided by Bruker Company. The diameter of nanocellulose was then plotted as in histogram for numerical diameter distribution after measurement of 100 randomly selected nanocellulose.

3.4.6 High resolution transmission electron microscope (HRTEM)

Transmission electron microscopy (TEM) is an advanced microscopic technique to visualize the sample material by using beam of high energy electrons (up to 300 kV accelerating voltage). In TEM, beam of high velocity electrons are liberated from the electron gun and accelerated under vacuum to focus the coherent beam onto the specimen by condenser lens. The beam strikes the specimen while parts of it are transmitted and focused by objective lens to enlarge and project into the image on phosphor screen or captured by charge coupled device (CCD) camera. The images obtained is usually the highly magnified view of the nano- and microstructure and present in high resolution mode ultimately.

High resolution transmission electron miscroscope (HRTEM) is one of the important tool for the morphological characterization of nanomaterials. The morphology and dimension of nanocellulose were assessed using a HRTEM (JEOL JEM-2100F) operated at 200 kV accelerating voltage with insertion of a GATAN camera. Prior to observation, a drop of diluted suspension (0.002 wt%) of nanocellulose was loaded on a glow-discharged carbon-coated copper grid (300-mesh, formvar-carbon, Ted Pella Inc). The excess liquid was blotted with a filter paper and the grid was allowed to dry at ambient

temperature. The length and width or diameter of nanocellulose were measured using Image J version 1.48 (National Institutes of Health, USA) and the results were reported as the mean value of the data.

3.4.7 Thermogravimetric analysis (TGA)

Thermogravimetric analysis (TGA) is practically used to determine the thermal stability of a material by measuring variation of mass with respect to temperature under a controlled atmosphere. The basic principle of TGA is to determine changes of mass profile when the sample is gradually heated in a furnace. The mass changes can used to infer thermal stability of a sample or determine the composition of a material. Mass loss is typical for thermal event and can be ascribed to evaporation, reduction, decomposition or loss of volatile component. Other than that, a sample can retain or gain weight due to oxidation or absorption. TGA can tracks the mass changes of the sample via a micro-thermobalance. The plot of weight percentage of sample against temperature or time is depicted as a thermogram to understand thermal transition behavior of the material.

TGA was carried out using Mettler Toledo (TGA/SDTA 851) in order to evaluate the thermal stability of the cellulosic samples. Approximately 4 mg of each sample was heated from room temperature to 600 °C at a heating rate of 10 °C/min. All measurements were performed under a nitrogen atmosphere with a gas flow of 20 mL/min in order to prevent any premature thermo-oxidative degradation and also fast pyrolysis of cellulosic materials. The curve of percentage of weight loss against the temperature was plotted as a thermogram. Derivative TG (DTG) curves expressed the weight-loss rate as a function of time.

CHAPTER 4: RESULTS AND DISCUSSION

4.1 Introduction

This chapter presents the results obtained from the characterization of synthesized nanocellulose and the discussion of the analysis. There are two main sections in this chapter where the first section presents the results and data analysis regarding to the formation of nanocrystalline cellulose (NCC) by using Bronsted acidic IL (1-butyl-3-methylimidazolium hydrogen sulfate, $BmimHSO_4$). While the second section demonstrates the results and data analysis of regenerated cellulose nanoparticles (CNPs) with 1-butyl-3-methylimidazolium acetate (BmimOAc). The influence of synthesis parameters such as reaction temperature and time, cellulose concentration (mass loading of MCC) as well as ultrasonication conditions are evaluated in detail on the formation and properties of the synthesized nanocellulose. This study aims to optimize the synthesis conditions such that highly crystalline nanocellulose with small size can be formed by utilizing IL.

4.2 Synthesis of Nanocrystalline Cellulose (NCC) by $BmimHSO_4$

4.2.1 Mechanism of NCC Synthesis with $BmimHSO_4$

In the current section, the preparation of nanocrystalline cellulose (NCC) was conducted with heat treatment with $BmimHSO_4$. The process involves is a thermochemical process, followed by mechanical treatment to ensure uniform dispersion of NCC. The heat treatment is essentially to increase the rate of catalytic reaction (hydrolysis) in $BmimHSO_4$. Also, it is important to lower the viscosity of IL so that the ions of IL could gained sufficient energy to promote the mobility as well as diffusion of the ions into cellulose matrix for interaction. It is suggested that the temperature and time of hydrolysis reaction as well as cellulose concentration (mass loading of MCC into IL) are the main factors that strongly influenced the properties and dimensions of the synthesized NCC. Therefore, the effects of these parameters will be discussed in details

within this chapter. The proposed mechanism of formation of NCC with $BmimHSO_4$ is discussed as below.

Acid hydrolysis is a frequently used method for the production of cellulose nanocrystals (CNCs) or NCC. Instead of using concentrated sulfuric acid, acidic $BmimHSO_4$ is adopted as catalyst for cellulose hydrolysis in the present study owing to the more advantageous properties of IL. Nevertheless, the hydrolysis of MCC by $BmimHSO_4$ is found to have some similarity with the working principle of acid hydrolysis method (Man et al., 2011). In this context, $BmimHSO_4$ is found to behave like an acid in acid hydrolysis during its interaction with MCC. $BmimHSO_4$ is a Bronsted acidic IL because its $[HSO_4]^-$ anions have a low pKa value of 2 in water. Besides that, the acid to anhydroglucose molar ratio ($[H^+]$/[AGU]) is 0.24 mol/mol within the acidic environment (pH 1) of $BmimHSO_4$. In contrast to strong acid hydrolysis (i.e. concentrated sulfuric acid hydrolysis), $BmimHSO_4$ mediated hydrolysis route has 2 to 3 lower magnitude orders. This indicates $BmimHSO_4$ enables a more efficient hydrolysis reaction in a mild acidic condition (Mao et al., 2013).

In light of these, $BmimHSO_4$ is suggested to distinctively perform dual functions by initiating swelling of cellulose, and followed by catalysing the hydrolytic cleavage of β-glycosidic linkages. This means that $BmimHSO_4$ functions as both the solvent and catalyst for cellulose hydrolysis (Tian et al., 2014). Despite that, it is able to be recovered, recycled and eventually be reused after the reaction. In the present study, the yield of $BmimHSO_4$ recovered is about 90 % after removing excess water through evaporation and subsequent concentrating under vacuum. This provides a green and environmental friendly approach as compared to traditional strong acid hydrolysis because IL is highly recoverable and recyclable as well as no discharge of any toxic or hazardous waste products.

$BmimHSO_4$ has intrinsically acidic character (pH 1) in which its acidity comes from the hydrogen of $[HSO_4]^-$ which has a pKa value of about 2 in water (To, 2012). It is expected that higher acidity of $BmimHSO_4$ is induced at elevated temperatures. Interestingly, dissociation of ion pairs of $BmimHSO_4$ into individual $[Bmim]^+$ cations and $[HSO_4]^-$ anions is promoted at higher temperatures (Jin, Wang, Wang, & Zhao, 2012). In the meantime, formation of electron donor-electron acceptor (EDA) complexes is favoured due to the interaction between charged species of $BmimHSO_4$ and cellulose molecules. The charged species are then diffused into intermolecular space between the cellulose chains, causing them to swell. $BmimHSO_4$ significantly altered and broke the inter and intramolecular hydrogen bonding within cellulose and gradually exposed the hydroxyl groups (Han et al., 2013; Kosan et al., 2008; Pinkert et al., 2009). As a consequence, cellulose swelled as the interval between macromolecular chains of cellulose is increased. This indicates that $BmimHSO_4$ could swell cellulose and could destroy the hydrogen bonding as well as cause the space between the stacked sheets of cellulose molecules to increase (Han et al., 2013; Man et al., 2011). The diffusion of $[HSO_4]^-$ into the cellular matrix is facilitated and the presence of higher density of $[HSO_4]^-$ caused the environment inside the cellulose to become more acidic and favourable for hydrolysis (Tian et al., 2014).

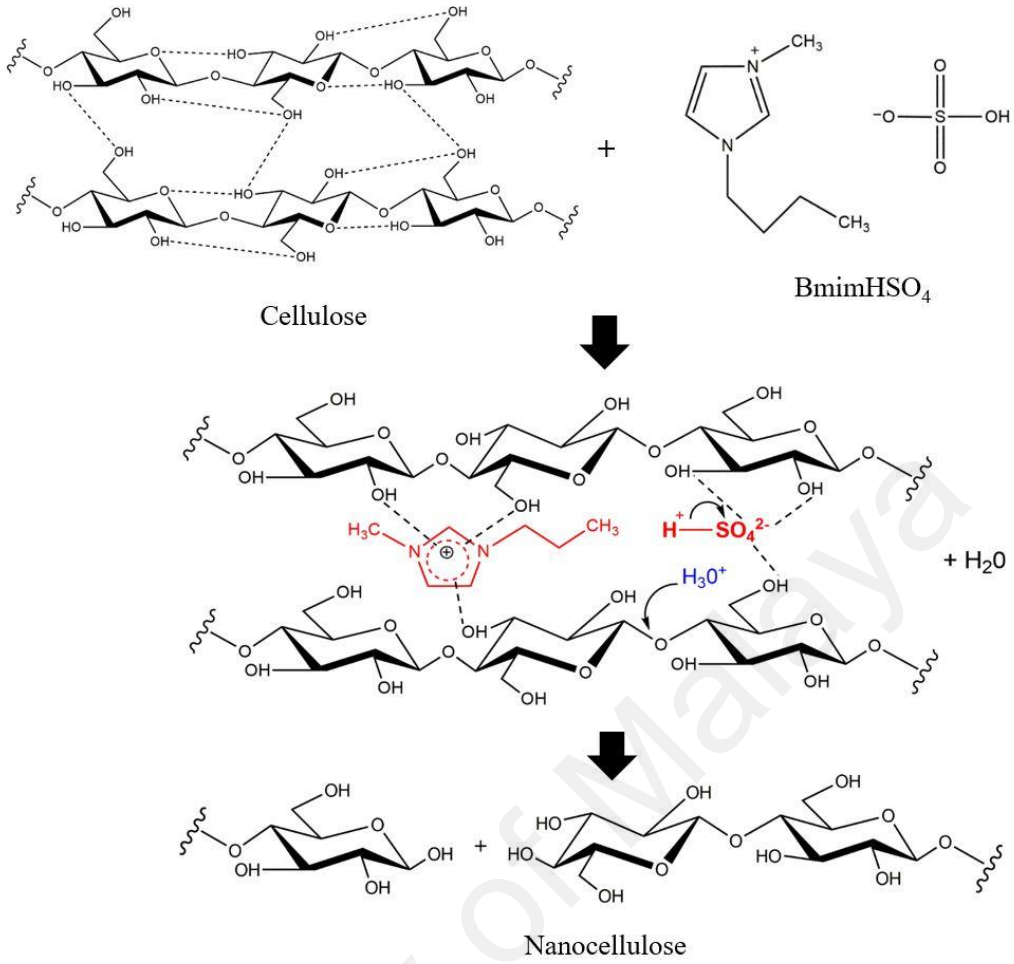

Figure 4.1: Proposed mechanism on formation of NCC by $BmimHSO_4$ mediated hydrolysis.

$BmimHSO_4$ is a poor solvent for cellulose, yet it can be a good swelling agent. On top of that, the mild or moderate acidic character of its $[HSO_4]^-$ anions can essentially initiates cellulose hydrolysis (Mao, Heck, Reiter, & Laborie, 2015). Therefore, $BmimHSO_4$ mediated hydrolysis of cellulose is a heterogeneous process. Initially, the process involves diffusion of $[HSO_4]^-$ anions into the cellulose fibers, and subsequently catalyzes the cleavage of glycosidic bonds (Mao et al., 2013). Due to the hygroscopic character of IL, water is usually retained in IL as impurities. It is suggested that presence of small amount of water in $BmimHSO_4$ (~3.1 to 4% (w/w)) likely sufficient to trigger the release of protons $[H^+]$ from the IL to allow the hydrolysis reaction (Abushammala, Krossing, & Laborie, 2015; Mao et al., 2015). Apart from that, the intrinsic acidic character of $BmimHSO_4$ caused the mixture to have acidic condition of pH 1 (To, 2012). As

mentioned previously, the acidity is attributed to the hydrogen of $[HSO_4]^-$ and have a pKa of 2. Theoretically, pKa value greater than 0 indicates a weak acid. Thus, $[HSO_4]^-$ is a weaker acid than sulfuric acid (pKa -3) and will only partially dissociated into hydronium ions $[H_3O]^+$ and sulfate anions $[SO_4]^{2-}$.The acidity is attributed to the electronegative oxygens in drawing the electron density away from the hydrogen atom that is bonded to one of the oxygens. Therefore, hydrogen are more partially positive and more reactive (Tian et al., 2014). A small fractions of protons $[H^+]$ that dissociated from the $[HSO_4]^-$ are suggested to react with water molecules in the aqueous solution to facilitate the formation of hydronium ions. As a consequence, most protons exist in the form of hydronium ions in the system. The highly reactive hydronium ions are important to further catalyze the hydrolytic cleavage of glycosidic bonds by causing the protonation of glycosidic oxygen that consequently induced splitting of glycosidic bonds and resulted in the release of shorter fragments of cellulose chains as NCC. Thus, hydrolysis of cellulose is effectively catalyzed by Bronsted acid IL in the presence of trace amount of water (Abushammala et al., 2015).

Protonation of glycosidic oxygen induced by hydronium ions initiated cellulose hydrolysis and subsequently lead to splitting of glycosidic bonds. The hydrolytic cleavage of glycosidic bonds between two anhydroglucose units results in the rearrangement of interlinking chain ends, which rendered the release of internal strain (Man et al., 2011). In native cellulose, amorphous regions have greater accessibility for $[HSO_4]^-$ and, therefore, are more susceptible to hydrolytic cleavage than the crystalline region (Shimada, Takahashi, Hon, & Shiraishi, 1991). The amorphous regions are hydrolyzed at a much faster rate due to their disordered structure and consist of weak van der Waals forces. On contrary, a much slower rate for the reducing end and surface of residual crystalline domains because they have stronger and ordered structure (Mao et al., 2013; Millet, Moore, & Saeman, 1954). In other words, the crystalline regions are recalcitrant

to hydrolysis than the amorphous parts because of their intricate network of strong hydrogen bonding. Consequently, the amorphous regions were selectively hydrolyzed and dissolved in $BmimHSO_4$ and leaving the crystalline regions remained intact in NCC (Lu & Hsieh, 2010). However, controllable hydrolysis conditions is required in order to prevent over degradation or complete hydrolysis of cellulose to its molecular units such as glucose. In addition, mechanical treatment such as ultrasonication after the hydrolysis reaction is essential to ensure the NCC was uniformly dispersed in the suspension and also, to disintegrate the bulk cellulose aggregates into smaller dimensions with uniform size distribution (Maiti et al., 2013; Man et al., 2011). Mechanical agitation is also important to avoid the possible formation of aggregation and agglomeration of cellulose crystallites.

In addition to chain scission, esterification of hydroxyl groups due to the $[HSO_4]^-$ also occurred during the cellulose hydrolysis catalyzed by $BmimHSO_4$. The sulfate groups were introduced along the surface of the cellulose crystallites which eventually imparted a negative charge on the surface of NCC. This anionic stabilization via the electrostatic repulsion forces of electrical double layers were able to effectively prevent the aggregation of NCC driven by hydrogen bonding which accounted for the stability of the colloidal suspension. Hydrogen bonding formed between the hydroxyl groups and greater surface area of smaller NCC particles with high surface energy contributed to the aggregation of NCC (Marchessault, Morehead & Koch, 1961; Lu & Hsieh, 2010).

After the hydrolysis and mechanical agitation process, regeneration of cellulose from the cellulose/$[BmimHSO_4]$ suspension is possible with the addition of water as the anti-solvent. Rapid mixing of water (a polar solvent) with cellulose in IL leads to the precipitation of cellulose as powdery flocks. Hydrogen bonding properties are mainly involves in the reconstruction of cellulose within the cellulose/water/$BmimHSO_4$ system

(Swatloski et al., 2002). $BmimHSO_4$ has strong water absorbability due to its preference to form hydrogen bonding with water molecules as O-H bonding has higher electronegativity and therefore, is much stronger than the corresponding C-H type hydrogen bonds (Ding et al., 2012). The bonding between cellulose and $BmimHSO_4$ is then weakened due to the fast addition of water. Reconnection of hydrogen bonding between cellulose chains during the regeneration process resulted in the reconstitution and precipitation of highly ordered or crystalline structure of cellulose (Han et al., 2013).

In summary, $BmimHSO_4$ is a Bronsted acidic IL which can performs dual function of swelling and catalyzing cellulose hydrolysis. Therefore, the NCC produced by $BmimHSO_4$ mediated hydrolysis exhibit higher crystallinity and smaller size. Overall, this synthesis route provided by $BmimHSO_4$ offers a promising alternative to the utilization of concentrated acid approach due to its more advantageous properties in terms of higher yield and quality of NCC formed, recovery of IL and less toxic. This is an environmental friendly approach in which the IL is recoverable and recyclable without any hazardous waste products are being produced.

4.2.2 X-ray Diffraction Analysis

XRD analysis is conducted to determine the changes in crystallinity and crystallite size of untreated MCC and NCC prepared by $BmimHSO_4$. The crystallinity and crystallite size of NCC are analysed based on Segal's formula and Scherrer's equation, respectively and are summarized in Table 4.1. Figure 4.2 shows the XRD patterns of pristine MCC and NCC that are synthesized with $BmimHSO_4$ at different synthesis conditions. As illustrated in the Figure, NCC exhibit similar diffraction peaks as MCC at $2\theta = 14.7^{\circ}$, 16.5°, 22.5° and a small peak at 34.5° corresponding to the (-110), (110), (200) and (040) crystallographic planes of typical cellulose *I* structure respectively. These characteristic peaks are attributed to the monoclinic crystalline cellulose I_{β} structure which consists of

repeating units of β-D-glucopyranose units joined together via strong intermolecular hydrogen bonding (Lu et al., 2015). Crystalline cellulose *I* structure is preserved in the synthesized NCC. During the hydrolysis catalyzed by $BmimHSO_4$, cellulose amorphous regions were selectively hydrolyzed and removed in IL. This resulted in the release of internal strain as cellulose crystalline domains in which the crystallinity was retained or improved. The crystalline structure was preserved as crystalline regions were predominantly retained in NCC whereas the amorphous regions were removed and dissolved in IL. Thereafter, the amorphous contents of NCC were significantly lowered and yield in the production of highly crystalline structure of NCC.

The crystallinity index (CrI) of NCC is notably affected by hydrolysis temperature, time, cellulose concentrations as well as ultrasonication conditions. A relatively ordered structure with strong and resolve peak at position 22.5º (200) corresponds to the crystallinity peak, and the CrI can be determined based on the intensity of this peak. A sharper diffraction peak at 22.5º (200) indicates higher crystallinity and thus, higher CrI.

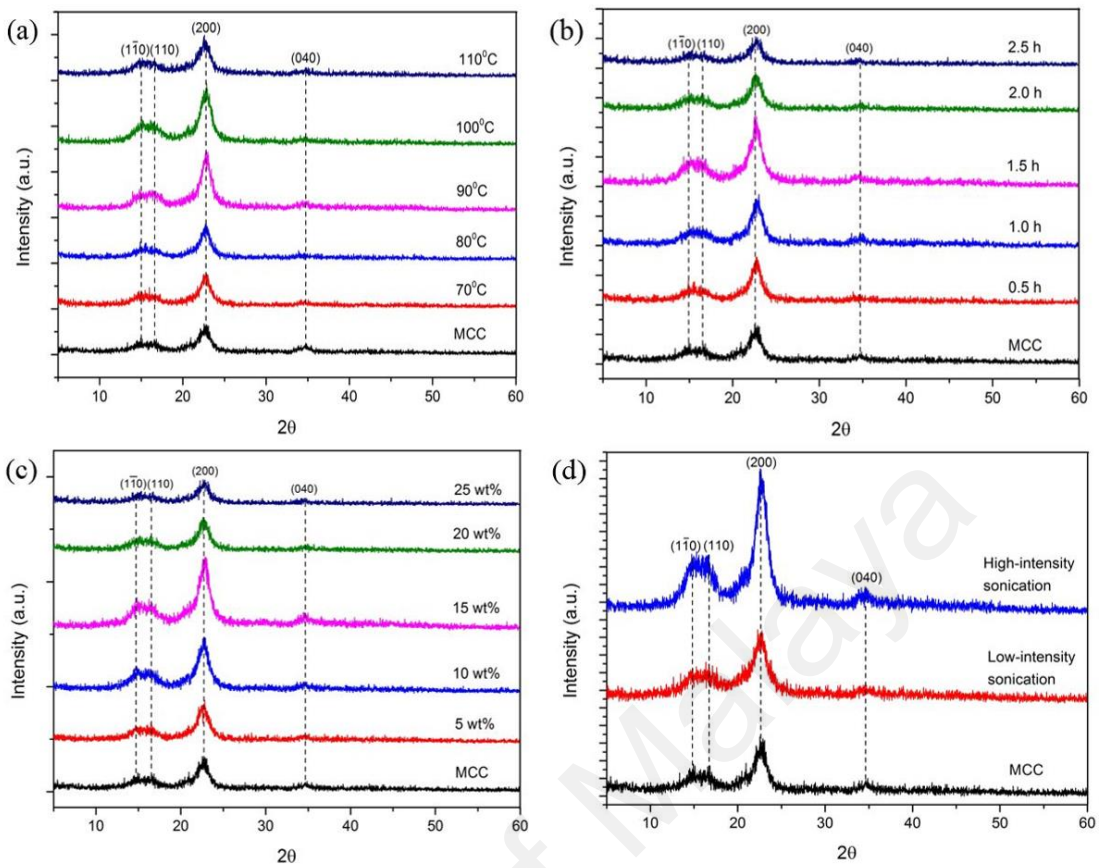

Figure 4.2: XRD patterns of MCC and NCC optimized with different parameters (a) temperature, (b) time, (c) cellulose concentration (mass loading of MCC), and (d) ultrasonication conditions.

The peak positioned at 22.5º corresponds to the (200) crystalline plane of NCC become sharper as illustrated in Figure 4.2 which indicates higher perfection of the crystal lattice in (200) plane in NCC than the pristine MCC. The peak at 14.7º become more intense and is separated from the peak at 16.5º indicates a more compact and ordered crystalline structure (Lu et al., 2014).

Table 4.1: Crystallinity index and crystallite size of NCC.

Sample	Crystallinity index, CrI (%)	Crystallite size, D_{XRD} (nm)
MCC	78.0	25.3
a) Temperature (ºC)		
70	86.8	5.9
80	89.7	5.8
90	92.2	4.8
100	92.2	4.6
110	85.3	4.3
b) Time (hour)		
0.5	88.5	5.9
1.0	90.1	5.3
1.5	92.2	4.8
2.0	84.7	4.5
2.5	80.3	4.1
c) Percent mass loading of MCC (wt%)		
5	86.6	5.4
10	89.5	5.3
15	92.2	4.8
20	85.8	5.1
25	80.7	5.2
d) Sonication treatment		
Low-intensity sonication	83.4	4.5
High-intensity sonication	94.5	5.0

In general, reaction temperature is one of the important factors that influence the hydrolysis of cellulose and has notably affected the crystallinity of NCC. Based on Table 4.1, the crystallinity of NCC increased with temperature rising from 70 ºC to 90 ºC and reaches the highest CrI of 92.2 at 90 ºC and 100 ºC. Interestingly, it is noteworthy that the crystallinity of NCC synthesized by $BmimHSO_4$ is significantly higher in comparison to pristine MCC (78%). The relative increase in the crystallinity with increasing temperature is attributed to the increase in the dissociation of higher number of $[Bmim]^+$ cations and $[HSO_4]^-$ anions from $BmimHSO_4$ and caused the diffusion coefficient of $[H^+]$ to increase in the aqueous solution at higher temperature (Han et al., 2013). Subsequently, hydrolytic cleavage of glycosidic bonds is facilitated at elevated temperature and individual crystallites are then released (Li et al., 2009). The amorphous regions are selectively hydrolysed and removed as they are more susceptible to hydrolysis than the crystalline

counterparts. Therefore, higher crystallinity of NCC is obtained at high temperature hydrolysis reaction with $BmimHSO_4$ because the removal of amorphous parts essentially increased the crystallinity of NCC (Man et al., 2011).

On the other hand, crystallinity of NCC gradually decreased from 92.2 to 85.3 when heated beyond 100 ºC. This is presumably due to the hydrolysis of crystalline components taking place at higher temperature after the removal of amorphous fractions. In addition, excessive hydrolysis of cellulose into glucose monomers suggesting loss of NCC, and indirectly can lead to decrease in its crystallinity. This is further evidenced by the darkening of cellulose suspension due to dehydration and carbonization or the existence of some coloring matter arising from the glucose as temperature rose to 110 ºC, as illustrated in Figure 4.3 (Fan & Li, 2002; Lu, Gui, Zheng, & Liu, 2013). Moreover, the broadening of the crystalline peaks indicates the decrease in the crystallite size of NCC as the reaction temperature increased. Cellulose with loose structure is favorable for the changes in the crystallite size during hydrolysis. It has been suggested that the growth of the defective crystallites and degradation of smaller crystallites influenced the crystallite size during hydrolysis (Liu et al., 2013). Thus, smaller crystallite size NCC is formed at high temperature as the degradation of crystallites took place to a large extent during hydrolysis. At higher reaction temperature, the hydrolytic cleavage of glycosidic linkages catalyzed by IL took place extensively and performed at a higher rate. Consequently, this phenomenon induced the progressive reduction of cellulose crystallites and eventually degradation of crystalline domains that resulted in the production of smaller crystallite sizes of NCC at higher operating temperature. In summary, 90 ºC is selected to be the optimal reaction temperature owing to higher crystallinity of NCC produced and also to avoid excessive hydrolysis and possible degradation of cellulose, leading to lower NCC yield and lower crystallinity. Excessive hydrolysis can be essentially avoided by adopting a low-to-moderate reaction temperature for hydrolysis.

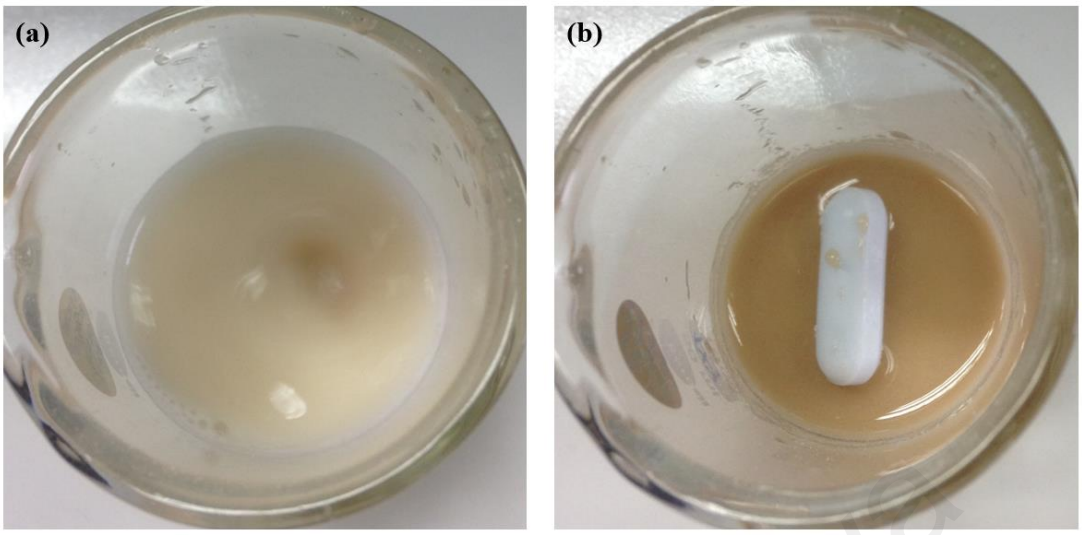

Figure 4.3: Observation of color of cellulose/BmimHSO$_4$ suspension during the reaction at (a) temperature below 100 °C and (b) temperature of 110 °C.

Reaction time is also one of the important parameters that essentially governed the crystallinity of NCC. Figure 4.2 (b) clearly shows the XRD patterns of NCC synthesized at different reaction time. It is worth noting that the intensity of (200) crystalline peaks become sharper and prominent when the reaction time is increased from 0.5 to 1.5 hours. Apparent broadening and weakening of the crystalline peaks are observed when the reaction time is prolonged to 2.5 hours. This implies the crystallinity of NCC increased relatively with the reaction time from 0.5 to 1.5 hours. The highest crystallinity NCC is acquired at the optimal reaction time of 1.5 hours. However, crystallinity of NCC is decline significantly when hydrolyzed for more than 1.5 hours. When the reaction time is too short (0.5 hours), cellulose is not able to hydrolyze effectively, provided that only a small number of cellulose is being hydrolyzed. Hydrolysis of amorphous cellulose and isolation of NCC took place at a much lower rate which resulted in the lower crystallinity of NCC. In general, longer time can promote hydrolysis of cellulose more extensively. The diffusion of $[HSO_4]^-$ anions into the cellulose fibers increased with time and subsequently breakdown the glycosidic bonds to release the internal strain. This in turns, leads to the production of NCC with higher crystallinity because the amorphous regions were selectively hydrolyzed.

Amorphous regions are first and more easily decomposed than crystalline domains because they consist of disordered microstructure and therefore, more susceptible to hydrolysis reaction. However, prolonged exposure to hydrolysis can further improved the cellulose hydrolysis which resulted in significant reduction in the crystallinity of NCC. The lower crystallinity is attributed to the crystalline domains are increasingly subject to extensive hydrolysis, and thus NCC is partly destroyed. The crystalline domain of cellulose is gradually hydrolyzed and eventually degrade into glucose monomers after prolonged hydrolysis treatment (Ahmadi et al., 2015; Fan & Li, 2012). Besides that, crystallite size of NCC is decreased relatively with increasing reaction time. The crystallite size is larger at short hydrolysis time (0.5 hour) which presumably is attributed to the growth of defective crystallites during regeneration process. The size reduction of crystallites was resulted from the excessive hydrolysis and eventually, the degradation of the crystalline domains due to the prolonged exposure to hydrolysis. As a consequence, the crystalline domains are increasingly subjected to hydrolytic cleavage and resulted in the formation of smaller cellulose crystallites with lower crystallinity contents. Therefore, 1.5 hours of reaction time is chosen as the optimization of synthesis conditions.

Based on Table 4.1, cellulose concentrations (expressed in mass loading of MCC into IL) also significantly influenced the crystallinity of NCC. Crystallinity of NCC increased from 86.6 to 92.2 when the mass loading of MCC increased from 5 to 15 wt% and the highest crystallinity is obtained at 15 wt%. The crystallinity declines drastically with the further increase in the concentration of MCC beyond 15 wt%. The initial increase in the crystallinity of NCC is attributed to the increase in the diffusion of $[HSO_4]^-$ anions into the cellulose fibers. The increase in the catalytic activity of $BmimHSO_4$ caused the hydrolytic cleavage of glycosidic bonds as there are greater number of $BmimHSO_4$ molecules present in the system. Additionally, better solvating and catalytic power of $BmimHSO_4$ are suggested at lower cellulose concentrations. Lower cellulose

concentration implies the presence of higher concentrations of IL within the system. In this context, the proportionate higher concentration of IL signifies the existence of greater amount of ions of IL which able to acquire higher mobility to diffuse into the cellulose polymer chains to initiate the hydrolysis and solvation of cellulose. Hence, BmimHSO4 is capable to perform dual functions of catalyzing and dissolution effectively at lower cellulose concentration state.

On the other hand, gradual reduction of crystallinity is mainly due to the weakening of the catalytic as well as solvation ability of $BmimHSO_4$ with increasing cellulose concentration. Besides that, the number of $BmimHSO_4$ molecules present in the system is much lower with respect to increasing cellulose concentrations which slow down the diffusion of anions into the fibers. Consequently, the hydrolysis reaction took place at a lower rate that essentially lead to lower crystallinity. This implies that $BmimHSO_4$ is in supersaturation state such that increasing cellulose concentration most likely slow down or halted the hydrolysis reaction (Sun, Chen, Jiang, & Lynch, 2015).

Moreover, when the cellulose concentration is beyond the optimum concentration (> 15 wt% of MCC), apparent lower crystallinity in NCC has been observed because some portion of MCC cannot dissolve completely in $BmimHSO_4$ and become critical for the hydrolysis (Lu et al., 2013). The viscosity of cellulose/$BmimHSO_4$ suspension is increased apparently with relatively higher cellulose concentrations. The viscous suspension renders difficulty to the stirring process as well as effective mixing of cellulose with $BmimHSO_4$. As a consequence, hydrolysis of cellulose is seriously impacted. The dimensions of the crystals related to the (200) plane is increased probably attributed to the recrystallization of the amorphous regions in the border of the crystalline regions of NCC (Nascimento et al., 2014). It is also suggested that the nucleation and growth of crystallite is accelerated due to supersaturation effect (Sun et al., 2015). In

summary, lower cellulose concentration favored the hydrolysis and beneficial to the production of highly crystalline NCC.

The crystallinity of NCC produced with low-intensity ultrasonic bath and high-intensity ultrasonic probe are 83.4% and 94.5%, respectively. This signifies that high-intensity ultrasonication produced higher crystallinity NCC due to stronger cavitation effect. High-intensity ultrasonication allows the formation, growth and collapse of the cavitation bubbles took place instantaneously (*in-situ*) and more intense in aqueous solution because the ultrasonic probe is immersed directly into the cellulose suspension. As a consequence, a greater intensity of cavitation and higher amplitude of vibrational energy are generated (Hamid, Zain, Das & Centi, 2016). However, weaker cavitation effect is produced by ultrasonic bath as the suspension is inserted into the water bath and thereby, generating lower vibrational energy. The resulting ultrasound energy is transferred to the cellulose chains through cavitation process. Consequently, the mechanical shearing forces of higher intensity due to the collapse of the cavitation bubbles generally break down the interaction forces that hold the cellulose microfibrils after hydrolysis, which in turns facilitated the disintegration of cellulosic fibres into nanofibers. In addition, it is suggested that greater cavitation effect due to high-intensity ultrasonication selectively damaged the amorphous and defective crystalline regions (Guo, Guo, Wang & Yin, 2016). Crystallinity enhancement for NCC with high-intensity ultrasonication is more profound as the (200) crystalline peaks become sharper and more resolve. This indicates the formation of a more compact and ordered crystalline structure NCC with higher crystal lattice perfection is successful with the utilization of high-intensity ultrasonication. Therefore, it can be concluded that high-intensity ultrasonication shows more favorable effect on crystallinity enhancement as well as beneficial to the isolation of NCC following hydrolysis.

Apart from that, high-intensity ultrasonication give rise to the formation of slightly bigger cellulose crystallites because the treatment promotes the growth of the crystallites and meanwhile, enhanced the crystallinity of NCC. On the contrary, low-intensity sonication was less effectively in promoting the crystallites growth after the hydrolysis process. Hence, the crystallites were comparably smaller due to the less profound vibrational forces generated by the cavitation.

Overall, it is confirmed that $BmimHSO_4$-mediated hydrolysis predominantly liberates cellulose *I* structure with higher crystallinity than the precursor materials under mildly acidic conditions. The synthesis conditions are optimized at 90 ºC for 1.5 hours with a cellulose concentration of 15 wt% MCC. The controllable synthesis conditions are essentially to avoid serious degradation of cellulose into sugar molecules and prolonged hydrolysis will be not productive. The hydrolysis conditions can be controlled through have a good monitoring and controllable parameters such as reaction temperature and time. Low operating temperature and moderate reaction time are adopted for efficient production of NCC through the hydrolysis process.

4.2.3 Hydrodynamic Size and Zeta Potential Analysis

Table 4.2 shows the hydrodynamic size, polydispersity index (PDI) and zeta potential measurement of NCC synthesized with different reaction parameters. It is clearly illustrated that synthesis parameters such as temperature, time, cellulose concentrations as well as ultrasonication conditions are influenced the hydrodynamic size of NCC. Apparently, the average hydrodynamic size of NCC is strongly dependent on the temperature and time of synthesis. Hydrodynamic size of NCC decrease relatively with increasing synthesis temperature and time. The size of NCC is decreased from 89.07 to 36.78 nm when the temperature is increased from 70 to 110 ºC. Meanwhile, drastic reduction of hydrodynamic size from 85.69 to 33.71 nm is observed as the reaction time

is increased from 0.5 to 2.5 hours. This signifies that large and poorly dispersed aggregation of NCC is formed with high polydispersity index (PDI) at low temperature and shorter time. In other words, higher temperature and longer reaction time essentially favored hydrolysis of cellulose by promoting the cleavage of glycosidic bonds. Consequently, the size of NCC is diminished with more uniform size distribution. Hence, small size NCC can be dispersed well in water to acquire a stable colloidal suspension (Ahmadi et al., 2015).

Apart from that, cellulose concentration is also known to play a crucial role in cellulose hydrolysis. Cellulose concentration yield significant impacts on the uniformity of NCC particles. In this context, a lower cellulose concentration meaning a higher proportionate concentration of IL in the system. The ions of IL capable to acquire higher mobility and diffusion of ions into the cellulose matrix is performed at a higher rate due to the presence of higher concentration of ions of IL. As a consequence, higher number of ions of IL are able to surround and interact with the cellulose molecules for the hydrolysis reaction and consequently resulted in the formation of NCC with smaller dimensional size and enhanced uniformity. On contrary, higher cellulose concentration suggested that there are lower concentration of IL in the system. The scarcity of ions of IL caused the interaction between IL and cellulose less likely to be performed at an optimum rate. Therefore, some of the cellulose molecules were effectively hydrolyzed into smaller particles, while some part of it would retained bulk and aggregate sizes of NCC.

The hydrodynamic size of NCC obviously increased with increasing cellulose concentrations. Interestingly, the PDI values also increased gradually. This manifests that NCC formed under higher cellulose concentration have larger size with less uniformity due to the weakening of the catalytic as well as solvation ability of $BmimHSO_4$ at its supersaturation state. Eventually, $BmimHSO_4$ acquired a supersaturation state at the

highest cellulose concentration (25 wt% MCC). At this stage, $BmimHSO_4$ is very viscous and its catalytic and solvation properties are not distinctively well performed. Besides that, the cellulose/$BmimHSO_4$ suspension become more viscous with increasing cellulose concentrations. This condition becomes critical for hydrolysis where the process is slow down and incomplete hydrolysis is expected. This resulted in the formation of much bigger size NCC with less uniform size distribution. Thus, lower cellulose concentrations favour the hydrolysis of cellulose and contributed to the production of smaller size NCC.

Table 4.2: Hydrodynamic size, polydispersity index and zeta potential of NCC.

Sample	Hydrodynamic size (nm)	Polydispersity index, PDI	Zeta Potential (mV)
a) Temperature (ºC)			
70	89.07	0.362	-19.6
80	67.10	0.347	-20.5
90	45.89	0.264	-37.5
100	42.39	0.258	-37.9
110	36.78	0.234	-38.2
b) Time (hour)			
0.5	85.69	0.385	-28.6
1.0	65.99	0.361	-37.2
1.5	45.89	0.264	-37.5
2.0	37.54	0.256	-38.4
2.5	33.71	0.244	-39.3
c) Percent mass loading of MCC (wt%)			
5	34.15	0.162	-51.4
10	42.63	0.227	-46.2
15	45.89	0.264	-37.5
20	67.93	0.280	-31.4
25	87.64	0.315	-25.0
d) Sonication treatment			
Low-intensity sonication	54.27	0.342	-33.2
High-intensity sonication	45.06	0.248	-40.1

The current section discusses the effect of ultrasonication conditions on the hydrodynamic size of NCC. It is noteworthy that high-intensity ultrasonication produced smaller size NCC with more uniform size distribution as compared to low-intensity sonication. This is reasonably attributed to the effect of acoustic cavitation where the

highly intense ultrasound energy is transmitted to the cellulose chains and caused delamination to diminish the interaction forces between the cellulose chains (Guo et al., 2016). High vibrational energy and violent shock waves generated by ultrasonication consequently break down the glycosidic bonds and interlayer hydrogen bonding between cellulose polymer chains which resulted in the delamination of the adjoining cellulose chains for the liberation of smaller size NCC. In summary, high-intensity ultrasonication provides a more profound cavitation effect and thereby, effectively disintegrates cellulose aggregates into individual smaller size NCC (Guo et al., 2016; Lu et al., 2014). NCC is observed to disperse well in water and have uniform size distribution when high-intensity ultrasonication treatment is present. On the other hand, weak cavitation provided by low-intensity sonication only breaks the intermolecular and van der Waals forces between the cellulose chains and therefore, is not benign to the isolation of smaller size NCC. In contrast to high-intensity ultrasonication, low-intensity sonication tend to give rise to the formation of bigger particulates NCC with less uniform size distribution.

Therefore, it can be concluded that higher temperature, longer reaction time, lower cellulose concentrations as well as with the aid of high-intensity ultrasonication significantly resulted in the production of uniform and smaller size NCC. Nevertheless, the hydrodynamic radius of spherical particles dispersed in a solution is indicated based on dynamic-light scattering (DLS) technique adopted by zeta sizer. The approximate sizes of NCC can be revealed by DLS. Apart from that, DLS was used to measure the sizes of nanocellulose and acts as an indicator to compare the different size of NCC prepared by varied reaction parameters in order to obtain a clear illustration on the process.

In DLS, rod-like cellulosic fibres are always treated as spherical particles, which are clearly far from reality. The principle of DLS is based on the measurement of the scattered light intensity due to Brownian motion of particles in a solvent without an applied electric

field. Hence, the particle size evaluated likely to be larger than the real dimensions of particles and the sizes obtained from DLS are also likely to be deviated from those measured by image analysis such as TEM and AFM (Qua, Hornsby, Sharma & Lyons, 2011). In addition, DLS technique is more biased to larger particles because they are prone to mask the intensity of light scattered over the smaller particles. Hence, smaller particles are difficult to be detected by the particle size analyzer (Satyamurthy & Vigneshwaran, 2013). Furthermore, cellulose molecules are known to be highly hydrophilic and very likely to swell in water. These resulted in significantly larger size of NCC is measured with DLS technique of the zetasizer.

Zeta potential can be used to indicate the stability of a colloidal suspension. Basically, it is derived from the measurement on mobility distribution of charged particles when they are subjected to an electric field. The formation of the electric double layer between a solid substrate and a liquid electrolyte or its dispersion medium result in zeta potential. In general, a colloidal suspension is said to have a good stability accounts for its high zeta potential value which larger than ±30 mV. Moderate zeta potential colloidal suspension ranging from ±10 to ±30 mV has incipient instability, and the suspension with low zeta potential ranging from 0 to ±5 mV will rapidly flocculate (Li, Zhang, Zhang, Xiu, & He, 2015). This means that higher zeta potential values indicate higher capacity to disperse in water, while lower values indicate low dispersion (Lu et al., 2014).

Polar solvents have large dipole moments (partial charges) as the atoms with different electronegativities are bonded together. In this context, DI water is adopted as the solvent for cellulose suspension because it is a polar solvent. NCC spontaneously acquired a negatively surface electrical charges when brought into contact with the DI water. The greater surface charges of NCC suspension is attributed to the presence of higher number of negatively charged sulfate groups that contribute to the electrostatic repulsion between

the cellulose chains to prevent the agglomeration and aggregation of NCC. The stability of NCC suspension is evidenced by the high absolute values of the zeta potential.

Zeta potential values decreased progressively with increasing reaction temperature and time. The zeta potential values decreased from -19.6 to -38.2 mV when the temperature increased from 70 to 110 ºC. While the zeta potential is decreased from -28.6 to -39.3 mV with increasing hydrolysis time from 0.5 to 2.5 hours. NCC synthesized at higher temperature and prolonged exposure to hydrolysis have higher dispersion capability in water and therefore, higher colloidal stability. The suspension of NCC is considered stable as the absolute value is higher than 25 mV. The higher zeta potential values indicate NCC suspension is stabilized by electrostatic repulsion due to $BmimHSO_4$-mediated hydrolysis that induced grafting of sulfate groups that randomly adsorbed on the surface of NCC. Consequently, a negative electrostatic layer is formed on the surface of NCC due to the negatively charged sulfate groups that repelled the adjoining cellulose chains. Hence, the NCC suspension is stabilized with a greater mean surface charge. NCC suspension will neither precipitate nor flocculate due to the electrostatic repulsion between the negatively charged particles (Guo et al., 2016). The prevalent acidic contribution is due to the proton of the hydrogen sulfate groups that help in catalyzing the hydrolysis of cellulose. A greater number of $BmimHSO_4$ molecules are dissociated into individual charged species at higher temperature and leads to more sulfate groups being adsorbed on the surface of NCC (Ahmadi et al., 2015). The aggregation of particles are overcome due to the sufficient repulsive forces between the negatively charged particles.

Besides that, NCC suspension is more stable after prolonged exposure to hydrolysis because more thorough hydrolysis reaction is favored at longer time. Larger size particles (low surface area per unit mass) with a lower mean surface charge favored the interaction between particles due to inadequate cellulose hydrolysis as only a small number of sulfate

groups were attached on the surface of NCC. Expectedly, increase in the surface charges of NCC is evidenced with the gradual reduction of zeta potential values with increasing hydrolysis time. The stabilization of NCC by electrostatic repulsion is due to the presence of higher number of sulfate groups from IL to adsorb on the NCC. Ideally, the electrostatic repulsion forces are strong enough to prevent the aggregation of NCC while some agglomeration might dominated by van der Waals forces of attraction. Thus, NCC suspension is considered stable because neither precipitation nor flocculation will be occurred.

On the other hand, the zeta potential values of NCC increased proportionally with increasing cellulose concentrations. This signifies the lower stability of NCC suspension because incomplete or slower rate of hydrolysis presumably happen at higher cellulose concentration due to the weakening of catalytic as well as solvation power of $BmimHSO_4$ at highly viscous condition. NCC with a lower mean surface charges is formed because there are only a limited number of sulfate groups present on the surface of NCC due to ineffective hydrolysis. Weak repulsive forces lead to the agglomeration and aggregation of particles in water which caused the suspension to become less stable.

Lastly, high-intensity ultrasonication confers the NCC suspension with higher colloidal stability due to the stabilization of NCC by entanglement and steric hindrance generated from the mechanical process (Abraham et al., 2013). Ultrasound energy can be transferred to the cellulose chains through a cavitation process. Due to the acosutic cavitation effect generated by high-intensity ultrasonication, it is postulates that intense mechanical shearing forces generally breakdown the interaction forces between the cellulose chains which subsequently caused delamination and disintegration of cellulose into smaller particles (Bittmann, Haupert & Schlarb, 2009; Filson & Dawson-Andoh, 2009). Thereafter, smaller size particles with higher surface area would exhibit higher

mean surface charge that essentially contributed to the electrostatic repulsion accounted for their colloidal stability.

4.2.4 Fourier Transform Infrared Spectroscopy (FTIR) Analysis

FTIR is one of the most important analytical techniques that is being widely used nowadays. It is an indispensable technique to determine the chemical composition of pristine MCC and changes in the chemical structure of NCC obtained after hydrolysis. In general, changes in the chemical structure of cellulose can be inferred by disappearance or increase/reduction in intensity of certain IR bands of the crystalline domains of cellulose (Jonoobi, Khazaeian, Tahir, Azry, & Oksman, 2011; Shankar & Rhim, 2016). Figure 4.4 demonstrates the FTIR spectra of pristine MCC and synthesized NCC at different reaction parameters. As shown in Figure 4.4, NCC exhibit similar FTIR spectra as MCC, indicates that preservation of chemical structure of cellulose *I* took place, which is in good accordance with XRD results reported in the Section 4.2.2.

Both MCC and NCC exhibit relatively strong broad band in 3300-3450 cm^{-1} corresponds to stretching vibration of hydroxyl groups (-OH) in cellulose molecules (Maiti et al., 2013; Pang et al., 2015). The band shifted to lower wavenumber after hydrolysis, indicates that hydrolysis weakened the hydrogen bonding of cellulose. Intricate network of hydrogen bonding between cellulose chains produced strong crystalline structure of cellulose molecules that organized in the form of microfibrils. The hydroxyl groups are responsible for the establishment of various inter and intramolecular hydrogen bonding.

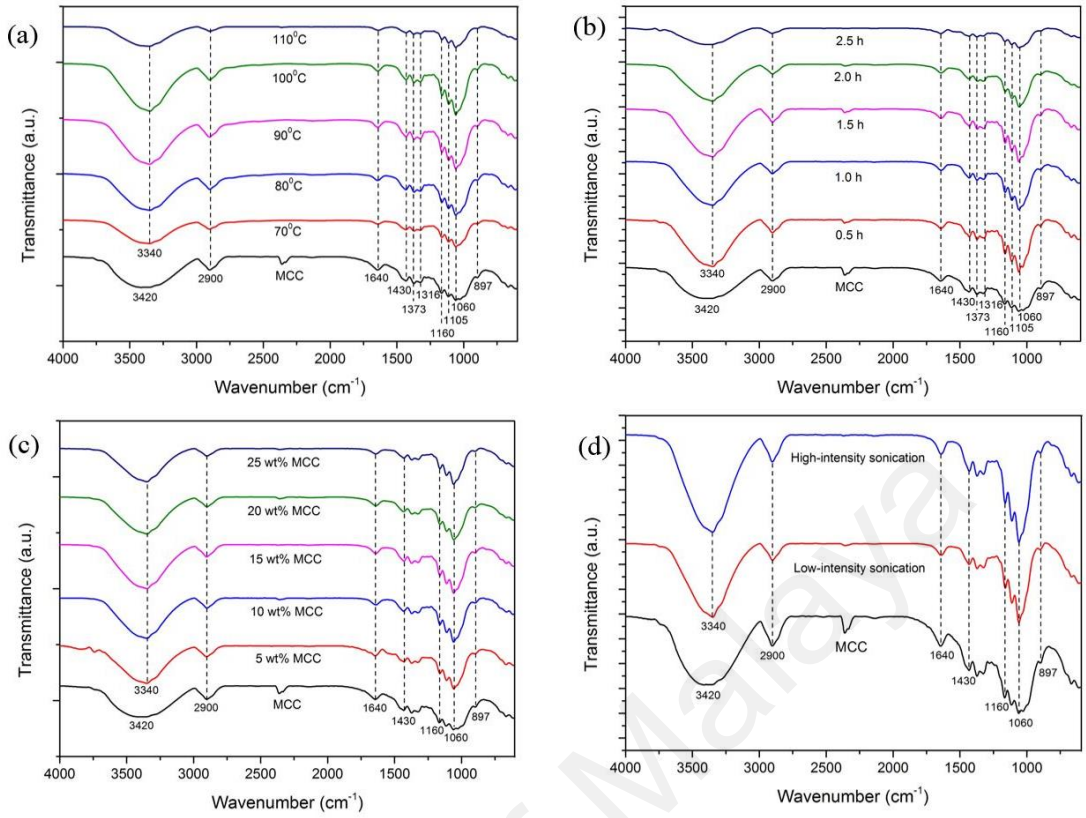

Figure 4.4: FTIR spectra of NCC optimized with different parameters (a) temperature, (b) time, (c) cellulose concentration (mass loading of MCC), and (d) ultrasonication conditions.

FTIR has been proven to be one of the most useful technique in the characterization of hydrogen bonds in cellulose. From Figure 4.4, pristine MCC (3420 cm^{-1}) exhibits stretching vibration at slightly higher wavenumber than NCC (3340 cm^{-1}). The band position at 3420 cm^{-1} is assigned to intramolecular O(2)H---O(6) bonding whereas 3340 cm^{-1} is correspond to intramolecular O(3)H---O(5) bonding. These bands are the characteristic stretching vibration of intramolecular hydroxyl groups of typical cellulose *I* (Fan, Dai, & Huang, 2012; Guo et al., 2016). It is interesting to note that the bands are shifted to lower wavenumber for NCC obtained after hydrolysis. This signifies strong intra-chain hydrogen bonding between O(3)H---O(5) bonds exist predominantly in NCC because this bonds have lower hydrogen bond distance values of about 2.782 ± 0.001 Å and thus, have higher energy of hydrogen bond values (22 ± 1 kJ). In contrast, intramolecular O(2)H---O(6) bonding have larger hydrogen bond distance values of approximately 2.8 ± 0.001 Å and consist of lower hydrogen bond energy (16 kJ).

Therefore, the higher values for hydrogen bond energy associated with lower hydrogen bond distance imply that stronger interactions between O(3)H---O(5) intramolecular cellulose chains in NCC because they are closer to each other. The cellulose chains have stronger interactions within the adjacent cellulose polymer chains and resulted in the establishment of stronger and higher number of intramolecular hydrogen bonds which significantly lead to more stable packing of cellulose chains (Poletto, Ornaghi, & Zattera, 2014). Many of the intermolecular hydrogen bonds are breakdown during the hydrolysis process while most of the intramolecular hydrogen bonds are remained intact in NCC after the hydrolysis. There are higher number of O(3)H---O(5) intramolecular bonds within NCC because this bonds are shorter and thus, more stronger in dictated the crystalline packing of cellulose. In short, the reduction of intermolecular hydrogen bonds was much profound for NCC. This is because the intra-chain hydrogen bonds are stronger than the inter-chain hydrogen bonds as the intra-chain bonds length are relatively shorter.

Based on the figure, it is observed that higher crystallinity NCC have much sharper and stronger bands at 3340 cm^{-1} as higher number of O(3)H---O(5) bonds dictate the crystalline structure by acquire ordered packing of cellulose chains (Poletto et al., 2014). The intensity of this bands is increased relatively with higher crystallinity of NCC (as determined by XRD previously) whereas the bands become broader and weak for lower crystallinity or amorphous NCC. A decrease in the intensity of hydroxyl groups stretching bands for lower crystallinity or amorphous NCC indicates the reduction in hydroxyl group contents in NCC after exposure to hydrolysis at higher temperature and longer time.

In addition, the spectra of all samples show the characteristic C-H stretching vibration around 2900 cm^{-1} and O-H bending mode of adsorbed water at 1640 cm^{-1} (Ahmadi et al., 2015; Lu et al., 2015). FTIR spectra in the 700-1500 cm^{-1} have been used to characterize the polymorphs of highly crystalline cellulose and to give details information regarding

the bonding in polysaccharide rings. Small peaks at 1373 cm^{-1} and 1316 cm^{-1} are attributed to bending vibration of C-H and C-O groups of the aromatic ring in polysaccharides, respectively (Fan et al., 2012; Ibrahim, El-Zawawy, Jüttke, Koschella, & Heinze, 2013). The peak at 1160 cm^{-1} is assigned to C-O asymmetrical stretching vibration within the anhydroglucose ring. It is noteworthy that C-O stretching vibration is almost identical for all samples which indicates that the degradation of cellulose can hardly take place at glucose rings. The main degradation point should occur at glycosidic bonds where preferable site to hydrolysis attack. A shoulder band at 1105 cm^{-1} arises due to C-O-C glycosidic ether band of the polysaccharide component. A prominent band observed at 1060 cm^{-1} is caused by asymmetrical stretching vibration of C-O-C pyranose ring (within the plane ring) (Jonoobi et al., 2011; Maiti et al., 2013; Pang et al., 2014).

The crystalline structure of cellulose can be illustrated by comparing the intensity of peaks at 1430 cm^{-1} and 897 cm^{-1}. Absorption bands at 1430 cm^{-1} is associated with CH_2 bending vibration and usually designated as crystalline bands for cellulose. This band is strong and more predominant in cellulose *I* structure while it becomes very weak and eventually shifts to lower wavenumber (1420 cm^{-1}) in cellulose *II* and amorphous cellulose (Lu et al., 2015; Shankar & Rhim, 2016). All NCC show stronger intensity of this crystalline bands which indicates the preservation or crystallinity enhancement in NCC after the hydrolysis. The intensity of crystalline band is increased relatively with increasing temperature and time as well as with the aid of high-intensity ultrasonication. Therefore, highly crystalline NCC exhibits stronger intensity of this band.

On the other hand, a small peak at 897 cm^{-1} in the anomeric region (700-950 cm^{-1}) represents stretching vibration of C-O-C at β-(1→4)-glycosidic linkages and is assigned as an amorphous band for cellulose (Jiang & Hsieh, 2013; Poletto et al., 2014; Shankar & Rhim, 2016). Apparently, this band appears weaker for NCC which inferred scissoring

of glycosidic bonds between glucose units in cellulose by hydrolysis and ultrasonic treatment. NCC shows weaker amorphous band, suggesting a lower amorphous content because the amorphous parts are highly susceptible and more prone to hydrolysis than the crystalline regions. A significant increase in the intensity of the crystallinity band alongside with a decrease in the intensity of the amorphous band in the FTIR spectra of NCC clearly manifests the improved crystallinity of NCC at higher temperature, longer time and with the aid of high-intensity ultrasonication. The results obtained by FTIR were found to agree well with the finding of XRD. Moreover, the absence of IL peaks ($BmimHSO_4$) in the spectra implies the complete removal of IL during the washing process (Han et al., 2013; Man et al., 2011).

In addition, a FTIR analysis is subjected to pure $BmimHSO_4$ and regenerated $BmimHSO_4$ in order to investigate the changes in the chemical structure after the reaction. Figure 4.5 shows FTIR spectra of pure $BmimHSO_4$, and $BmimHSO_4$ that is regenerated and recovered after the catalytic reaction with cellulose. As depicted in Figure 4.5, the spectrum of regenerated $BmimHSO_4$ looks identical to the spectrum of pure $BmimHSO_4$ except for the presence of one extra broad peak within 3200-3800 cm^{-1}. The presence of broad band at 3440 cm^{-1} for regenerated $BmimHSO_4$ is corresponds to the intermolecular hydrogen bonds (–OH) between $BmimHSO_4$ and water due to the water retained in regenerated IL. Most of the IL including $BmimHSO_4$ is highly hygroscopic in nature and they have high affinity for water molecules.

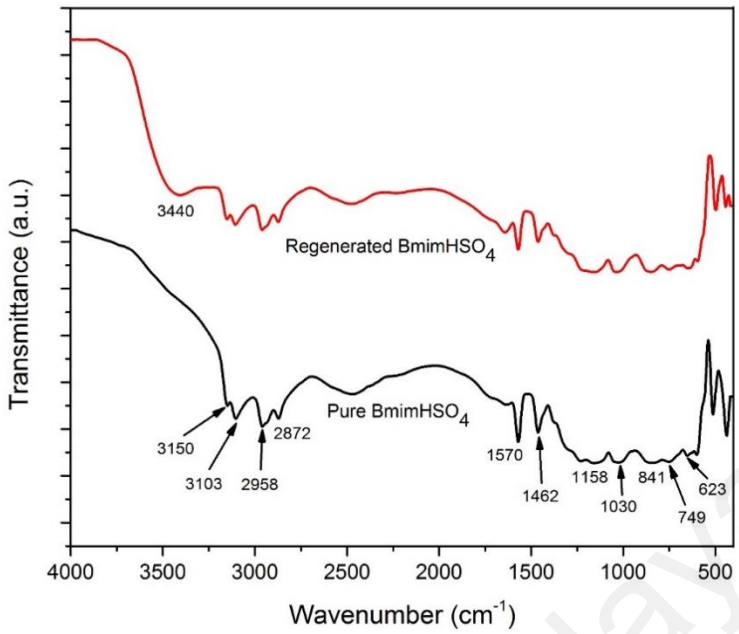

Figure 4.5: FTIR spectra of pure $BmimHSO_4$ and regenerated $BmimHSO_4$.

Besides the presence of additional –OH bands for regenerated $BmimHSO_4$, similar spectra obtained confirm that the chemical structure of regenerated $BmimHSO_4$ is unchanged after the reaction. This indicates they have the same functional groups and manifests the significant properties of $BmimHSO_4$ as it is recyclable and reusable (Man et al., 2011). $BmimHSO_4$ can be easily recovered via simple distillation process and vacuum evaporation by taking advantages of the distinct boiling point differences of $BmimHSO_4$ and water. The boiling point of $BmimHSO_4$ is above 200 °C which is relatively higher than that of water (100 °C at standard conditions) (Cao et al., 2009). Therefore, water can be easily removed from the $BmimHSO_4$-water solution through evaporation and subsequently concentrated under vacuum condition to regenerate the IL. In the present study, the yield of recovered $BmimHSO_4$ is about 90 %. The high recovery yield and recyclable nature of IL make this synthesis route become attractive and environmental friendly approach to prepare nanocellulose.

Both pure and regenerated $BmimHSO_4$ exhibit a small peak at around 3103 cm^{-1}, which is attributed to the stretching vibration of aromatic =C-H. Besides that, a small

band at 3150 cm^{-1} is attributed to quaternary amine salt formation with hydrogen sulfate. Distinct peaks at 2958 and 2872 cm^{-1} are associated with the aliphatic asymmetric and symmetric (C-H) stretching vibrations due to methyl groups in the alkyl substituents. The band at 1570 cm^{-1} is correspond to in-plane stretching of C=C bonds and 1462 cm^{-1} is due to C=N stretching. Peaks at 1030, 841, 749 and 623 cm^{-1} are the characteristic stretching vibration of C-N of aliphatic amines (Dharaskar, Varma, Shende, Yoo & Wasewar, 2013; Socrates, 2004). While the band at 1158 cm^{-1} is due to hydrogen sulfate anion (Socrates, 2004). Based on FTIR analysis, it confirms that the regenerated $BmimHSO_4$ has similar chemical structure as pure $BmimHSO_4$, thus its integrity is preserved.

4.2.5 Morphological analysis by Field Emission Scanning Electron Microscopy (FESEM), Atomic Force Microscope (AFM) and Transmission Electron Microscopy (TEM)

In the present study, FESEM is employed to study the surface morphology of NCC after the hydrolysis. Figure 4.6 shows the FESEM images of NCC obtained at different reaction temperatures. Figure 4.6 (a) demonstrates pristine MCC primarily consists of bundled of aggregated cellulose fibrils with irregular shape and larger size of about 20 µm. Each cellulose fiber appears to be assembled from several to hundreds of microfibrils and constitutes for the compact structure of cellulose. Apparently, the cellulose fibers have diameter which are significantly larger with rough surface morphology and low aspect ratio. It is suggested that the aggregation of cellulose fibers are associated with strong hydrogen bonding between hundreds of individual cellulose microfibrils that assembled into a single structure (Liu, Zhong, Chang, Li, & Wu, 2010).

On the other hand, the aggregation of fibers of NCC is broken down to a greater extent after which the MCC is hydrolyzed with $BmimHSO_4$, as shown in Figure 4.6 (b-d). The glycosidic bonds and many of the intermolecular hydrogen bonds as well as a small

proportion of intramolecular hydrogen bonds were breakdown during the hydrolysis. As a consequence, the micro-sized cellulosic fibers tend to separate from the bundle of fibrils to form individual cellulose crystallites that consist of smaller diameter and shorter chain length. Besides that, the intermittent breakdown in the fibrillar structure due to the acidic IL caused the significant reduction in the diameters of cellulosic fibers at elevated temperature and prolonged exposure to hydrolysis (Haafiz, Hassan, Zakaria, & Inuwa, 2014). Apparently, NCC demonstrate as cylindrical-shaped fibrils with relatively smooth surface. In contrast to pristine MCC, NCC show comparatively refined fibrillar structure with smaller diameter of fibers. It is worth noting that the diameter of NCC fibrils decreased when the hydrolysis temperature is increased. As depicted in Figure 4.6 (d and e), hydrolysis conducted at higher temperatures (90 and 100 °C) produced smaller size and more refined structure NCC. This presumably give rise to the formation of higher aspect ratio NCC as longer and thinner cellulose fibrils are observed. Therefore, FESEM images illustrated that MCC are large, irregular-shaped cellulose fibers with rough surface while NCC are essentially smaller fibrils with homogenous and smooth fibrillar structure.

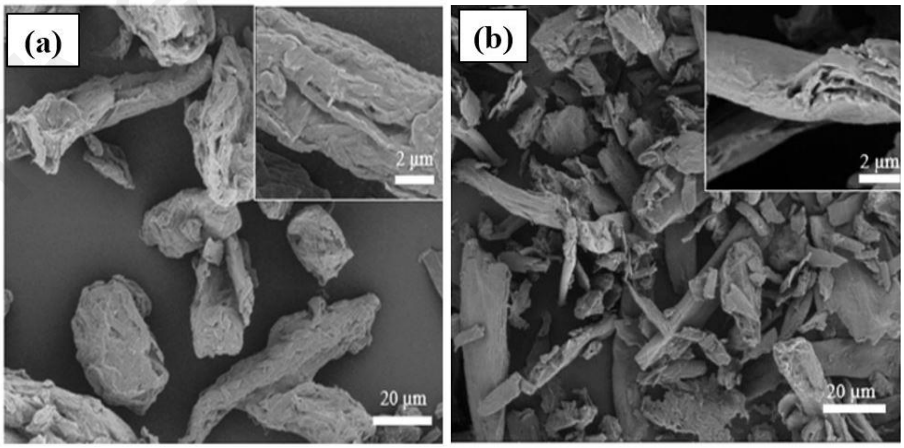

Figure 4.6: FESEM images of (a) MCC, (b) NCC synthesized at temperatures of (b) 70 °C, (c) 80 °C, (d) 90 °C and (e) 100 °C. Insets are the images of cellulose fibres at 15,000x magnification.

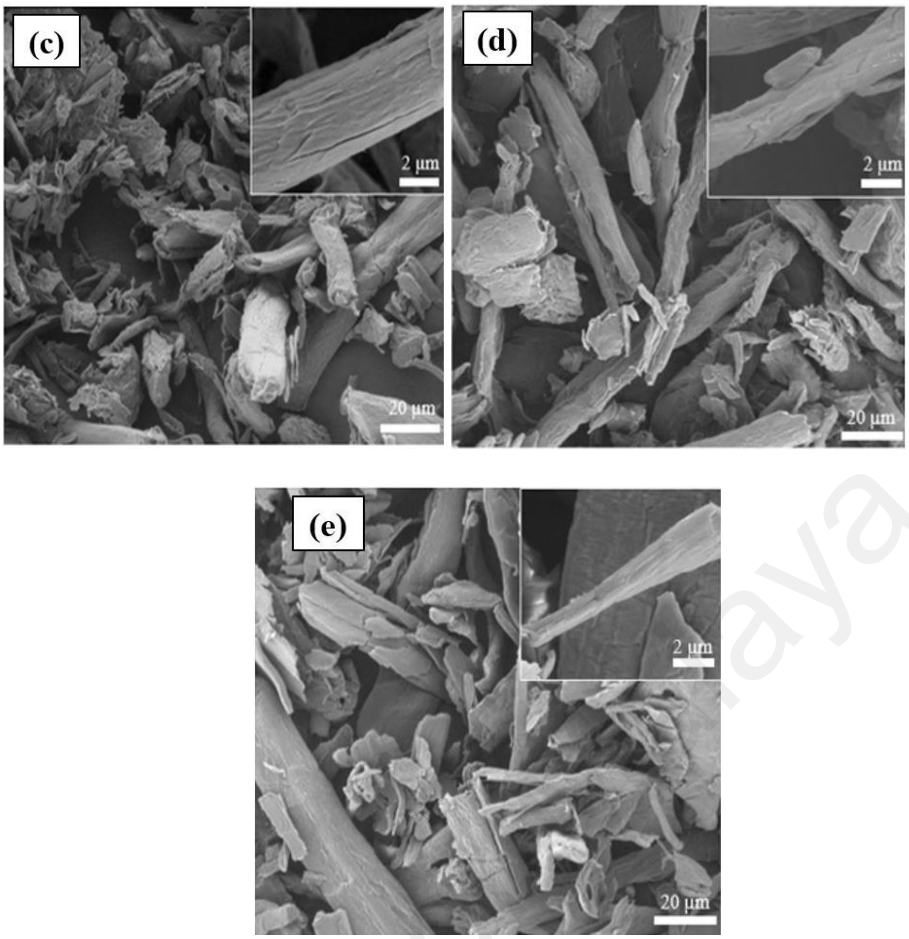

Figure 4.6, continued.

The morphology of NCC obtained at synthesis time of 0.5, 1.0, 1.5 and 2.0 hours using FESEM are shown in Figure 4.7. As depicted in Figure 4.7 (a), nano-size cellulose fibrils started to emerge from the peripheral and edge of cellulose fibers at short hydrolysis time of 0.5 hours. Rod-like nano-size cellulose fibrils can be found on the surface of cellulose fibers when the MCC is hydrolyzed for 1 hour. However, they tend to not distribute evenly on the fibers. Nevertheless, long and thin cellulose fibrils are observed to distribute evenly after 1.5 hours of hydrolysis which may account for its high aspect ratio. These rod-like cellulose fibrils are identified earlier by XRD and FTIR as NCC because of its higher crystallinity. The highest aspect ratio NCC was obtained at the optimum conditions of hydrolysis at 1.5 hours. Uniform nano-size NCC eventually appeared homogenous and distribute evenly on the surface of cellulose fibers after prolonged hydrolysis for 2 hours. Although 0.5 and 1.0 hour are able to generate nanocellulose, however, the nanocellulose

obtained does not have uniform size distribution and is only present in a relatively small area with lower crystallinity. This means that short hydrolysis time of 1 hour may not be sufficient enough to remove most of the amorphous parts of cellulose (Fan & Li, 2012). When the cellulose is prolonged exposed to the hydrolysis conditions, this will ensures more thorough and extensively breakdown of intermolecular hydrogen bonds during hydrolysis which resulted in the generation of smaller crystallites NCC with greater uniformity. Thus, the fibers of NCC distributed more evenly and the size of NCC are consists of enhanced uniformity.

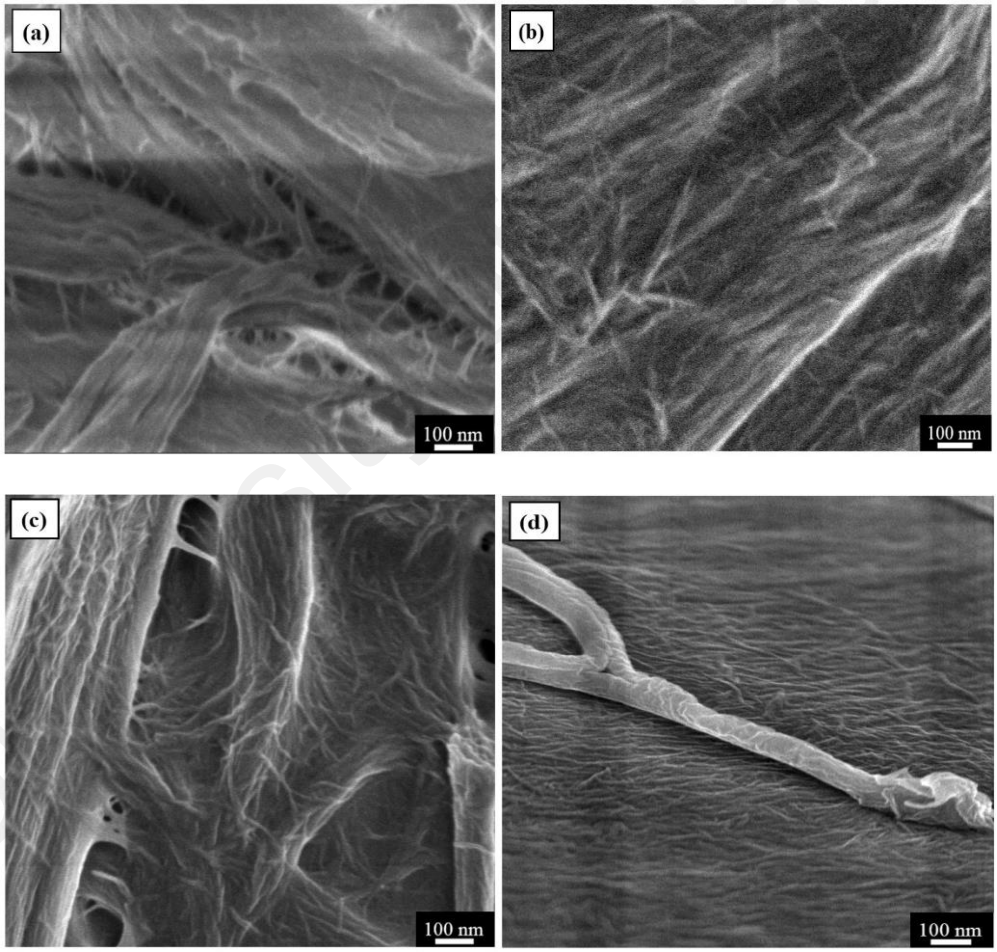

Figure 4.7: FESEM images of NCC obtained at different hydrolysis time: (a) 0.5 h, (b) 1.0 h, (c) 1.5 h and (d) 2.0 h.

The proposed mechanism of formation of NCC is the initial breakage of hydrogen bonding network between adjoining cellulose chains, and its subsequent cleavage of β-1,4-glycosidic bonds within the same cellulose chains to separate cellulose fibrils due to

interaction of cellulose with $BmimHSO_4$ (Ahmadi et al., 2015). Therefore, hydrolytic cleavage of glycosidic bonds rendered extensive reduction in particle size (diameter) and give rise to the formation of highly crystalline NCC.

In addition, corresponding AFM images of NCC at selected synthesis time are presented in Figure 4.8. The morphology and dimension (length and diameter) of synthesized NCC are determined by AFM analysis. Figure 4.8 demonstrates the AFM images and peak force error for a better illustration of the morphology and size of NCC obtained at 0.5, 1.0 and 1.5 hours of hydrolysis. The mean length, diameter and aspect ratio of NCC determined via AFM are then presented in Table 4.3, and the measurement of diameter size distribution were presented in Figure 4.9.

Table 4.3: Average length, diameter and aspect ratio of NCC determined from AFM analysis.

Sample	Average length, L (nm)	Average diameter, d (nm)	Aspect ratio (L/d)
(a) 0.5 h	282 ± 121	78 ± 2.6	4.96 ± 0.60
(b) 1.0 h	202 ± 76	63 ± 2.9	5.75 ± 0.58
(c) 1.5 h	512 ± 195	15 ± 3.1	15.85 ± 2.30

It is clearly seen that the average diameter of NCC decreased considerably from 78 nm to 15 nm as the hydrolysis time is increased from 0.5 to 1.5 hours. Apart from that, the aspect ratio of NCC increased proportionally with the increase in the hydrolysis time. NCC have greater size distribution at 0.5 hour of hydrolysis because the diameter distribution spans a wide range from 59 to 82 nm. From Figure 4.8 (a), it can be observed that some NCC intertwined with the larger fibrils and consist of non-uniform size NCC with lower aspect ratio. The size of NCC spans a relatively wide range at short hydrolysis time. This signifies that shorter hydrolysis time is not efficient as the hydrolysis was inadequate with the incomplete removal of amorphous contents. In addition, the

hydrolysis is a process which requires time for effective hydrolytic cleavage of β-glycosidic bonds (Moon et al., 2011).

As the hydrolysis time progress, the size distribution of NCC becomes narrower with greater uniformity, and reduction in its diameter. NCC obtained at 1.5 hours of hydrolysis has the smallest diameter of about 15 nm and the highest aspect ratio of about 15.85. A greater number of cellulose chains are broken down to smaller fragments when the hydrolysis time is increased because of the more extensive and thorough hydrolysis reaction which resulted in more efficient break down of glycosidic bonds. Consequently, the size of NCC is diminished to a greater extent and with high uniform size distribution (Fan & Li, 2012). Moreover, some agglomeration and aggregation of rod-like NCC structure are observed which might be ascribed to water evaporation during the sample preparation. Meanwhile, some isolated rods of NCC are observed. Highly crystalline structure and smaller size NCC with higher aspect ratio is suggested to use as strengthen material for composite applications. In principle, high aspect ratio nanocellulose fibers have better ability to sustain mechanical stress uniformly over the matrix than the shorter fibers. The effectiveness of reinforcement is presumably generated through the hydrogen bond formation between the NCC within the extended network, whose packing structure depends on the distribution as well as the aspect ratio (l/d, where l= length and d=diameter) (Klemm et al., 2011; Moon et al., 2011; Salas et al., 2014).

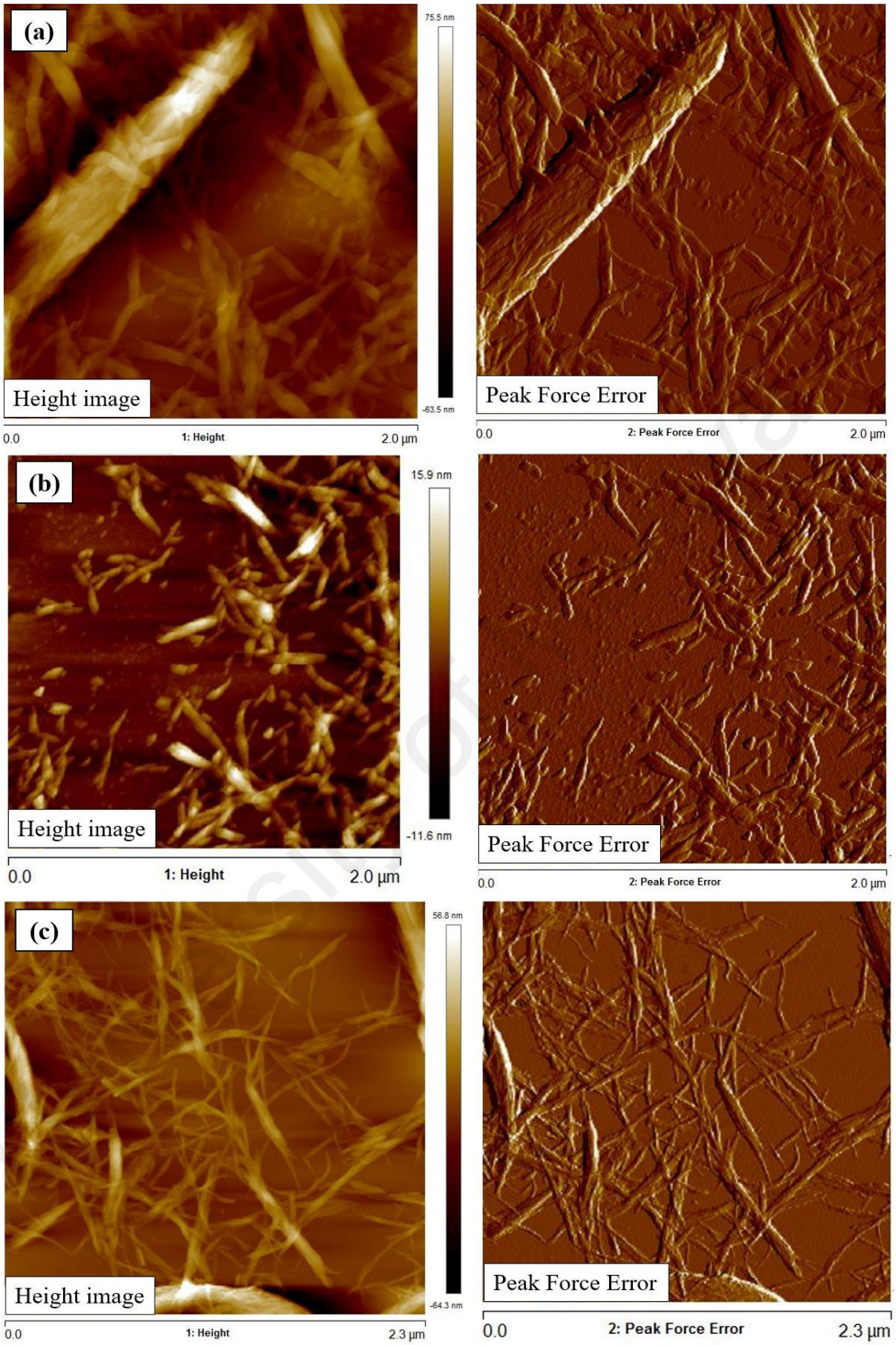

Figure 4.8: AFM height images and peak force error images of NCC obtained at different synthesis time: (a) 0.5 h, (b) 1 h and (c) 1.5 h.

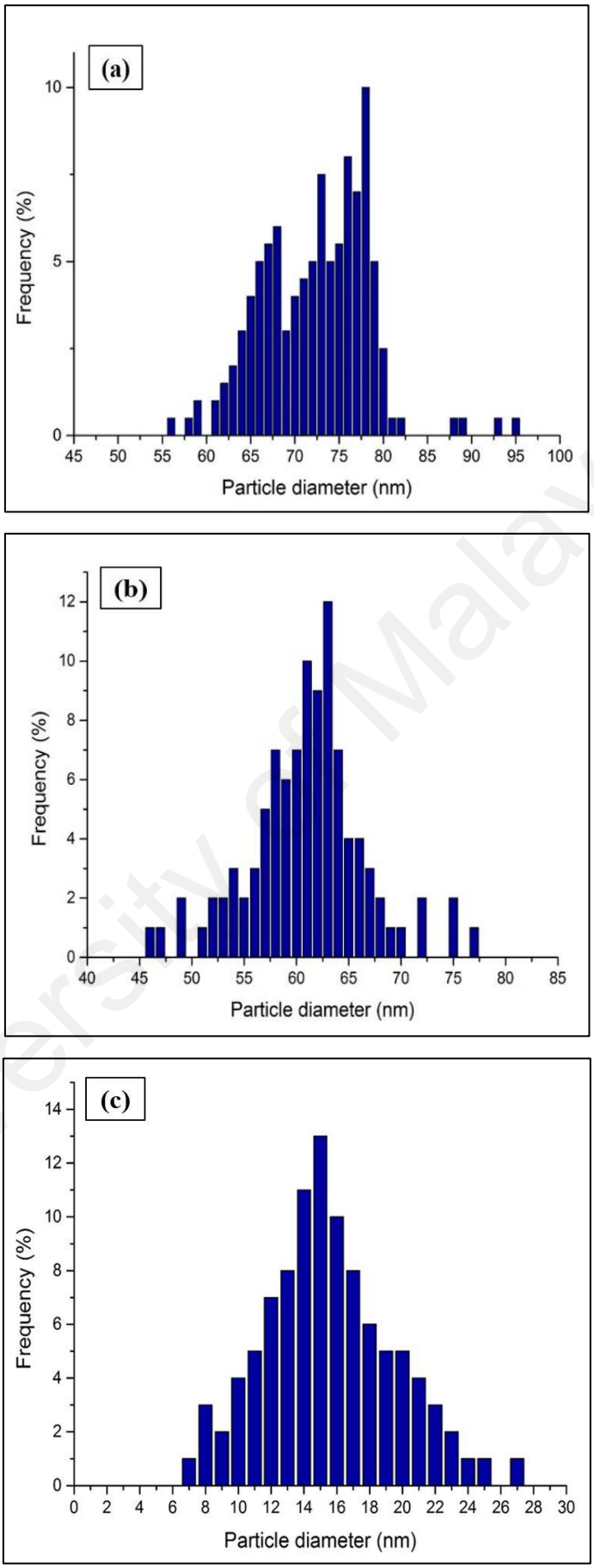

Figure 4.9: Size distribution (diameter) of NCC based on AFM analysis obtained at different synthesis time: (a) 0.5 h, (b) 1 h and (c) 1.5 h.

Figure 4.10 shows the high resolution TEM images of NCC obtained at selected synthesis time of 1.0, 1.5 and 2.0 hours. Under controlled conditions, the hydrolytic cleavage of amorphous parts of cellulose by $BmimHSO_4$ with heat treatment caused the crystalline domains to remain intact. The size of cellulose microfibrils could eventually be reduced from micron to nanometer scale after hydrolysis. Thereafter, highly crystalline NCC nanostructure could be produced upon hydrolysis. It should be noted that the distribution of length, width and percent crystallinity of the NCC are likely dependent on the type and conditions of the treatments applied to produce nanocellulose. In this context, smaller particle size and higher crystallinity of NCC were acquired at the prolonged exposure to hydrolysis conditions. When the smaller diameter of particles is obtained at longer hydrolysis time, this signifies that more amorphous regions were hydrolyzed by $BmimHSO_4$ during hydrolysis and resulted in the liberation of smaller crystallites of NCC with higher crystallinity as a larger fraction of amorphous regions were selectively removed by IL.

Based on the TEM images as illustrated in Figure 4.10, it is observed that rod-like NCC is acquired at 1 and 1.5 hours hydrolysis while thin and needle-like NCC is obtained at 2 hours. The length and diameter of NCC are determined via TEM analysis. The length and width of NCC are revealed to be 120-180 nm and 55-65 nm for 1 hour, 75-80 nm and 15-20 nm for 1.5 hours and lastly 85-95 nm and 10-15 nm for 2 hours of hydrolysis, respectively. The agglomeration of NCC are observed which presumably associated with the hydrogen bonding between adjacent cellulose molecules and high surface energy of the smaller size NCC. The smaller size and thin needle-like morphology of NCC are attributed to over degradation of crystalline domains, besides the hydrolysis of amorphous regions of cellulose at prolonged hydrolysis condition. This deduction can explained the lower crystallinity and smaller size of synthesized NCC. Interestingly, the size measurement of NCC by AFM analysis is somewhat larger than that of TEM presumably

due to tip broadening effect which are common in AFM technique (Goetz, Keltner, & Simon-Thomas, 2010; Lu & Hsieh, 2012).

In summary, NCC that is acquired at 1.5 hours hydrolysis has the highest crystallinity and smaller size. Thus, it is the optimum condition to synthesize highly crystalline NCC with uniform and narrower size distribution.

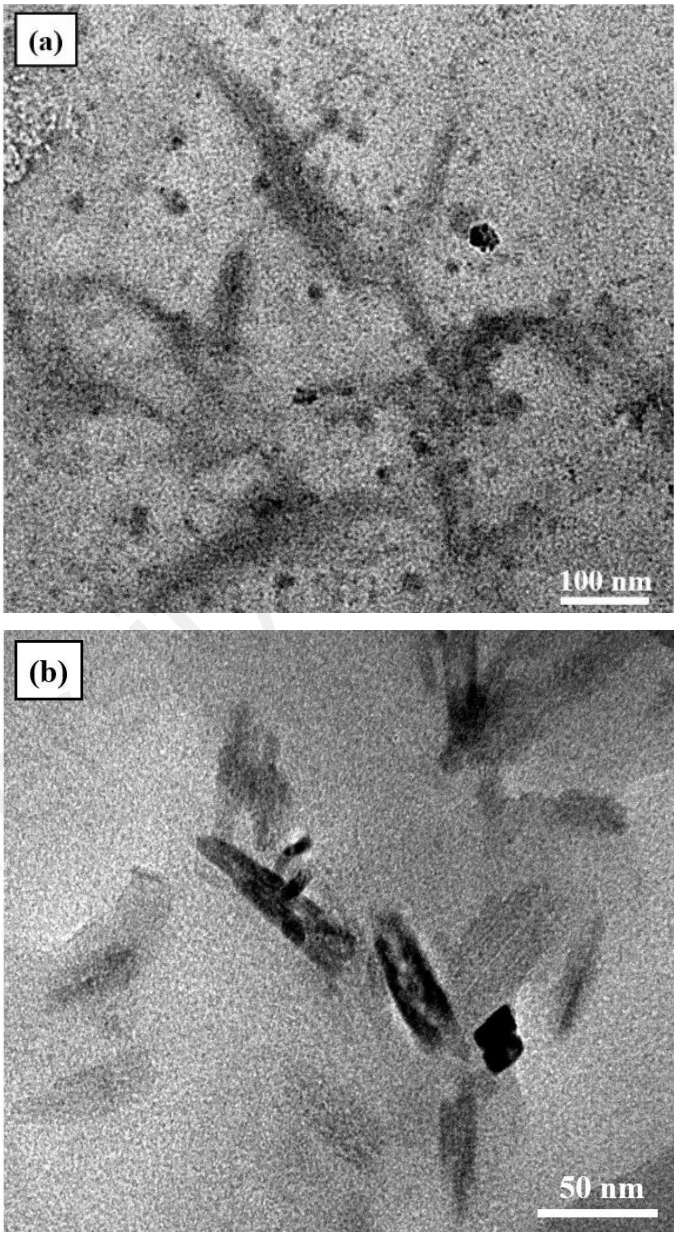

Figure 4.10: HRTEM images of NCC synthesized at (a) 1 h, (b) 1.5 h and (c) 2 h.

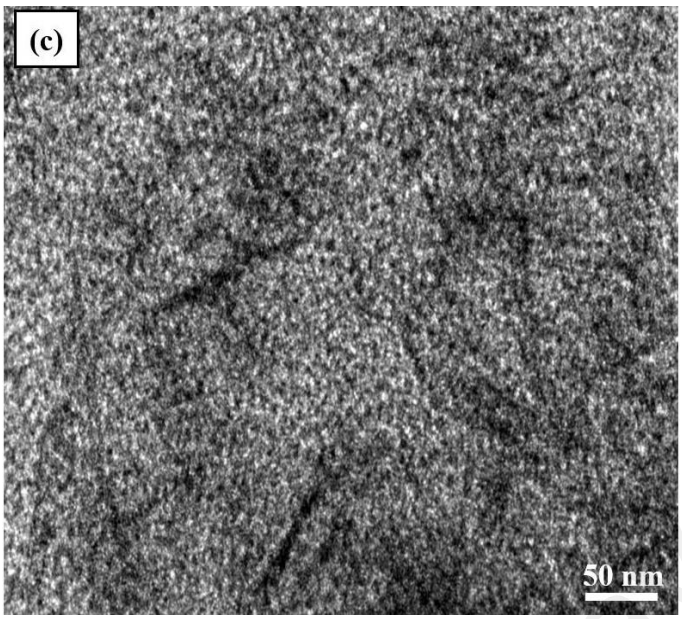

Figure 4.10, continued.

4.2.6 Thermal properties analysis by Thermogravimetric Analysis (TGA)

TGA analysis was conducted to investigate thermal stability of pristine MCC and NCC obtained after hydrolysis with $BmimHSO_4$. TGA and DTG thermograms of MCC and NCC prepared at different synthesis conditions are as shown in Figure 4.11. All samples including pristine MCC and synthesized NCC present an initial small amount of weight loss in the temperature at around 100 ºC which ascribed to evaporation of water molecules (Lu et al., 2015; Nascimento et al., 2014; Pang et al., 2015). This finding is in good accordance with the characteristic absorbance band of bending vibration of intermolecular bonded water interaction at 1640 cm^{-1} as observed in the FTIR spectra reported in earlier section. Both MCC and NCC are composed of cellulose, whose elementary unit is anhydroglucose that contains three hydroxyl groups. These hydroxyl groups formed intra and intermolecular hydrogen bonds, causing the cellulose to be hydrophilic. Hence, the hydroxyl groups present in the native structure of MCC and NCC contribute to their hydrophilic character (Kalia et al., 2011; Klemm et al., 2011).

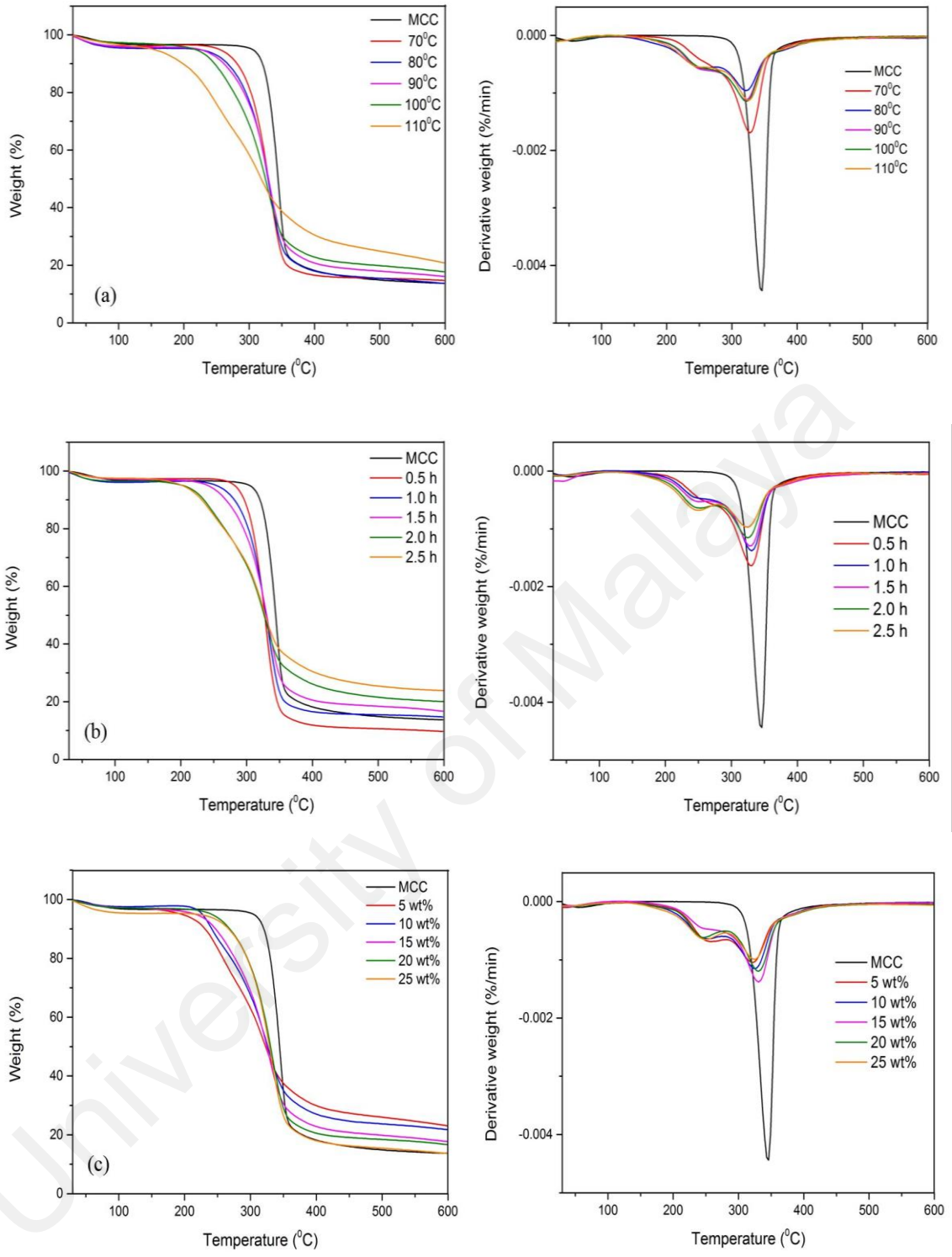

Figure 4.11: TGA and DTG curves of MCC and NCC optimized with different parameters (a) temperature, (b) time, (c) cellulose concentration (mass loading of MCC), and (d) ultrasonication conditions.

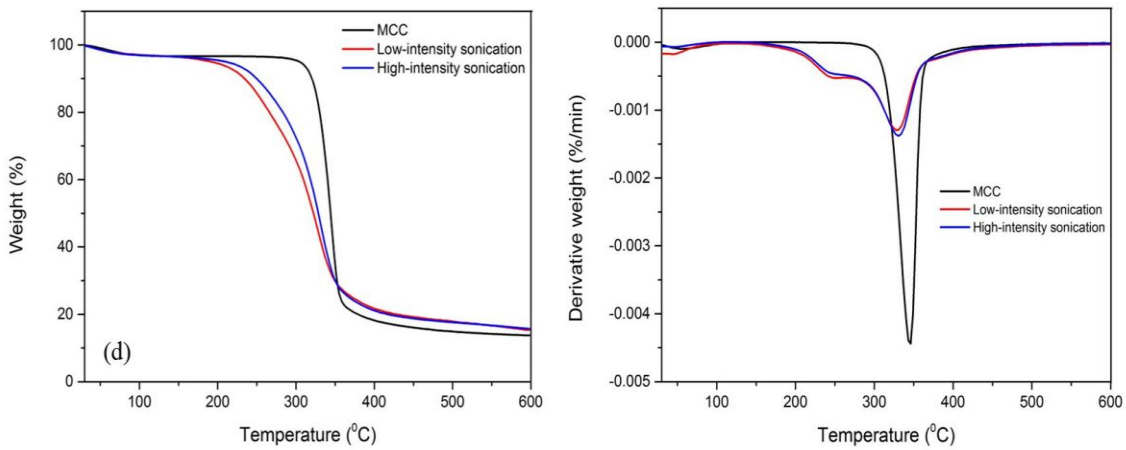

Figure 4.11, continued.

The onset decomposition temperature (T_0), maximum thermal decomposition temperature (T_{max}) and char yield of cellulose samples determined from TGA and DTG curves are given in Table 4.4. Apparently, decomposition of MCC occurs within a relatively narrow temperature range (300 to 370 ºC) and shows only one pyrolysis process as revealed in DTG curve. Typical decomposition behavior of MCC initially onsets at 300 ºC followed by a sudden weight lost with the T_{max} took place at 345 ºC with a relatively weight loss of 82 %. The high decomposition temperature of MCC is associated with the compact and highly dense structure of cellulose packing. Hence, pristine MCC has higher thermal stability than the synthesized NCC. The yield of char produced by MCC at 600 ºC is 13.7 % (Chen et al., 2011; Mandal & Chakrabarty, 2011).

By opposite, synthesized NCC show different decomposition behavior as compared to that of pristine MCC. Apparently, the decomposition of NCC took place within a wider range of temperatures with two distinct pyrolysis processes well separated in close proximity as revealed in DTG curves. The first pyrolysis is a slow weight lost process which occurs at relatively lower temperature range from 200 to 270 ºC with T_{max} peak at 240 ºC. On the other hand, the second process has greater dominance over the first pyrolysis, ranging from 270 to 360 ºC with pronounced T_{max} at around 330 ºC. Approximately 25 % of the original mass of NCC is lost during the first pyrolysis and

followed by another 52 % mass loss in the second (Mandal & Chakrabarty, 2011; Nascimento et al., 2014). Meanwhile, on contrary to corresponding MCC, NCC are producing slightly higher amount of char yield at 600 ºC, which is between 14 to 23 % (Han et al., 2013). The lower decomposition temperature of NCC indicates the lower thermal stability of NCC than MCC.

Table 4.4: Onset decomposition temperature, maximum decomposition temperature and char yield of MCC and NCC.

Sample	Onset decomposition temperature, T_0 (ºC)	Maximum decomposition temperature, T_{max} (ºC)	Char Yield (%)
MCC	300.0	345	13.7
a) Temperature (ºC)			
70	274.5	335	14.1
80	270.2	330	13.7
90	269.3	330	16.7
100	260.5	330	17.7
110	238.0	330	21.1
b) Time (hour)			
0.5	286.2	330	9.7
1.0	274.5	330	14.7
1.5	269.3	330	16.7
2.0	235.3	325	19.3
2.5	232.4	324	22.5
c) Percent mass loading of MCC (wt%)			
5	248.5	322	23.1
10	250.9	325	21.8
15	269.3	330	16.7
20	274.6	330	15.9
25	274.6	325	14.6
d) Sonication treatment			
Low-intensity sonication	247.3	328	15.6
High-intensity sonication	265.2	330	16.1

Therefore, it can be deduced that MCC has only one pyrolysis process and NCC have two-step pyrolysis processes (Chen, Wang, & Liu, 2012). The difference in the thermal decomposition behavior is assumed to be due to different decomposition-gasification processes or degree of crystallinity. Interestingly, NCC are noticeably decomposed at significantly lower temperature range than MCC, presumably attributed to reduction in

molecular weight of NCC. Consistent with onset decomposition temperature, T_{max} of NCC are lowered to 330 ºC. Pyrolysis process of NCC has been confirmed by the evidence of two distinct decomposition peak as revealed in the DTG curves. The first pyrolysis took place at lower temperature (240 ºC) corresponds to the decomposition of highly accessible and sulfated amorphous regions which are less thermally stable whereas the second pyrolysis occurred at higher temperature of 330 ºC represents the breakdown of crystal interior due to thermal degradation of cellulosic materials (Lu et al., 2013). The second pyrolysis indicates the cleavage of glycosidic linkage within cellulose which usually falls within the temperature range from 275 to 350 ºC (Kim, Kim, Kim, & Yang, 2006).

Reduction in thermal stability of NCC could be ascribed to several reasons. First, surface sulfation of NCC because the adhesion of sulfate groups from $BmimHSO_4$ caused the activation energy required for thermal decomposition was lowered. Sulfate groups that adsorbed on the cellulose chains will catalyzes the thermal degradation of cellulose at lower temperature by promoting dehydration reactions. Hence, the presence of sulfate groups are responsible to the reduced thermal stability of NCC as the thermal decomposition is occurred at lower temperature (de Morais Teixeira et al., 2010; Li, Yue & Liu, 2012). Expectedly, NCC are decomposed at lower temperature (Man et al., 2011; Morais et al., 2013; Xiong et al., 2012). Second, thermal stability diminished because of the higher surface area of smaller NCC fiber dimensions as compared to macroscopic cellulose which increased the exposure to heat that presumably contributes to lower decomposition temperature (Han et al., 2013; Jiang & Hsieh, 2013). A greater exposed surface area indicates that many of the sulfate groups adsorbed on the surface of cellulose chains and act as catalyst to promote the degradation of cellulose at lower temperature. Besides that, the increased exposure of surface sulfate groups to heat presumably

contributes to the lower decomposition temperature and therefore, lowered the thermal stability of NCC.

Despite that, the yield of char residue produced by NCC (14-23 %) are greater than MCC (13.7 %). Theoretically, pyrolysis of cellulose should produce an ideal yield of 44.4% of carbonaceous residuals during which the dehydration reaction will release all hydrogen and oxygen in the form of H_2O through dehydration reaction. However, pyrolysis reaction may involves other complex reactions such as decarbonylation to CO, decarboxylation to CO_2, as well as reactions to form gaseous products, for instance, H_2 and CH_4 (Jiang & Hsieh, 2013). The pyrolysis of cellulose generally involves dehydration, which occurs below 300 °C, followed by char formation. Dehydration and char formation were predominantly occurred for cellulose with lower degree of crystallinity and more favorable in the amorphous regions or disordered structure. The pyrolytic reaction of cellulose usually proceeds with dehydration, which is the loss of water molecules from the cellulose components. After the dehydration, there was subsequent breakdown of the anhydrocellulose into the carbonaceous residuals at higher temperature which known as char yield residuals. The formation of char yield is accelerated by dehydration reaction which lead to a higher amount of char remnants, whose structures are not further degraded into low volatile compounds (Broido & Nelson, 1975; Shafizadeh, 2012).

The higher char yield residues of NCC can be attributed to a few reasons. First, the dehydration effect catalyzed by sulfate groups would facilitates the formation of char residues. Moreover, the smaller dimensional size of NCC induced a greater amount of free end chains. The formation of char residues is favorable as the decomposition of free end chains took place at a lower temperature (Wang, Ding, & Cheng, 2007). During hydrolysis, the cleavage of glycosidic linkages and breakdown of the inter and intra

hydrogen bonds resulted in the formation of NCC fragments with reduced chain length and smaller dimensional size. Lower chain length NCC possess an increase in the exposed surface area with sulfate bearing groups as well as increase in the number of free end chains. Hence, the formation of char residues of NCC is favorable due to the dehydration effect catalyzed by the sulfate groups at lower temperature and constitutes for the increased char yield content (Li, Yue & Liu, 2012). Additionally, the intrinsically flame resistant characteristic of the sulfated amorphous and crystalline regions of cellulose caused an increase in char remnant for NCC (Johar, Ahmad, & Dufresne, 2012; Mandal & Chakrabarty, 2011).

On top of that, decreasing trend of onset decomposition temperature is observed for NCC that synthesized with higher reaction temperature and longer time. When the temperature and time increased, onset decomposition temperature of NCC decreased gradually with T_{max} remain unchanged. This presumably attributed to a greater number of sulfate groups adsorbed onto the surface of NCC with exposure to hydrolysis conditions at higher temperature and prolonged reaction. Thereafter, surface sulfation of NCC occurred more readily at higher temperature and prolonged time which eventually lead to lower onset decomposition temperature (Xiong et al., 2012). Nonetheless, the highly crystalline NCC fabricated at temperature of 90 ºC may compromise the effect of surface sulfation and the onset decomposition temperature did not decrease drastically. Highly crystalline NCC constitutes of more closely packed structure and ordered arrangement of cellulose chains due to existence of higher number of hydrogen bonding established between adjoining cellulose chains that resulted in a more thermally stable structure (Ashori et al., 2006; Yang et al., 2007). Furthermore, the cellulose molecules of NCC are stabilized by intramolecular hydrogen bonds to suppress thermal expansion along the cellulose chains to enhance the thermal stability (Hidaka, Kim, & Wada, 2010). Therefore, thermal stability is improved for higher crystallinity NCC because the closed

packed structure makes it difficult for heat transfer. The higher crystallinity cellulose domains act as barriers for the heat transfer as well as thermal degradation (Poletto et al., 2014). As a consequence, the onset decomposition temperature of NCC is not drastically decrease to significantly lower temperature. This finding is supported by work of Kim and his colleagues which demonstrated that high crystallinity cellulose has shifted the thermal decomposition to higher temperatures (Kim, Eom, & Wada, 2010).

However, on further increasing the reaction temperature and time, many of the hydrogen bonding and parts of the molecular cellulose chains are ruptured and eventually degraded which lead to less thermally stable structure that started to decompose at apparently lower temperature (Chen et al., 2012). In addition, onset decomposition temperature of NCC is shifted to lower temperature for 5 wt% cellulose concentration because there is a greater amount of sulfate groups are available for surface sulfation. Meanwhile, ultrasonication conditions have no significant impact on the thermal properties of NCC. Similar finding was reported by Chen and his co-workers on 2011.

On the other hand, char yield of NCC is increased proportionally with increasing reaction time. The surface sulfation of cellulose chains took place extensively with prolonged exposure to the hydrolysis conditions because reasonably a greater number of sulfate groups adsorbed onto the surface of NCC and then the char formation is favorable. It is the sulfate groups that catalyzed the dehydration reaction which contribute to the formation of char remnants. In addition, the smaller dimensional size of NCC obtained through longer hydrolysis time would induced a greater number of free end chains. As a consequence, the formation of char residues is favorable. Less sulfation phenomenon occurred on the cellulose chains with increasing cellulose concentration as restriction of ion mobility at viscous suspension and consequently resulted in reduction of char yield residues. It is well-known that sulfate groups have flame-retardants characteristics

because they prompt to form char and act as a catalyst in accelerating dehydration and desaturation of pyranose rings (Johar et al., 2012; Kokol et al., 2015).

4.3 Synthesis of Cellulose Nanoparticles (CNPs) by BmimOAc

4.3.1 Mechanism of CNPs Synthesis with BmimOAc

The synthesis of regenerated cellulose nanoparticles (CNPs) in 1-butyl-3-methylimidazolium acetate (BmimOAc) is investigated. Besides that, the influence of different synthesis parameters on the preparation of CNPs are extensively studied. Practically, cellulose is difficult to dissolve in water and most common organic solvents due to its compact crystalline structure. The insolubility of cellulose is mainly attributed to the stiff molecules as well as closed chain packing via van der Waals forces and intricate network of inter- and intramolecular hydrogen bonds (Blackley, 2012; Dadi, Schall, & Varanasi, 2007; Damodaran, Parkin, & Fennema, 2007). However, IL has been proven to be effective in dissolving complex macromolecules and polymeric components of lignocellulosic biomass by breaking the hydrogen bond network which in turns, facilitated the dissolution of cellulose (Swatloski et al., 2002). The details of the proposed working principle or mechanism is discussed as below.

Generally, dissolution of cellulose in IL is influenced by the interactions between hydroxyl groups of cellulose and anion of the IL. The anion of the IL functions as hydrogen-bond acceptor in dissolution process during which it interacts specifically with hydroxyl proton of the cellulose. In particular, physicochemical properties such as hydrogen-bonding basicity (β) and viscosity of IL determined the extent and ability of anion of IL to accept the hydrogen bonding. Acetate anion has strong hydrogen-bonding basicity (1.09) based on the Kamlet-Taft parameters of [Bmim] salts (MacFarlane et al., 2006; Ohno & Fukaya, 2009) and BmimOAc has a relatively low viscosity of 646 mPa (at 25 ºC) (Bonhote et al., 1996; Olivier-Bourbigou et al., 2010). As a result, BmimOAc

can be an excellent candidate to dissolve cellulose due to the ability of acetate anion to accept and established the hydrogen bonding with cellulose. In addition, the low viscosity of BmimOAc can essentially promotes the dissolution process due to the higher ions mobility (Ha, Mai, An, & Koo, 2011).

Generally, IL is composed entirely of cations and anions. The ionic species in BmimOAc dissociated into respective $[Bmim]^+$ cations and $[OAc]^-$ anions (acetate anion) as the interactions between charged species within BmimOAc are weakened at elevated temperature. The charged species interact specifically with hydroxyl proton and oxygen of cellulose molecules to form electron donor-electron acceptor complexes (EDA) (Pinkert et al., 2009). On one hand, the dissociated charged species diffuse into the space between the cellulose chains. Free acetate anions are then interact specifically with hydroxyl proton of cellulose while $[Bmim]^+$ cations preferably to associate with hydroxyl oxygen of cellulose (Ha et al., 2011). These interactions result in the separation of hydroxyl groups and increase the interlayer spacing between the adjoining cellulose chains which consequently lead to swelling behavior of cellulose fibrils. Thus, cellulose dissolution is facilitated (Kosan et al., 2008). The proposed mechanism of formation of CNPs with BmimOAc solvolysis approach is illustrated in Figure 4.12.

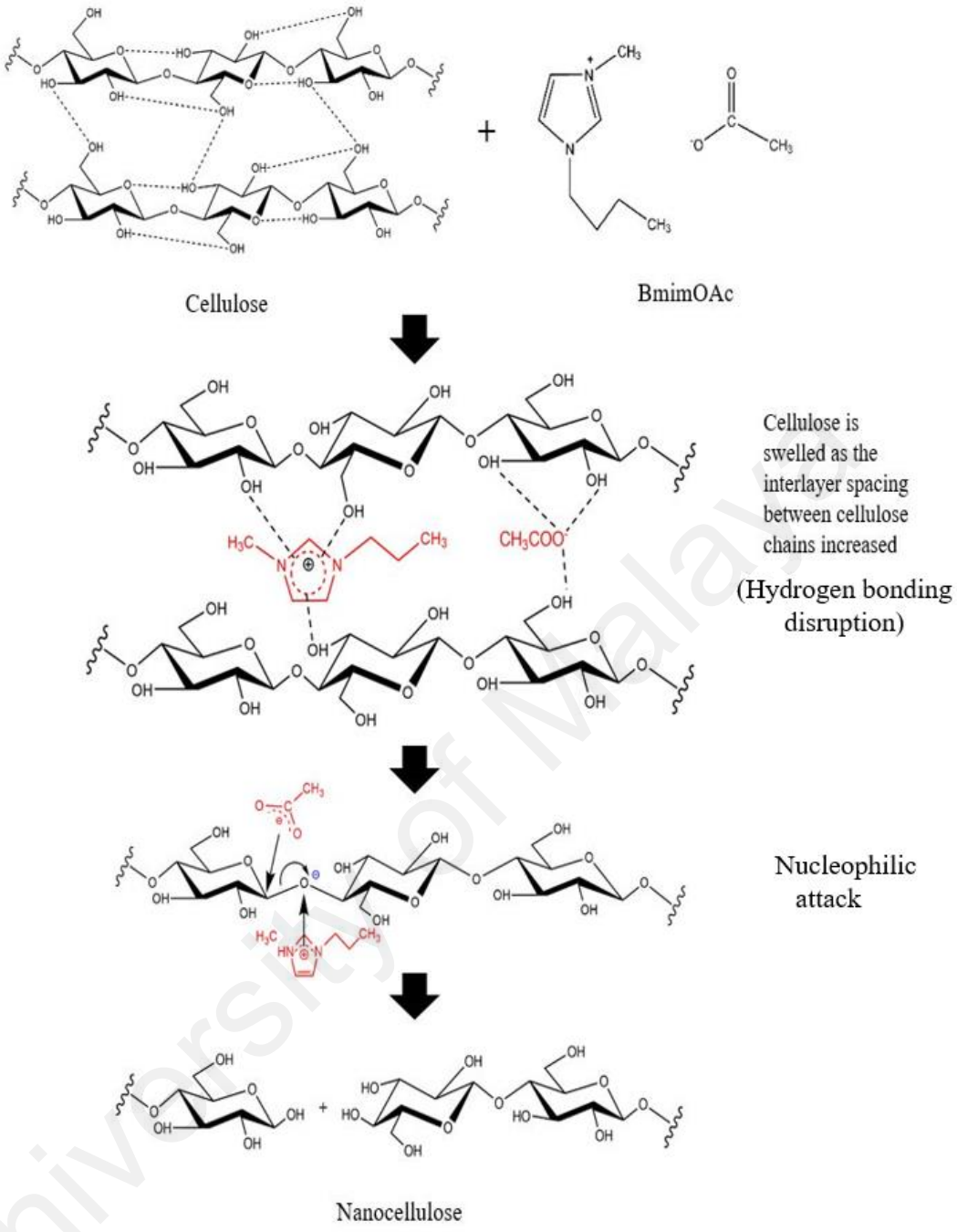

Figure 4.12: Proposed mechanism of formation of CNPs with BmimOAc solvolysis.

On the other hand, breakage of β-1,4-glycosidic bonds is possible to occur within the cellulose chains. Ordinarily, the β-1,4-glycosidic bonds are not too difficult to break. However, because of these hydrogen bonds, cellulose can form very tightly packed crystallites which constitute for its stiffness such that neither water molecules can penetrate through it. These bonds are required to be broken to render cellulose to be

inactively strong such that high electronegativity molecules have good affinity on it (Otulugbu, 2012; Soni, Hayes, & Srivastava, 2004). Acetate anions are good nucleophile but they are not sufficiently strong to substitute the hydroxyl groups. The carbon atom of β-1,4-glycosidic bonds is attacked by acetate anions whereas the glycosidic oxygen atom is interacted with the electron-rich aromatic π system of $[Bmim]^+$ via non-bonding or π electrons. As a result, network of intermolecular hydrogen bonding between neighbouring cellulose chains and β-1,4-glycosidic bonds within the same cellulose chains are broken down which lead to dissolution and degradation of cellulose into molecular level (Han et al., 2013; Kosan et al., 2008). It is suggested that the acetate anions are particularly playing major role in governing the effective dissolution of cellulose. The dissolution of cellulose in BmimOAc is inferred by the establishment of strong hydrogen bonding between acetate anions with hydroxyl groups of cellulose.

On contrary, $[Bmim]^+$ cations only weakly interact with hydroxyl groups through hydrogen-bonding (Jiang et al., 2012). The existence of aromatic imidazolium ring of $[Bmim]^+$ cations are to promote electron delocalization in order to enhance the electronegativity of the anions which in turns, dominate the hydrogen bonds forming capability with the cellulose. Joint interactions of both $[Bmim]^+$ cations and acetate anions with hydroxyl groups contributed to the dissolution of cellulose in IL (Ha et al., 2011). As a consequence, pristine hydrogen bonding network within cellulose is extensively disrupted while the formation of hydrogen bonds between cellulose and BmimOAc is facilitated and more established. The disruption on inter and intra hydrogen bonding within cellulose is attributed to the swelling of cellulose induced by IL. Consequently, the hydrogen bonds within the pristine cellulose get disrupted in such a way that they lose their tightly, rigid and ordered packed structure. Meanwhile, intercalation of ions of IL increased the interlayer spacing between cellulose and disrupted the hydrogen bonding

within the crystalline domains. Hence, the cellulose dissolution is accompanied with swelling of cellulose with certain degree of structural disruption.

Apparently, the regenerated CNPs are swelled after the dissolution process, in comparison to pristine MCC. The diffusion of charged species of BmimOAc into the matrix of cellulose chains caused the interlayer spacing between chains to increase. This contributed to the swelling behavior of regenerated CNPs that subsequently enhanced the dissolution in BmimOAc (Brandt et al., 2010). As a result, CNPs that regenerated from BmimOAc dissolution experience certain degree of swelling at different synthesis conditions (Ang et al., 2012). It is noteworthy that dissolution and swelling of cellulose in BmimOAc are mainly temperature and time-dependent. High temperature and prolonged dissolution likely facilitate the dissolution and swelling of cellulose. Thus, hydrogen bonding within cellulose are disrupted and break down due to the interactions of acetate anions at higher temperature as rapid dissolution occurred and are intensified over time (Wang, Li, Cao, & Tang, 2011).

Hydrogen bonding properties also plays a crucial role in the regeneration and reconstruction of cellulose structure (Swatloski et al., 2002). CNPs can be easily reconstituted from the BmimOAc/cellulose mixture by the addition of anti-solvent such as water. Water is functions as an anti-solvent because it benign for the withdrawal of acetate anions from cellulose by means of competitive hydrogen bonding that results in the precipitation of cellulose. The hydrogen bonding between BmimOAc and cellulose is weakened and get disrupted when excess water is added into the system as BmimOAc has higher affinity to water and more preferentially to form hydrogen bonding with water molecules.

The interaction energies between BmimOAc and cellulose prone to decrease as more water is present in the system. On the other hand, the number of hydrogen bonding

increases because of the preferentially of BmimOAc to form hydrogen bonding with water molecules. As a consequence, the interaction energies and number of hydrogen bonds between BmimOAc and water molecules are increase when more water is present in BmimOAc/cellulose system. It is evidenced that OH…O type hydrogen bonds are much stronger than the CH…O type hydrogen bonds as O-H bonding has higher electronegativity than the corresponding C-H type hydrogen bonding. Hence, the number of OH…O type hydrogen bonds are higher than CH…O type hydrogen bonds and formed readily with the addition of water. It is suggested that interaction energies for BmimOAc-water are much higher than that of BmimOAc-cellulose when two or more water molecules interact specifically with BmimOAc. This signifies precipitation of cellulose is due to preference of water molecules to interact with BmimOAc. Therefore, reconnection of hydrogen bonding between loose cellulose molecules caused the cellulose to precipitate as the regenerated cellulose and contributes to the changes in the crystalline structure of CNPs (Ding et al., 2012; Han et al., 2013; Swatloski et al., 2002).

Furthermore, anions of IL proven to be of critical importance in dictate the interaction of IL with water molecules while the cations are of less significance (Cammarata, Kazarian, Salter, & Welton, 2001). The absolute value of interaction energy is 5.24 kJ/mol when there is only one water molecule interacts with acetate-based IL through the cationic component. In opposite, the absolute value of interaction energy is 75.05 kJ/mol when the interaction is based on anion parts for one water molecule. This implies that anions of IL interact more specifically with water molecules than the cations. The strength of interactions of ionic species of IL with water molecules has been reported to follow the trend of anion–H_2O > cation–H_2O (Ding et al., 2012).

In summary, CNPs can be acquired from BmimOAc via a solvolysis approach in which the effective dissolution of cellulose is prompted and meantime, it catalyzes the

nucleophilic attacks to the glycosidic bonds. The significance of interactions between IL and hydroxyl groups of cellulose lead to the breakage of hydrogen bonding between the cellulose chains. Meanwhile, the cleavage of β-glycosidic bonds caused the formation of molecular level cellulose at nanometer scale.

4.3.2 X-ray Diffraction Analysis

XRD analysis is adopted to study the changes in the crystalline structure, crystallinity as well as crystallite size of CNPs after the dissolution and regeneration in BmimOAc. Figure 4.13 presents the XRD diffraction patterns of CNPs obtained at different synthesis parameters. Interestingly, XRD patterns of CNPs are apparently different from MCC as the diffraction peaks were shifted to lower Bragg angle. MCC exhibits a sharp and prominent crystalline peak at 2θ=22.5º which attributed to the characteristic cellulose *I* structure. However, a less crystalline structure of CNPs is confirmed by XRD analysis with the existence of a broad crystalline peak at position 20.2º corresponds to the characteristic cellulose *II* structure. The diffraction peaks of CNPs at 2θ= 12.2º, 20.2º and 21.7º are corresponding to (-110), (110) and (020) crystallographic planes of typical cellulose *II* structure respectively (Lu et al., 2015).

In comparison to the diffraction pattern of pristine MCC (cellulose *I*), a new peak is evidenced at 12.2º and the (200) crystalline peak of cellulose *I* is split into two broad and overlapped peaks around 20.2º and 21.7º. The shift of the main peaks to lower Bragg angle manifests the increase in the space between stacked sheets of cellulose molecules and the broader peak indicates smaller crystallites structure of CNPs. This implies that transformation of crystalline structure from initial cellulose *I* to cellulose *II* has took place after the dissolution and regeneration (solvolysis) in BmimOAc (Han et al., 2013). It is suggested that the dissolution of cellulose in BmimOAc reasonably caused the swelling

of cellulose and substantially disrupted the van der Waals forces as well as hydrogen bonding between the cellulose chains (Tian et al., 2014).

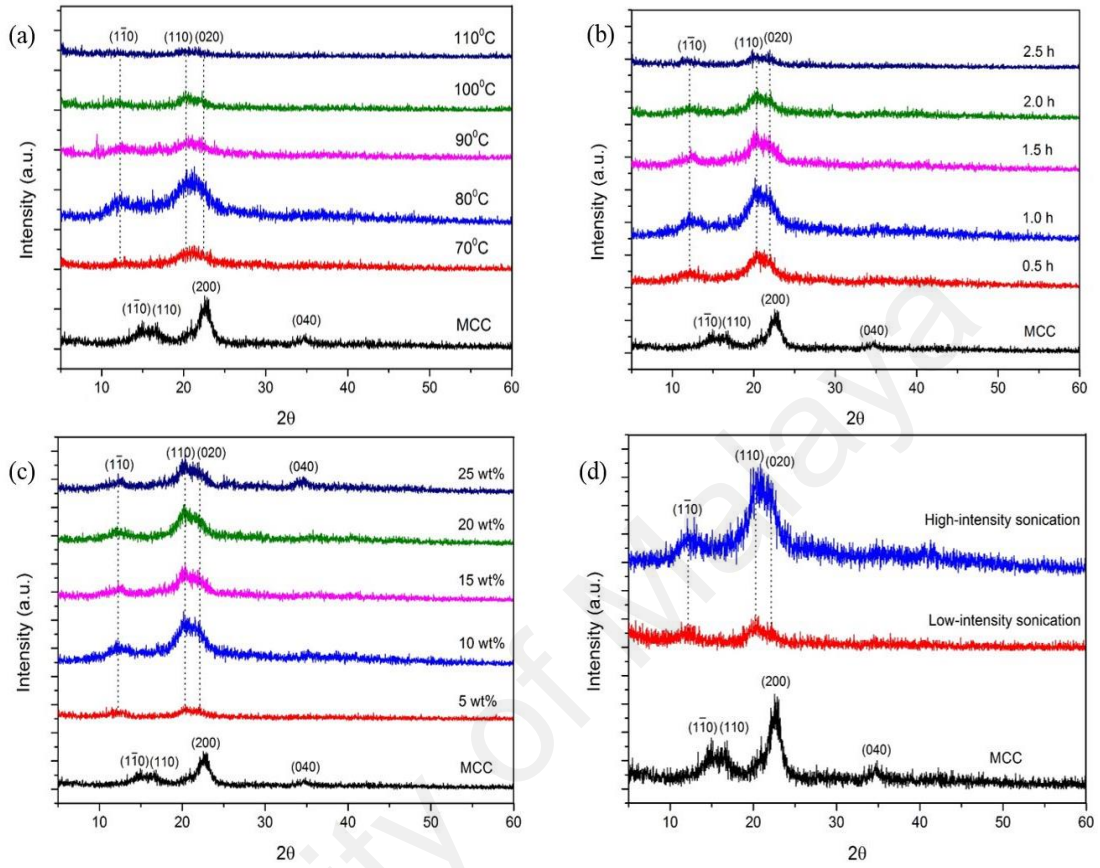

Figure 4.13: XRD patterns of MCC and CNPs optimized with different parameters (a) temperature, (b) time, (c) cellulose concentration (mass loading of MCC), and (d) ultrasonication conditions.

It is noteworthy that the intensity of the crystalline peaks of CNPs are reduced significantly as compared to the pristine MCC. This implies the lower crystallinity of CNPs than MCC as CNPs likely have a higher amorphous content. Lower crystallinity signifies a more amorphous structure of cellulose *II* and hence, a more disordered structure (Han et al., 2013; Sun et al., 2015). Overall, the synthesis of CNPs in BmimOAc comprising three essential steps: fibers swelling, disruption of the crystalline areas and formation of new crystalline lattice upon addition of anti-solvent. During the solvolysis, it is suggested that swelling of cellulose is attributed to the intercalation of ions of IL into the matrix which increased the interlayer spacing of cellulose chains. The free ions of IL not only disrupted the van der Waals forces within the amorphous regions, but also

induced the breakdown of interconnected hydrogen bonds within the crystallite domains. The cellulose loses its stiffness and bonds were reconnected to form a more amorphous structure of CNPs. Transition of the crystalline form probably due to the easy association and rearrangement in intermolecular hydrogen bonding or aggregation of cellulose chains in BmimOAc upon dissolution and regeneration (Pang et al., 2015). The lower crystallinity of CNPs are ascribed to the disruption of hydrogen bonding primarily within the crystalline domains of cellulose chains by interaction with BmimOAc that resulted in higher amorphousity of CNPs.

Table 4.5 shows the crystallinity index and crystallite size of CNPs calculated based on Segal's formula and Scherrer's equation, respectively from XRD results. Temperature of reaction is known to be the main factor to influence the crystallinity of CNPs. The crystallinity of CNPs initially increased from 59.4 to 78.8 when the reaction temperature is increased from 70 ºC to 80 ºC. However, crystallinity of CNPs dropped tremendously from 78.8 to 39.2 with elevating temperature from 80 ºC to 110 ºC. Interestingly, the highest crystallinity CNPs is successfully obtained at a moderate temperature of 80 ºC. The proportional initial increase in the crystallinity of CNPs is postulated due to degradation of internal bonds (non-covalent interactions) in the amorphous parts of cellulose chains. On the other hand, crystallinity dropped with increasing temperature is due to the breakage of hydrogen bonds within the crystalline domains of cellulose chains after the degradation of amorphous fractions (Mohkami & Talaeipour, 2011). Low temperature is just able to overcome the weak van der Waals forces within the amorphous or disordered regions. While high temperature is essentially required to break the intricate network of hydrogen bonding within the crystalline domains.

Table 4.5: Crystallinity index and crystallite size of CNPs.

Sample	Crystallinity index, CrI (%)	Crystallite size, D_{XRD} (nm)
a) Temperature (ºC)		
70	59.4	1.9
80	78.8	2.7
90	58.6	2.7
100	45.5	2.7
110	39.2	2.9
b) Time (hour)		
0.5	69.2	3.2
1.0	78.8	2.7
1.5	71.4	2.2
2.0	63.7	2.5
2.5	58.3	2.3
c) Percent mass loading of MCC (wt%)		
5	40.1	2.8
10	78.8	2.7
15	68.8	2.5
20	67.5	2.5
25	66.8	2.5
d) Sonication treatment		
Low-intensity sonication	64.1	4.3
High-intensity sonication	82.3	2.4

The lower crystallinity of CNPs is presumably attributed to the swelling of cellulose structure due to interaction of BmimOAc that facilitated at higher temperature. In general, dissolution of cellulose is prompted relatively to the increasing reaction temperature (Kosan et al., 2008). The charged species of BmimOAc are dissociated readily into individual $[Bmim]^+$ and $[OAc]^-$ ions as the bonds are weakened at higher temperature (Pinkert et al., 2009). The free acetate anions with higher mobility are then interact specifically with hydroxyl groups of cellulose and established the hydrogen bonding with cellulose chains (Han et al., 2013). Thereafter, the pristine hydrogen bonding network between cellulose chains are disrupted or breakdown and lead to higher dissolution rate of cellulose in BmimOAc at higher temperature. The extensive decomposition of hydrogen bonding within the crystalline domains of cellulose results in the crystallinity reduction of CNPs at elevated temperature (Han et al., 2013; Kosan et al., 2008; Mohkami & Talaeipour, 2011). The dissolution of cellulose is attributed to the disruption made to

the intricate network of hydrogen bonding in cellulose. Cellulose loses its stiffness as well as structure rigidity and bonded to the free ions of IL to become a soluble complex. Hence, BmimOAc with electronegativity character is benign for the dissolution of cellulose.

In addition, apparent darkening of the cellulose suspension at temperature ≥100 ºC suggested the complete dissolution and possible degradation of cellulose into glucose monomer units. This was found in good agreement with the results reported by Wang et al. (2011) where swelling happened at a temperature of 70 ºC and dissolution at 100 ºC. Similar finding was obtained for increased dissolution rate with increasing temperature. Thus, dissolution and swelling of cellulose in IL is temperature-dependent and dissolution is promoted at temperature beyond 100 ºC. At higher temperature (≥100 ºC), dissolution rate is the fastest which evidenced by the disappearance or complete dissolution of MCC after only 10 minutes of addition and cellulose was observed to dissolve completely in BmimOAc in a shorter time. Moreover, cellulose was started to degrade at a higher temperature of 110 ºC which illustrated by the formation of yellowish-brown color suspension as shown in Figure 4.14. This phenomenon indicates the possible occurrence of degradation into glucose monomers. Therefore, experimental conditions of 80 ºC was selected as the optimum temperature of synthesis of CNPs in BmimOAc as a compromise to allow slow dissolution of cellulose at a moderate pace while avoiding the possibility of cellulose degradation.

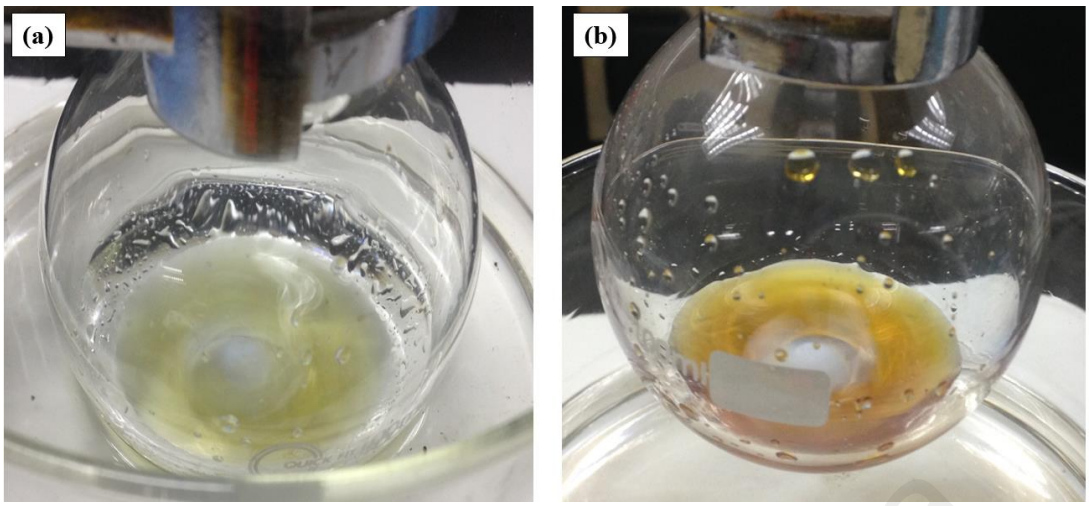

Figure 4.14: Observation of color of cellulose/BmimOAc suspension during the reaction at (a) temperature below 100 °C and (b) temperature of 110 °C.

Besides that, the crystallinity of CNPs also influenced by the reaction time. Crystallinity of CNPs is firstly increased from 69.2 to 78.8 when the reaction time was increased from 0.5 to 1 hour. When the dissolution time was extended up to 2.5 hours, crystallinity of CNPs dropped gradually from 78.8 to 58.3. This signifies the dissolution of cellulose increased proportionally with time and caused the crystallinity to decline over time. As the reaction time increased, a higher number of BmimOAc molecules acquired higher mobility and dissociated into the individual ions. The free ionic species of BmimOAc become more readily to diffuse into the cellulose matrix and consequently increased the interlayer spacing between cellulose chains (Han et al., 2013; Kosan et al., 2008). The swollen cellulose structure eases the breakage of hydrogen bonds in the crystalline regions of cellulose chains and contributed to the lower crystallinity of CNPs (Mohkami & Talaeipour, 2011).

The cellulose structure is swelled relatively with increasing dissolution time. It is noteworthy that the most severely swollen cellulose structure is obtained at prolonged dissolution (2.5 h). The crystallinity reduction of CNPs at prolonged dissolution is attributed to the highest degree of swelling and thus, structural disruption of cellulose. The disruption to the crystalline structure of CNPs results in the collapse of the pristine

cellulose ordered structure after the solvolysis due to the breakdown of hydrogen bonding network (Lu et al., 2015). Interestingly, CNPs with higher crystallinity could be obtained at 1 hour of dissolution in which the highest crystallinity is obtained throughout the time frame studied. Shorter dissolution time and moderate reaction temperature were preferably selected to allow sufficient dissolution while minimizing the possibility of extensive disruption caused to the crystalline structure. During the regeneration process, the crystallites most likely have incomplete growth and results in the increase of the amorphous content of CNPs. Crystallite size decrease is inferred by an increase in peak broadening with the incomplete growth of the crystallites.

In the current section, the effect of cellulose concentration (expressed in terms of mass loading of MCC into IL) on the crystallinity of CNPs is discussed. The lowest cellulose concentration (5 wt% MCC) indicates the presence of higher number of BmimOAc molecules in the mixture which resulted in the formation of CNPs with very low crystallinity (40.1). This is reflected by an apparent quite flat diffraction pattern for CNPs with very low crystallinity and higher amorphous content. Lower cellulose concentration favoured the dissolution of cellulose because of the greater solvating power of BmimOAc at low viscosity condition as the free ions acquired higher mobility. The lower viscosity of IL/cellulose suspension would beneficial for the mass transfer as well as promote the mobility of the ions. The ions in a lower viscosity medium can acquired higher kinetic energy and travelled faster for a reaction to take place. The increased diffusion of ions into the gap between the hydrogen bonded sheets of cellulose chains lead to more intercalation of ions into the cellulose lattice and subsequently disrupted the ordered lattice. After a complete swollen state is formed, the ions diffused into the inside of the crystals and underwent a thorough reaction with cellulose molecules. The breakdown of hydrogen bonds initiated cellulose dissolution and swelling of cellulose induced the

crystalline structure disruption which in turns, resulted in crystallinity reduction of CNPs after the solvolysis (Chen et al., 2012; Cheng et al., 2012; Sun et al., 2015).

Nevertheless, crystallinity decreased gradually for increasing cellulose concentrations from 10 to 25 wt%. The dissolution of MCC in BmimOAc becomes less effective with increasing cellulose concentrations. This is attributed to the decrease solvating power of BmimOAc with the viscosity increase of the cellulose suspension. Low viscosity will essentially promote the dissolution, presumably due to higher mobility of ions. On contrary, higher cellulose concentration contributes to viscosity build up that dramatically restrict the mobility of ions and eventually retard the ion diffusion to impede cellulose dissolution. The complete dissolution of 25 wt% MCC will not happen because BmimOAc is saturated with cellulose molecules and cannot effectively dissolve a higher quantity of cellulose. Consequently, less disruption is caused to the crystalline structure and lead to no drastic reduction in the crystallinity of CNPs. In addition, a small portions of cellulose *I* structure remained intact in CNPs after dissolution in BmimOAc at 25 wt% MCC. This is revealed by the presence of a distinct small peak at 34.5º (040) which signifies the coexistence of cellulose *I* and *II* structure with higher amorphous content. BmimOAc is in the supersaturation state with cellulose molecules. In summary, lower cellulose concentration is more favorable for the effective dissolution of cellulose.

Apart from that, different ultrasonication treatments also significantly affected the crystallinity of CNPs. On contrary to low-intensity sonication, high-intensity ultrasonication contributes to the formation of higher crystallinity CNPs. Improvement in crystallinity is evidenced by the existence of sharper and prominent of the (020) crystalline peak (Tang et al., 2013). This is because high-intensity ultrasonication produced a very strong and intense mechanical oscillating power due to acoustic cavitation phenomenon. During the process, cavitation leads to the formation, growth and

implosion of bubbles occurred continuously as the molecules absorb the ultrasound energy transmitted to the cellulose chains (Filson & Dawson-Andoh, 2009; Li, Yue, & Liu, 2012; Suslick et al., 1991). The collapse of these bubbles generates a large amount of energy and violent mechanical shock wave is given to the cellulose chains (Hamid et al., 2016). Consequently, high amplitude of vibrational energy due to high-intensity ultrasound transmits mechanical shearing forces to break down the interconnected network of hydrogen bonds and caused damage to the van der Waals forces between the cellulose chains within amorphous regions. Sonochemistry is the energy generated by cavitation and it is approximately 10−100 kJ/mol, which is within the hydrogen bond energy scale (Tischer, Sierakowski, Westfahl, & Tischer, 2010). Hence, the disintegration of macro-cellulosic fibres into nanofibers or nanoparticles is facilitated and beneficial for isolation of CNPs with higher crystallinity as the amorphous regions is seriously disrupted due to impact of ultrasonic. On the other hand, less profound cavitation effect and vibrational energy generated by ultrasonic bath only breaks the weak bonds of amorphous cellulose, while the inter layers of cellulose are remained partially disentangled and disintegrated. High-intensity ultrasonication deduced to be effective in the production of higher crystallinity of CNPs (Li et al., 2015).

In conclusion, XRD analysis verified the fact that native cellulose experienced a structural transformation from its initial cellulose *I* to terminated phase of cellulose *II* in CNPs with a remarkable reduction in crystallinity after the solvolysis process in BmimOAc. The hydrogen bonds in cellulose *II* are found between sheets, which manifesting a three-dimensional (3D) network whereas hydrogen bonds in cellulose *I* are among chains that exist merely in the same sheet. Therefore, CNPs achieved a more stable crystal structure due to reorganization and rearrangement of hydrogen bonds between cellulose (Pang et al., 2014; Pang et al., 2015).

4.3.3 Hydrodynamic Size and Zeta Potential Analysis

Table 4.6 shows the hydrodynamic size, PDI and zeta potential values of CNPs obtained at different synthesis parameters. The hydrodynamic size of CNPs increased dramatically with the increase in temperature and time, alongside with increase in PDI. This signifies that CNPs synthesized at higher temperature and exposed to prolong dissolution exhibit larger sizes with less uniformity in size distribution. Interaction between cation and anion of BmimOAc was weakened at higher temperature and with over time, so as the dissociation of ion pairs into individual charged species increased. The free ions acquired greater mobility at higher temperature and their motions become intensified over time. The diffusion of ions into the cellulose chains is then increased and subsequently, more intercalation of ions into the lattice resulted in the swelling of the cellulose structure (Zhao et al., 2012). The larger hydrodynamic sizes of CNPs at higher temperature and prolonged dissolution are inferred by extensive swelling of cellulose structure. The size distribution also becomes less uniform with increasing temperature and time, likely attributed to different degree of swelling of cellulose particles and hence, yield different hydrodynamic size when dissolved in water. Therefore, dissolution and swelling of cellulose in BmimOAc are both temperature and time-dependent. It is important to have controllable experiment parameters such that the extensive swelling of cellulose can be avoided by performed the solvolysis or dissolution process in shorter duration of time at relatively low-to-moderate reaction temperature.

Table 4.6: Hydrodynamic size, polydispersity index and zeta potential of CNPs.

Sample	Hydrodynamic size (nm)	Polydispersity index, PDI	Zeta Potential (mV)
a) Temperature (ºC)			
70	59.34	0.216	-19.7
80	66.67	0.245	-22.3
90	67.13	0.375	-23.5
100	76.78	0.433	-24.1
110	99.84	0.478	-25.2
b) Time (hour)			
0.5	60.13	0.193	-13.7
1.0	66.67	0.245	-22.3
1.5	85.21	0.282	-25.3
2.0	98.63	0.331	-27.0
2.5	109.00	0.448	-29.9
c) Percent mass loading of MCC (wt%)			
5	105.90	0.309	-27.5
10	66.67	0.245	-22.3
15	86.37	0.315	-20.0
20	92.94	0.477	-13.2
25	108.60	0.527	-10.0
d) Sonication treatment			
Low-intensity sonication	62.30	0.473	-17.1
High-intensity sonication	49.36	0.216	-23.9

Apart from that, it is worth noting that larger sizes of CNPs (105.90 nm) is obtained at the lowest cellulose concentration (5 wt%). This is because of the greater solvating power of BmimOAc at lower cellulose concentration is more favorable for cellulose dissolution. The formation of larger size CNPs is attributed to the presence of greater number of individual charged species with higher mobility to diffuse into the cellulose lattice to cause it to swell severely (Cheng et al., 2012). Hydrodynamic size of CNPs also dependent on the cellulose concentrations. Interestingly, the hydrodynamic size of CNPs is increased proportionally with increasing cellulose concentrations from 10 to 25 wt%. In addition, the PDI values also increased apparently, suggesting the lower uniformity in size distribution. This is ascribed to the lower solvating power of BmimOAc with the viscosity increase of BmimOAc/cellulose suspension for higher cellulose concentration. These slow down the ion diffusion and eventually impede the dissolution as the stiring

process becomes difficult (Quan et al., 2010). The larger hydrodynamic size of CNPs is presumably due to the ineffective dissolution because of the saturation of BmimOAc with cellulose molecules (Xu et al., 2013). For instance, the largest size CNPs (108.60 nm) is acquired at the highest cellulose concentrations of 25 wt%, likely due to the incomplete dissolution of MCC in BmimOAc. As a consequence, some cellulose are able to dissolve, whereas a small part of it might retained the crystalline cellulose *I* structure with bigger diameter. This essentially leads to the increase in PDI as cellulose molecules are constitute of different sizes and lowers the colloidal stability as some larger particles tend to precipitate down the solution.

Furthermore, hydrodynamic size of CNPs is also affected by the application of different ultrasonication treatments. Interestingly, CNPs prepared using high-intensity ultrasonication is significantly smaller in size with more uniform size distribution as compared to low-intensity sonication. This can be explained by the effect of acoustic cavitation. During high-intensity ultrasonication, the intense ultrasound energy is transmitted into the cellulose chains through a cavitation process via the growth and expansion of cavitation bubbles (Chen et al., 2011). The collapse of these bubbles generates an intense amount of energy to provide the powerful mechanical oscillating power which caused delamination or defibrillation to occur that diminished the interlayer hydrogen bonding network between the cellulose chains (Guo et al., 2016). Consequently, the ether linkages, as well as the hydrogen bonding network are broken down upon ultrasonication treatment due to highly intensive and violent shock waves, thereby releasing CNPs with smaller dimensions. The cellulose particles were further disintegrated and fragmented into smaller dimensions under the intensive mechanical shearing force (Lu et al., 2014). Thus, high-intensity ultrasonication is useful to isolate smaller dimensions of CNPs by hydrodynamic forces of ultrasound (Cheng, Wang & Rials, 2009). Mishra et al. (2012) have suggested the use of high-intensity ultrasound

probe to be more efficient for the production of nanocellulose, instead of using ultrasound bath. They reported a higher yield of nanocellulose can be obtained in a shorter time (yield 100% in 25 min) by using ultrasound probe in contrast to lower yield of nanocellulose to be obtained in a longer time (yield 50% in 60 min) by using ultrasound bath (Mishra, Manent, Chabot, & Daneault,2012). CNPs produced by high-intensity ultrasonication are constitute of smaller size and more uniformly distributed.

Zeta potential is the measure of electric potential in the interfacial double layer. It is important to denote the stability of a colloidal suspension. The mobility distribution of charged particles under an electric field is measured and determined as zeta potential (Satyamurthy & Vigneshwaran, 2013). Zeta potential characterization enables a clear illustration of surface charge and colloidal stability in a solvent. The surface charges of CNPs are influenced by the breakdown of hydrogen bonds as revealed from the zeta potential measurement presented in Table 4.6. In general, value between 0 to ± 15 mV indicates the onset of agglomeration and flocculation. Values between 15 to ± 30 mV are used to represent good stability of the colloidal suspension due to mutual repulsion of charges.

In the present study, improved colloidal stability of CNPs suspension is inferred by higher absolute zeta potential values with increasing temperature and time. The fracture of molecular chains in cellulose is prompted at higher temperature and prolonged dissolution as the individual ions of BmimOAc acquired greater mobility and their motions being intensified. As a consequence, the hydrogen bonding within cellulose are disrupted (Zhao et al., 2012). The breakage of intermolecular O(6)-O(3) hydrogen bonds network underlies between the cellulose polymer chains suggested to generate a higher density of hydroxyl groups exposed on their surface (Guo et al., 2016). The exposure of free hydroxyl groups on the surface of CNPs as negatively charged groups favoured the

formation of electrostatic layer to cover the particles and enhanced the dispersion in water (Lu et al., 2015). Therefore, the higher stability of the colloidal suspension is associated with the exposure of higher number of free hydroxyl groups.

Besides that, the colloidal suspension is much more stable at lower cellulose concentration. This is presumably due to the effective dissolution of cellulose and better solvating power of BmimOAc which caused disruption and breakage of hydrogen bonds to increase the exposure of hydroxyl groups on the surface in order to create a more stable colloidal suspension (Zhao et al., 2012). However, the colloidal stability decreased with increasing cellulose concentrations because less disruption and hydrogen bonds breakage took place due to the lower solvating power of BmimOAc. This implies the presence of small number of negatively charged hydroxyl groups is available for the electrostatic repulsion. The higher the cellulose concentration, the lower the stability of the colloidal suspension.

Moreover, high-intensity ultrasonication confers CNPs suspension with higher colloidal stability. By comparison, lower stability of CNPs suspension is provided by low-intensity sonication treatment which revealed by its higher zeta potential value. The highly intensive vibrational energy and violent mechanical shock generated by high-intensity ultrasonication have created significant impact on the delamination and defibrillation of cellulose fibers as well as breakage of hydrogen bonding between the cellulose polymer chains (Guo et al., 2016; Hamid et al., 2016; Lan et al., 2011; Lu et al., 2014). As a result, the chains are separated between each other from van der Waals forces and interconnected hydrogen bonds to expose many of the hydroxyl groups on the cellulose surface for electrostatic repulsion and accounted for its higher stability. In addition, the higher stability of CNPs suspension is also presumably attributed to smaller size particles that bear more charges on their surface for repulsion. In contrast, low-

intensity sonication only breaks the weak bonds such as van der Waals forces in cellulose. Steric hindrance and/or entanglement effect due to high-intensity ultrasonication effectively stabilized the CNPs suspension (Satyamurthy & Vigneshwaran, 2013). High-intensity ultrasonication is able to produce good stability of nanocellulose colloidal suspension with enhanced dispersion.

4.3.4 Fourier Transform Infrared Spectroscopy (FTIR) Analysis

FTIR analysis is conducted in order to gain more insight into the effects of varying synthesis parameters on the chemical and structural characteristics of CNPs. The changes in the structural modification after solvolysis in BmimOAc were also investigated by FTIR spectroscopy. There are some important functional groups within the linear polymeric structure of cellulose units. Figure 4.15 presents FTIR spectra of CNPs synthesized with BmimOAc at different synthesis parameters.

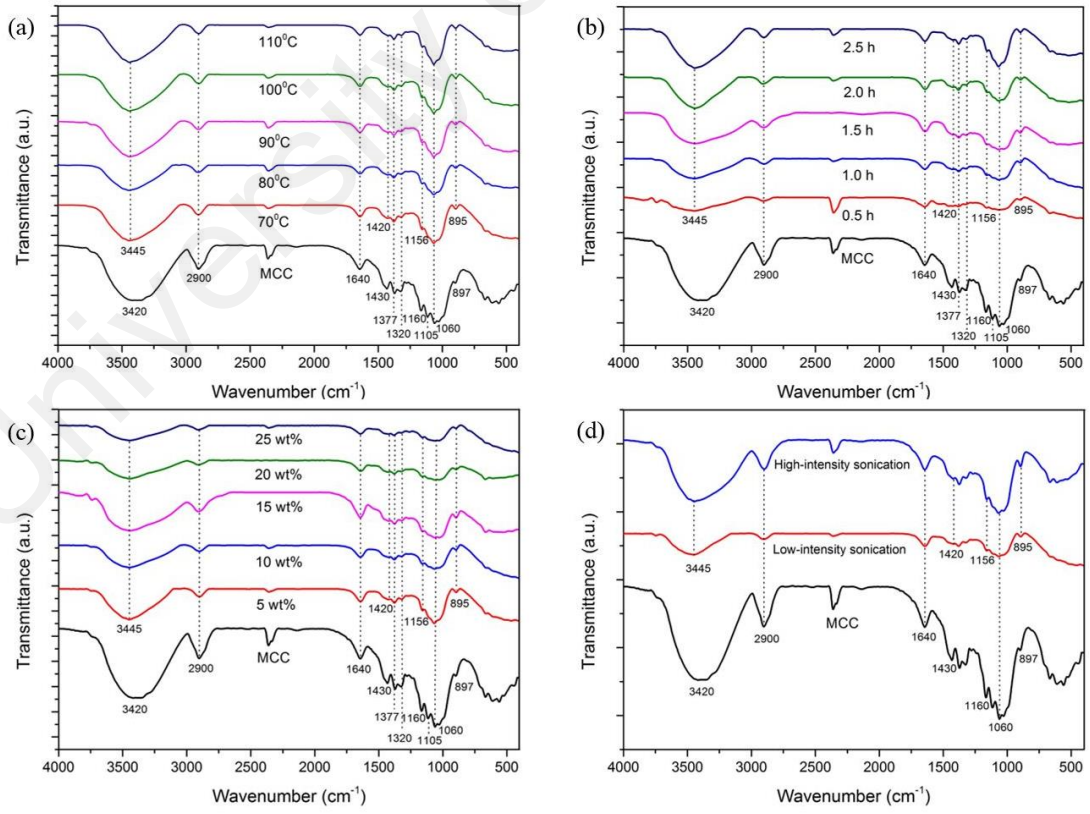

Figure 4.15: FTIR spectra of CNPs optimized with different parameters (a) temperature, (b) time, (c) cellulose concentration (mass loading of MCC), and (d) ultrasonication conditions.

In general, all cellulose samples including pristine MCC and synthesized CNPs exhibit broad band in the region of 3000 to 3600 cm^{-1} which is attributed to the stretching vibration of O-H due to existence of hydroxyl groups. In particular, the band at 3420 and 3445 cm^{-1} are mainly related to the intramolecular O(2)H--O(6) bonding within the cellulose chains (Chen et al., 2012; Fan et al., 2012; Poletto et al., 2014). Interestingly, the free O-H stretching of CNPs is shifted to slightly higher wavenumber as compared to corresponding MCC. In addition, the apparent much weaker and broader bands signify the weakened hydrogen bonding within CNPs after solvolysis in BmimOAc. This implies disruption of hydrogen bonding network occurred in CNPs during dissolution process. Besides that, it is likely that the number of hydrogen bonding in CNPs is diminished which caused the bands to shift from 3420 cm^{-1} in pristine MCC to a higher wavenumber of 3445 cm^{-1} in CNPs.

The band at 2900 cm^{-1} and 1640 cm^{-1} are assigned to the characteristic C-H stretching vibration and O-H bending vibration of absorbed water, respectively (Han et al., 2013). Cellulose *II* is observed to exhibit higher intensity of this peak as it reflects a greater number of surface hydroxyl groups on CNPs. The hydroxyl groups on CNPs are capable to form ion-dipole and/or dipole-dipole interactions with water molecules which in turns, draw more hydroxyl groups into contact with the surrounding water molecules and makes them more hydrophilic (Ahmadi et al., 2015). Despite that, sufficient space and freedom is provided for each glucose monomer to rotate and bend around the ether linkage for maximizing favorable molecule sub-phase interactions in the amorphous regions of cellulose. While on increasing the crystallinity, the chain flexibility is reduced and render the reorientation of the monomer segments as well as the hydrophilic/water interactions preferentially maximized at the near surface. Small peaks at 1377 cm^{-1} and 1320 cm^{-1} are associated with bending vibration of C-H and CH_2 wagging of the polysaccharide aromatic ring, respectively. The presence of a small peak at 1156 cm^{-1} is due to the C-O

anti-symmetric bridge stretching, whereas a sharp band at 1066 cm^{-1} is attributed to C-O-C pyranose ring skeletal vibration (Maiti et al., 2013; Kokol et al., 2015).

The absorption bands at 1420 cm^{-1} and 895 cm^{-1} can be used to study the polymorphs form of crystalline cellulose and crystallinity changes as FTIR spectrum of cellulose *I* is different from that of cellulose *II* and amorphous cellulose in terms of intensity and position of particular bands (Nelson & O'Connor, 1964a). On contrary to cellulose *I*, the bands at 1430 cm^{-1} is disappeared and eventually shifted to lower wavenumber of 1420 cm^{-1} in cellulose *II*. The band corresponds to $–CH_2$ bending vibration and is the characteristic crystalline band for cellulose *II* and amorphous cellulose (Pang et al., 2015). It is worth noting that CNPs exhibited lower intensity of crystalline band as compared to pristine MCC to evidence the crystallinity reduction in CNPs. Extensive disruption to the hydrogen bonding network of cellulose is due to the interaction with BmimOAc during dissolution which is responsible for the structural transformation and lower crystallinity of CNPs.

The reduced intensity of crystalline bands is simultaneously followed with an increase in the intensity of amorphous band at 895 cm^{-1}. The band at 895 cm^{-1} is the characteristic C-O-C stretching vibration of β-glycosidic linkages and is known as the amorphous band of typical cellulose. This band is more outstanding in cellulose *II* and amorphous cellulose because it is more sensitive to the amorphous content in cellulose. Apparently, the broadening and more resolved of this band signify the higher amorphousity of CNPs as in cellulose *II* structure. Thus, synthesized CNPs are more amorphous than the corresponding MCC in which demonstrates a higher content of disordered structure. The disordered structure of CNPs is likely results from deformation vibration of β-glycosidic linkages as well as the rearrangement in hydrogen bonding during regeneration process. A significant reduction in the intensity of the crystallinity band alongside with an increase

in the intensity of the amorphous band in spectra of CNPs clearly evidenced that MCC lost its crystallinity and integrity as well as underwent a structural transformation from original cellulose *I* into cellulose *II* after solvolysis process in BmimOAc (Adsul, Soni, Bhargava, & Bansal, 2012; Kuo & Lee, 2009; Liu et al., 2015). Therefore, CNPs are mainly composed of crystalline cellulose *II* and amorphous cellulose which is in good accordance with XRD results reported in the earlier section. In addition, the absence of peaks of BmimOAc suggesting the complete removal of IL during the washing step. It can be concluded that the chemical structure of cellulose remains unchanged after solvolysis, and hence, BmimOAc is a non-derivatizing solvent for cellulose (Liu et al., 2015).

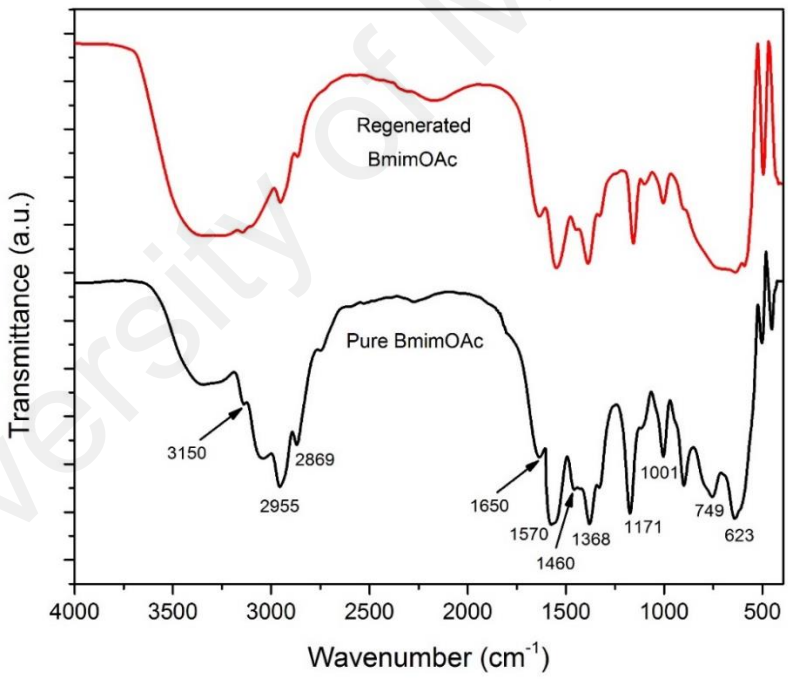

Figure 4.16: FTIR spectra of pure BmimOAc and regenerated BmimOAc.

Apart from that, a FTIR analysis is carried out on pure BmimOAc and regenerated BmimOAc to determine possible changes in chemical structure after the reaction. Figure 4.16 shows FTIR spectra of pure unreacted BmimOAc and regenerated BmimOAc that was recovered after interaction with cellulose. Regenerated BmimOAc exhibits almost similar spectra to the pure BmimOAc which indicates that no significant changes in the

chemical structure of regenerated BmimOAc after the reaction. However, the presence of an additional broad band in the range 3200-3700 cm^{-1} is distinct for the regenerated BmimOAc. The band is the characteristic stretching vibration of –OH that is present in water due to water absorption by IL because IL is highly hygroscopic. Both pure and regenerated BmimOAc exhibit almost similar functional groups and this signifies the potential usage of BmimOAc as a catalyst cum solvent for cellulose depolymerisation because it is recyclable and reusable (Man et al., 2011). In the present study, the yield of recovered BmimOAc is about 86 %. The highly recoverable yield and recyclable properties of IL contribute to the attractive and environmental benign synthetic approach to produce nanocellulose.

From Figure 4.16, a small band at 3150 cm^{-1} is observed in both pure and regenerated BmimOAc, which is attributed to quaternary amine salt formation with acetate anion. Besides that, small peak at around 3103 cm^{-1} is related to the stretching vibration of aromatic =C-H. Two distinct peaks of close proximity at 2955 and 2869 cm^{-1} are associated with the aliphatic asymmetric and symmetric (C-H) stretching vibrations due to methyl groups (Pielesz & Biniaś, 2010). The presence of an absorption band at 1570 cm^{-1} corresponds to in-plane stretching of C=C bonds and 1460 cm^{-1} is due to C=N stretching. A strong band appeared at 1171 cm^{-1} is attributed to the in-plane bending vibration due to methyl groups (CH_2). The existence of several bands at 890-1000 cm^{-1} is the bending vibration of =C-H. Furthermore, peaks at 749 and 623 cm^{-1} are associated with C-N stretching vibration (Dharaskar et al., 2013; Dharaskar et al., 2013; Socrates, 2004). Moreover, the confirmation of acetate anion is evidenced by the presence of bands at 1650 cm^{-1} (C=O stretching) and 1368 cm^{-1} [C-H in –O(C=O)-CH_3] (Adebajo, Frost, Kloprogge, & Kokot, 2006; Spagnol et al., 2012; Sun, Sun, & Sun, 2002). FTIR analysis reveals that regenerated BmimOAc has similar chemical structure as pure BmimOAc.

4.3.5 Morphological analysis by Field Emission Scanning Electron Microscopy (FESEM), Atomic Force Microscope (AFM) and Transmission Electron Microscopy (TEM)

FESEM is adopted to characterize the surface morphology of CNPs in order to study the changes that may be caused by solvolysis in BmimOAc. Figure 4.17 illustrates FESEM images of CNPs synthesized at different temperature. All CNPs showed smooth and homogenous surface morphology after regenerated from BmimOAc (Pang et al., 2015). Nevertheless, the original fibrous structure of cellulose is significantly altered, which give rise to the formation of conglomerate and homogenous texture with irregular shaped after dissolution. In contrast to pristine MCC, it is noteworthy that the intact and rough organized structure that commonly present in native cellulose is absent in CNPs. The images illustrate CNPs are generally composed of enlarged fascicular texture with porous structure organized disorderly in the matrix. This implies that the structure of CNPs is substantially disrupted and more amorphous or disordered with partly fused which indirectly signify the lower crystallinity of CNPs as compared to the pristine MCC (Han et al., 2013). The FESEM images further confirmed the cellulose dissolution in BmimOAc as discussed in the previous sections of XRD and FTIR.

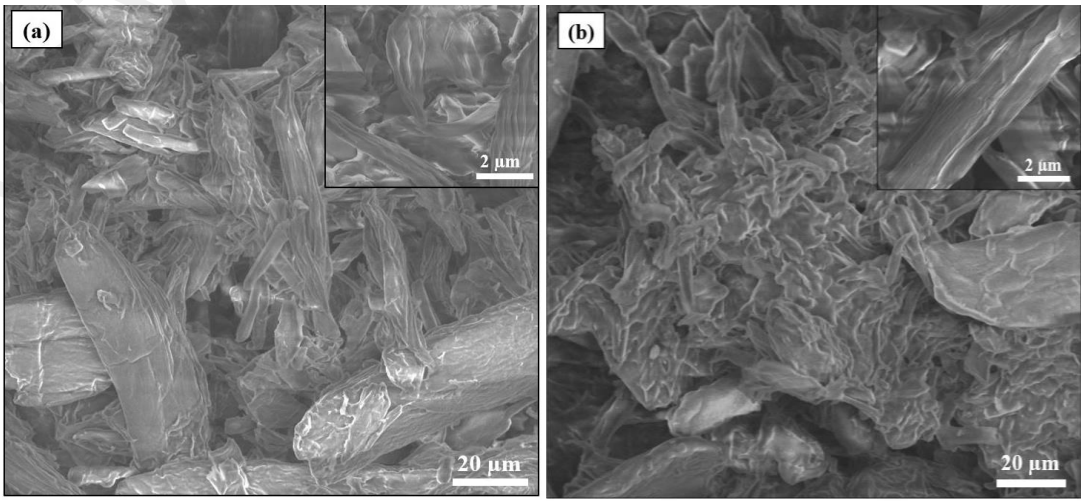

Figure 4.17: FESEM images of CNPs synthesized at temperatures of (a) 70 °C, (b) 80 °C, (c) 90 °C, (d) 100 °C and (e) 110 °C with BmimOAc. Insets are the images of cellulose fibres at 15,000x magnification.

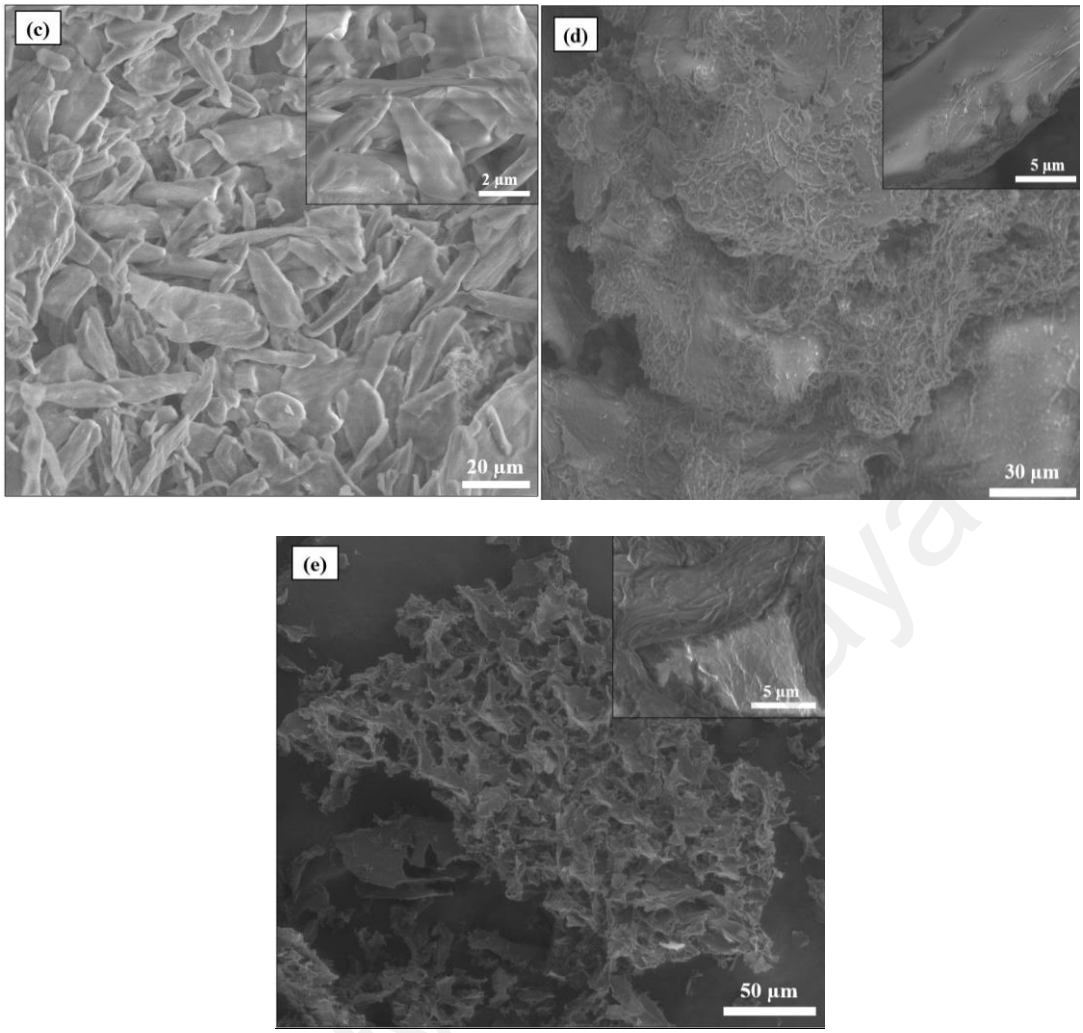

Figure 4.17, continued.

Interestingly, the surface structure of CNPs changed significantly with relatively increase in the synthesis (dissolution) temperature. As depicted in Figure 4.17, the width of the individual cellulosic fibers increased with increasing temperature. This indicates the swelling of cellulose has occurred and is prompted at higher temperature. CNPs experienced the most severe structural disruption when synthesized at higher dissolution temperature, particularly at 110 ºC, followed by synthesis condition at 100 ºC. The fascicular texture of fibers is significantly altered and enlarged with the existence of porous structure when CNPs are synthesized at temperature of ≥ 100 ºC. On contrary, fascicular fibers structure of CNPs is retained alongside with smaller width for the individual fibers when CNPs are acquired at lower temperatures (<100 ºC).

In general, higher temperature essentially facilitated cellulose dissolution. At higher temperature, more charged species dissociated from BmimOAc and they acquired greater mobility to diffuse into the matrix of cellulose. The intercalation of ions caused an increase in the interlayer spacing between cellulose chains and leads to swelling of cellulose structure. As a consequence, CNPs synthesized at higher temperature demonstrate substantially swelling on the surface structure due to serious disruption on the intricate network of hydrogen bonding within cellulose (Xu et al., 2013). The swollen appearance of fibers proved that swelling of cellulose has taken place during the dissolution process. On the other hand, CNPs obtained at lower temperature experienced a lower degree of structural disruption. CNPs are notably homogenous and dense at lower temperature while it becomes more porous at higher dissolution temperature. The uniform microstructure of CNPs fibers indicates that swelling is actually temperature dependent.

After subsequent dissolution and regeneration process, CNPs are obtained as white fluffy mass that consist of fibrillar structures with inter-connecting network of nanofibers after freeze dried. Freezing of dilute CNPs suspension caused free water to form ice crystals which concentrates CNPs to come closer to each other through hydrogen bonding both laterally and longitudinally. Consequently, freeze-drying caused the closely packed CNPs self-assembly to form white and fluffy fibrous mass containing sub-micron wide and micrometer long fibers. The formation of fluffy fibrous solid is facilitated by interfibrilliar attraction via hydrogen bonding among the abundant surface hydroxyl groups. Sublimation of ice crystals then leaves pores on the fibers structures which contributes to the formation of porous and disordered structure of CNPs. The white and fluffy fibrous CNPs are illustrated as aggregation of nanoparticles stringed together among sub-micron wide and exist as irregularly shaped fibers. Freeze drying process presumably contributes to the aggregation of nanoparticles while the intermolecular hydrogen bonding and strong hydrophilic interaction between cellulose chains render the

agglomeration (Chen et al., 2011a; Chirayil, Mathew, & Thomas, 2014a). Cellulose in a suspension tends to form aggregation of bulk structure instead of isolated nanofibers (Jiang & Hsieh, 2013).

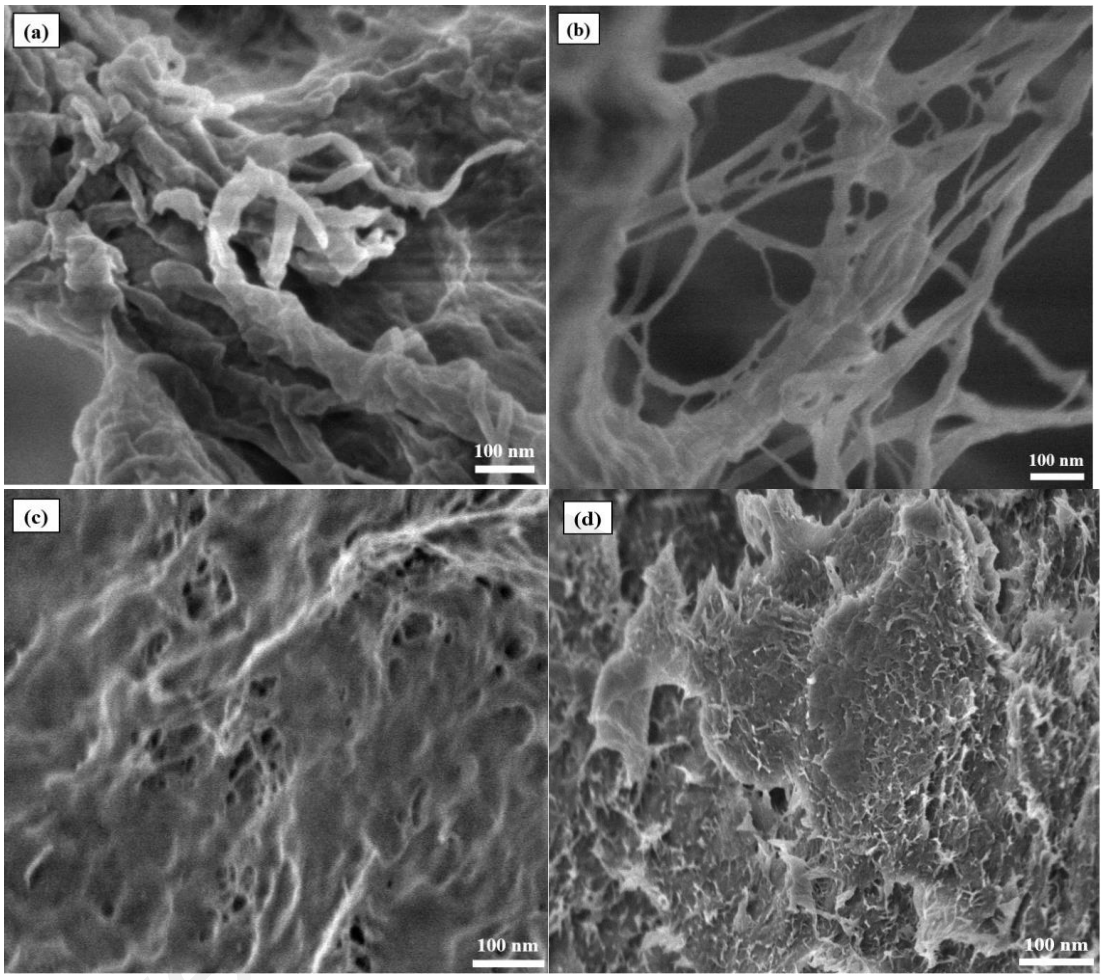

Figure 4.18: FESEM images of CNPs obtained at different dissolution time: (a) 0.5 h, (b) 1.0 h, (c) 1.5 h and (d) 2.0 h.

Figure 4.18 shows FESEM images regarding microstructure morphology of CNPs fibers obtained at different dissolution time, viewed at 50,000x magnification. From Figure 4.18 (a), there is a small number of cellulosic fibers in nanometer scale diameter present on the surface of microfibrils. However, most of the fibers tend to intervene themselves with microfibers and still exist in aggregation. The fibers have non-uniform size and distribute disorderly on the surface. Dissolution time of 1 hour is capable to produce narrower width of cellulosic fibers which can discerned and separated from the microfibers. The long and thin fibrilliar structure signifies lower degree of swelling took

place at short dissolution time and thus, less structural disruption happened. This in turns, leads to the formation of smaller dimension CNPs with retained crystallinity. Nevertheless, the intact fibrillar structure is rigorously altered and more porous structure is obtained at prolonged dissolution. The enlargement of fibers is demonstrated at 1.5 hours of dissolution due to serious swelling of cellulose structure. Cellulose swelled to a greater extent, and eventually the fibrilliar structure is completely destroyed after 2 hours of dissolution. This manifests that substantially surface and structural disruption are impacted on CNPs due to prolonged dissolution of cellulose in BmimOAc. CNPs regenerated after 2 hours experienced the most severe swollen structure and appearance with the existence of porous structure which responsible for their high amorphous content and lower crystallinity as well.

FESEM images are in good consensus with XRD findings in which lower crystallinity and amorphous cellulose structure are obtained after prolonged dissolution. The longer the dissolution time, the lower the crystallinity of CNPs and therefore, the more amorphous the cellulose become. As a matter of fact, the surface of cellulose *II* fibers is observed to be not so homogenous as compared to that of cellulose *I*, presumably related to different cellulose crystal structure.

AFM height images and peak force error of CNPs synthesized at 0.5, 1 and 1.5 hours of dissolution are presented in Figure 4.19. In general, CNPs have a typical granular or spherical shape (Pang et al., 2015). The sizes of granules/particles were measured, as shown in Figure 4.20. The mean particle size is obtained from it. There are some aggregations of particles observed, which presumably is due to the evaporation of water during sample preparation. Meanwhile, some individual CNPs particles are apparently clear in some images. At 0.5 hour, CNPs span larger size distribution where most of them have sizes range from 40 to 60 nm with mean particle size of 53 ± 4.8 nm. Besides that,

there is also some larger particles in the sizes range from 64 to 78 nm which are likely resulting from the ineffective dissolution due to insufficient dissolution time. Interestingly, as dissolution progress to 1 hour, CNPs obtained have smaller and more uniform size distribution within the range 35-51 nm with a mean size of 45 ± 3.1 nm in diameter. On the other hand, wider size distribution in the range 57-82 nm with a larger mean size of 76 ± 2.7 nm CNPs are acquired after 1.5 hours. However, the size distribution is not uniformly distributed for longer dissolution time as it tends to span a relatively larger area. In summary, dissolution time of 1 hour is able to produce smaller dimension and uniform size CNPs.

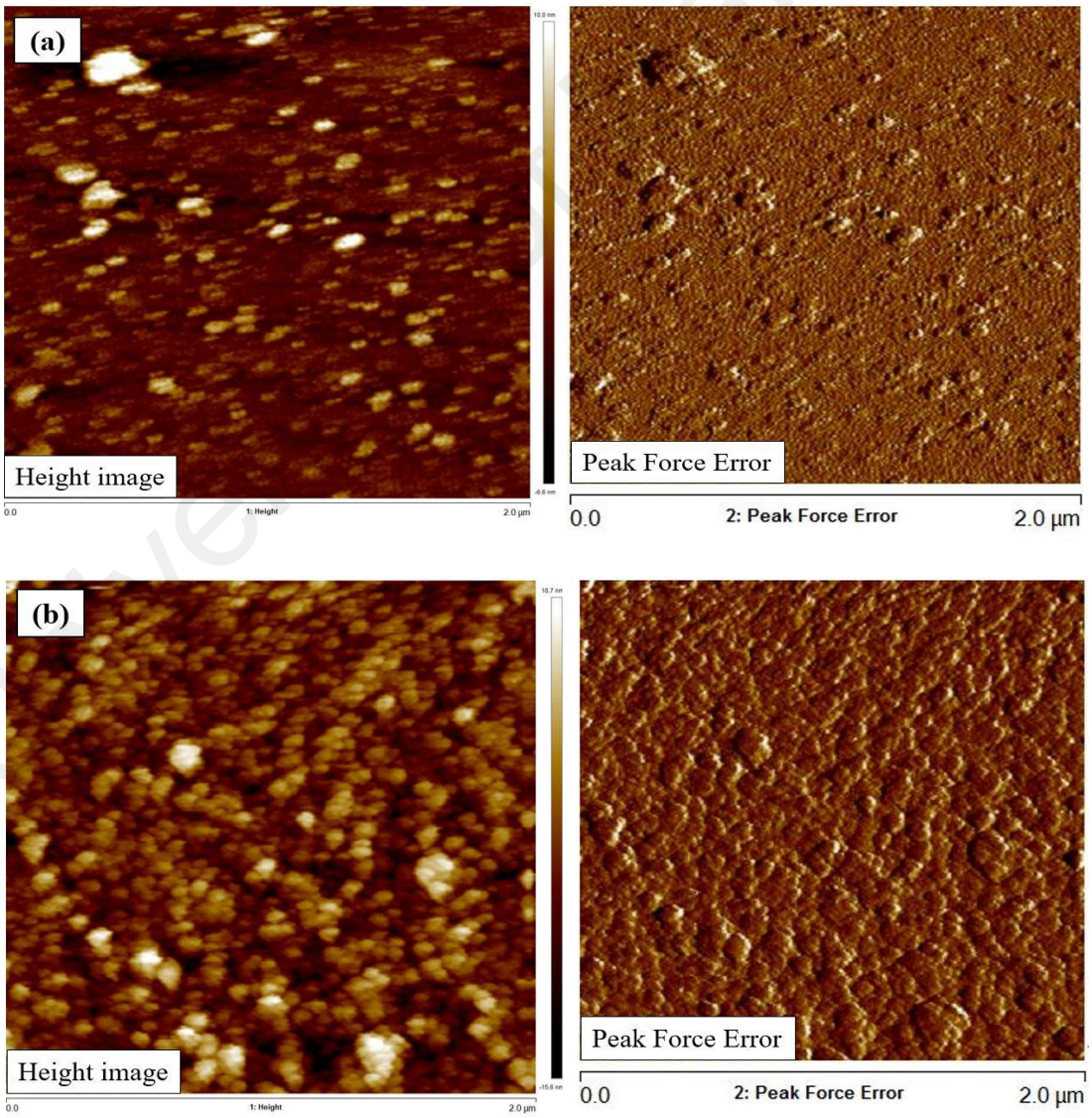

Figure 4.19: AFM height images and peak force error images of CNPs obtained at different synthesis time: (a) 0.5 h, (b) 1 h and (c) 1.5 h.

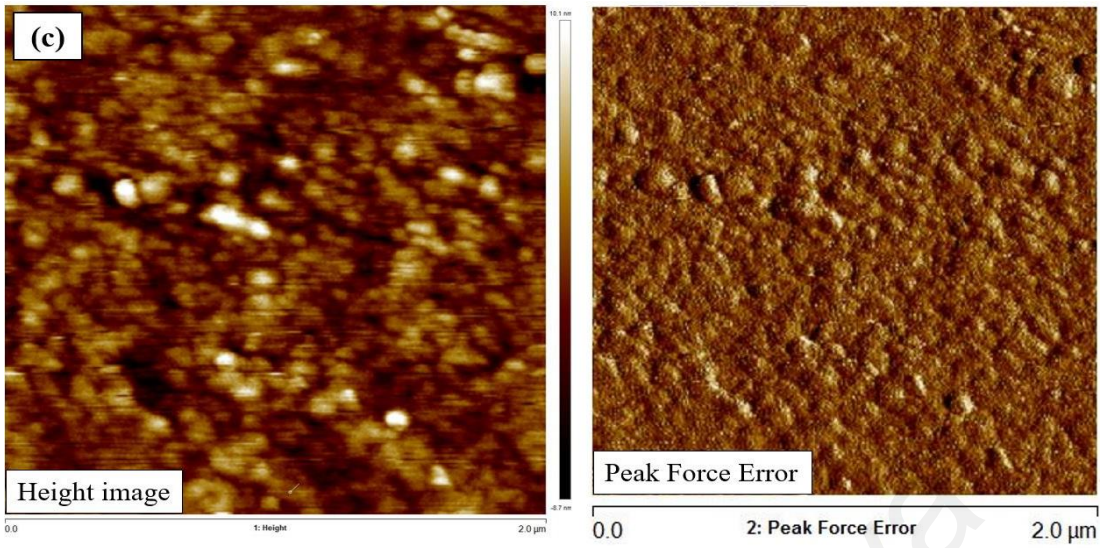

Figure 4.19, continued.

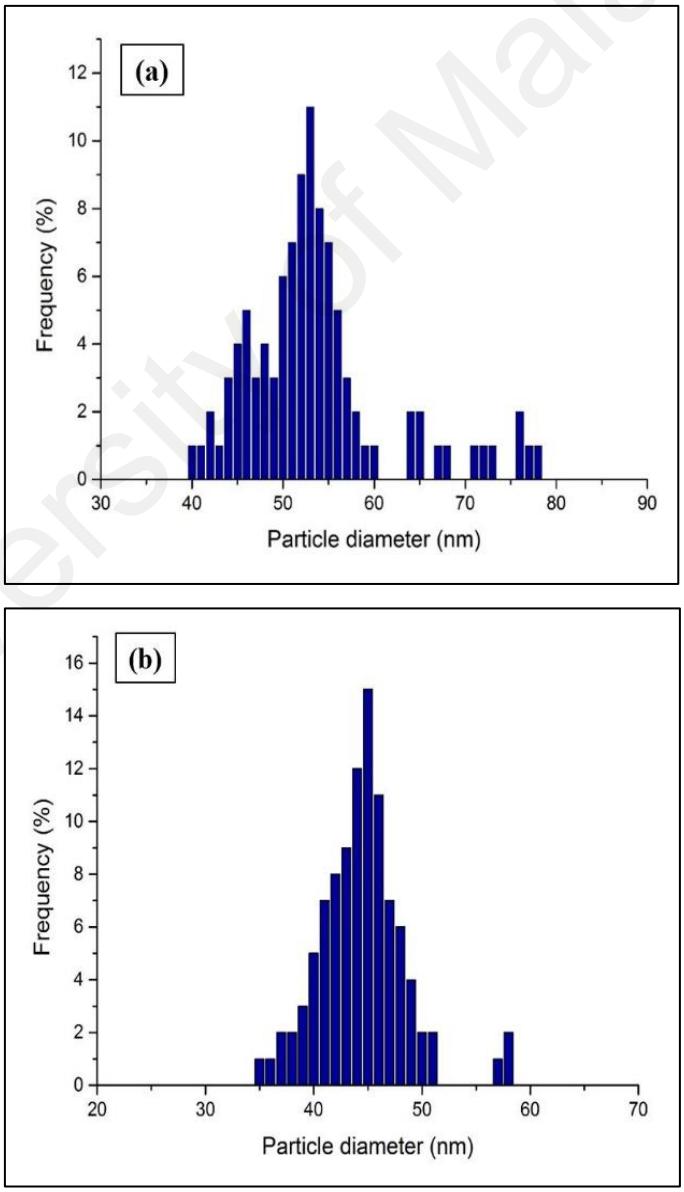

Figure 4.20: Size distribution (diameter) of CNPs based on AFM analysis obtained at different synthesis time: (a) 0.5 h, (b) 1 h and (c) 1.5 h.

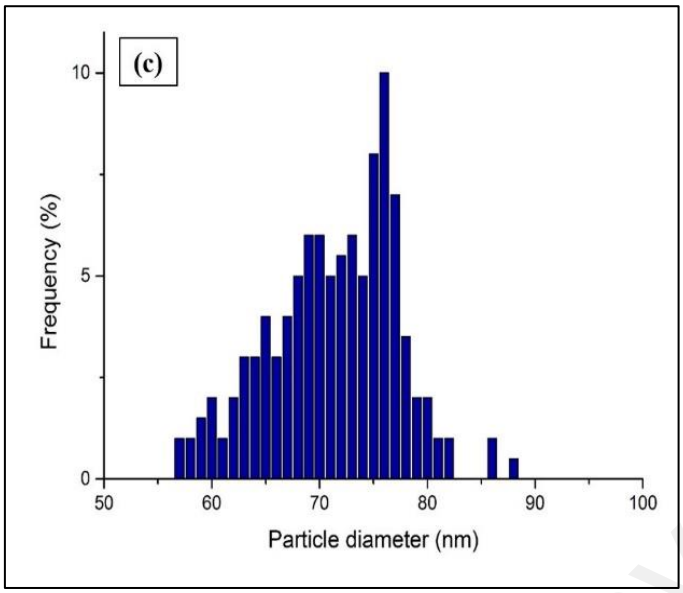

Figure 4.20, continued.

TEM images of synthesized CNPs at 1, 1.5 and 2 hours of dissolution time are illustrated in Figure 4.21. TEM images support the findings of AFM that the CNPs are evidenced to be of spherical shape. Aggregation of particles are generally observed for morphological characterization because it is the peculiar phenomenon of nanoscale materials. This is likely attributed to the small sizes of CNPs particles which prone to have high specific surface area and surface energy. Hence, the nanoparticles are easily conglutinated and stacked with each other by van der Waals forces. Moreover, the agglomeration of particles is possible as the presence of high density of surface hydroxyl groups facilitated the formation of hydrogen bonds (Lu et al., 2013).

TEM observation clearly demonstrates that CNPs have regular spherical shape. The diameter of each particles is then measured using Image J software. TEM measurements revealed that spherical CNPs synthesized at 1 hour have uniform diameters range approximately 30 to 40 nm. Larger size CNPs with diameter around 45 to 55 nm are acquired after 1.5 hours. However, significantly larger and irregular shape CNPs with diameters of 98 to 185 nm were regenerated from BmimOAc after 2 hours. Surprisingly, the longer the dissolution time, the larger the sizes of CNPs. The swollen appearance of

CNPs is attributed to the severe disruption on intricate hydrogen bonding within cellulose due to intercalation of ions of BmimOAc between the cellulose chains. The increased interlayer spacing between cellulose chains results in the extensively swelling of cellulose after prolonged dissolution. Therefore, 1 hour is selected as the optimum time for the effective dissolution of cellulose in BmimOAc.

On top of that, it is worth noting that the sizes of CNPs obtained from AFM and TEM analysis are comparably smaller than the corresponding hydrodynamic size measured by Zeta sizer. This is because CNPs are quasi-spherical nanoparticles and hence, TEM and AFM analysis provide the physical size of particles in dried form. Whereas Zeta sizer indicates the hydrodynamic radius of particles in colloidal suspensions by utilizing DLS technique and is more biased to larger size particles (Oliveri et al., 2013). Larger size particles tend to mask the effects or size measurements provided by the smaller particles. As a matter of fact, cellulose molecules are highly hydrophilic and much prone to swelling in water. Therefore, the size reported by Zeta sizer results in significantly larger particle sizes as compared to TEM and AFM analysis (Adsul et al., 2012). Besides that, the sizes of CNPs reported by AFM are somewhat deviated from the actual size measurements provided by TEM. The larger sizes of CNPs measured by AFM are reasonably due to tip broadening effect which is common in AFM technique (Goetz et al., 2010; Lu & Hsieh, 2012).

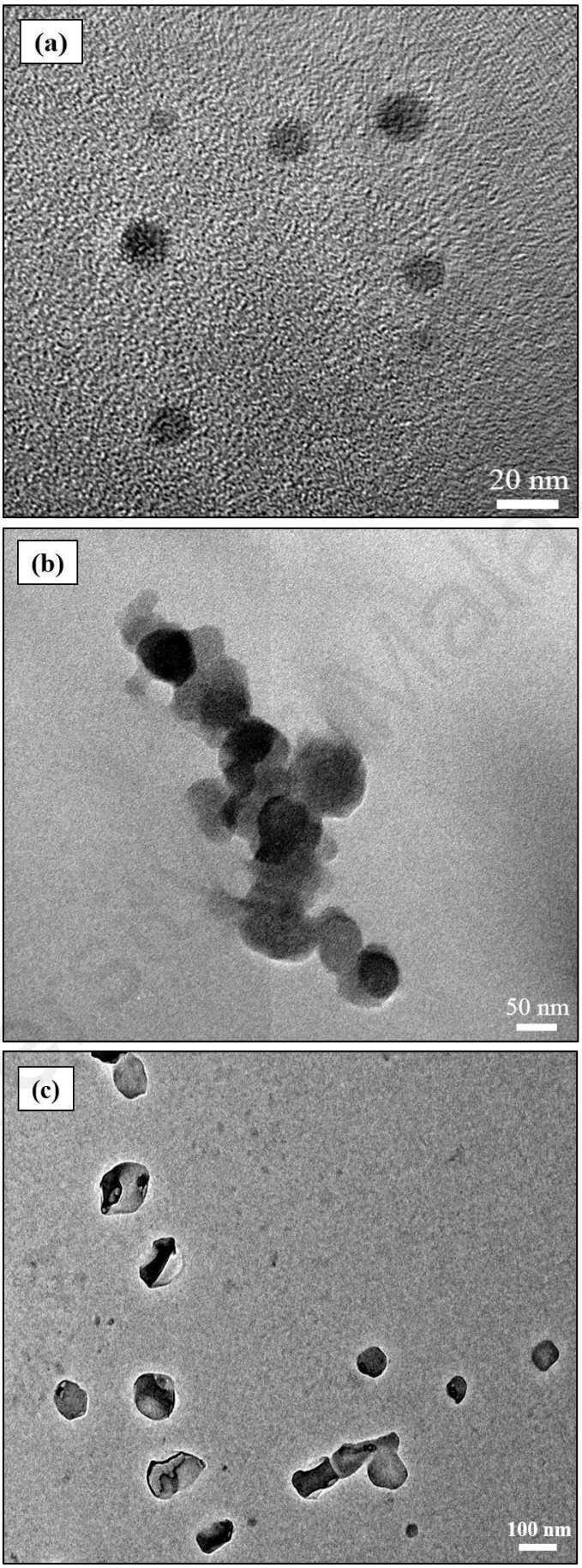

Figure 4.21: HRTEM images of CNPs synthesized at (a) 1 h, (b) 1.5 h and (c) 2 h.

4.3.6 Thermal properties analysis by Thermogravimetric Analysis (TGA)

In the current section, thermal stability of pristine MCC and synthesized CNPs were investigated by means of TGA studies. Thermogravimetric and its derivative curves of MCC and CNPs of different synthesis parameters are presented in Figure 4.22. An initial small amount of weight loss particularly at temperature below 100 ºC is observed in typical TG curves of all samples, corresponds to a mass loss of approximately 5 % due to the evaporation of retained moisture. This is associated with the hydrophilic behaviour of cellulosic polymers and caused water desorption (Pang et al., 2014; Pang et al., 2015).

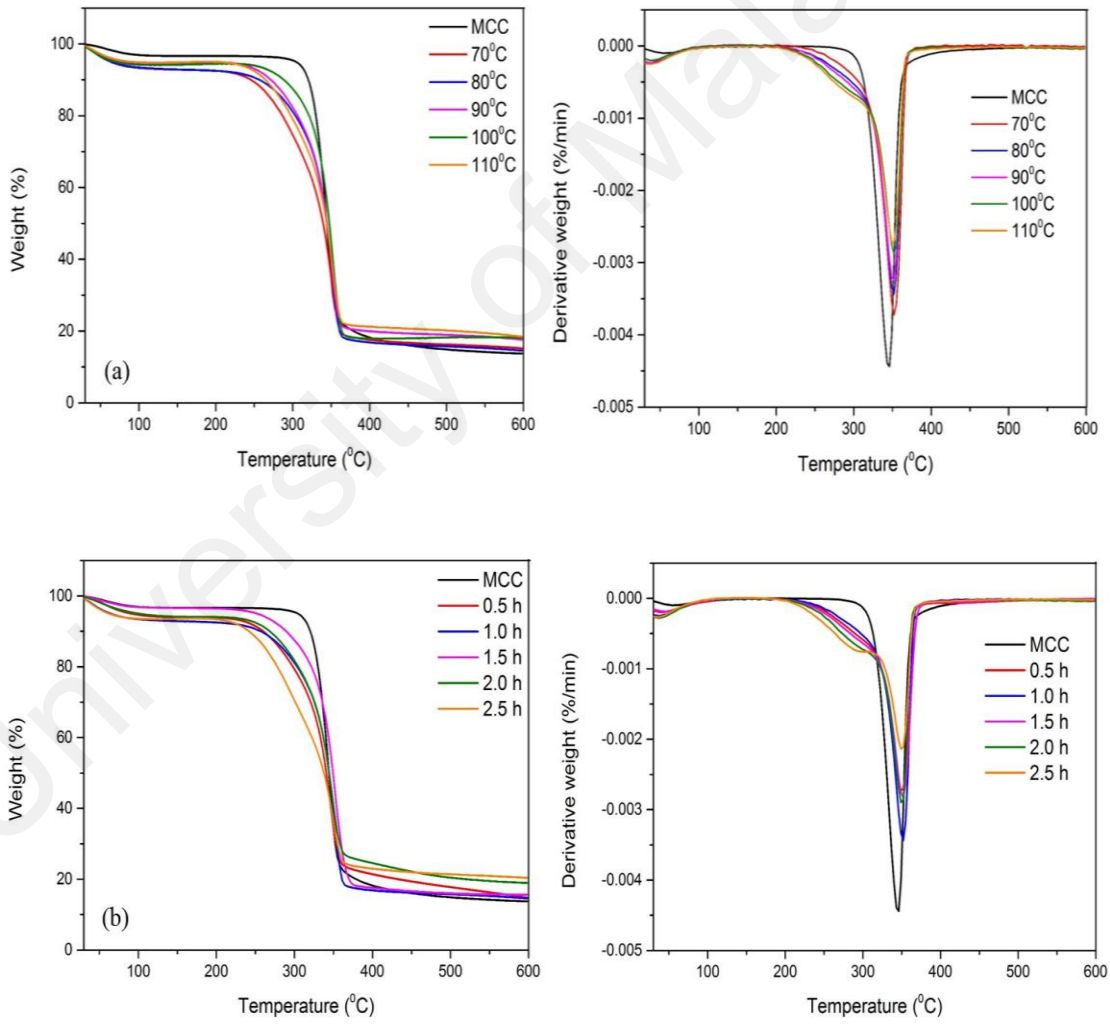

Figure 4.22: TGA and DTG curves of MCC and CNPs optimized with different parameters (a) temperature, (b) time, (c) cellulose concentration (mass loading of MCC), and (d) ultrasonication conditions.

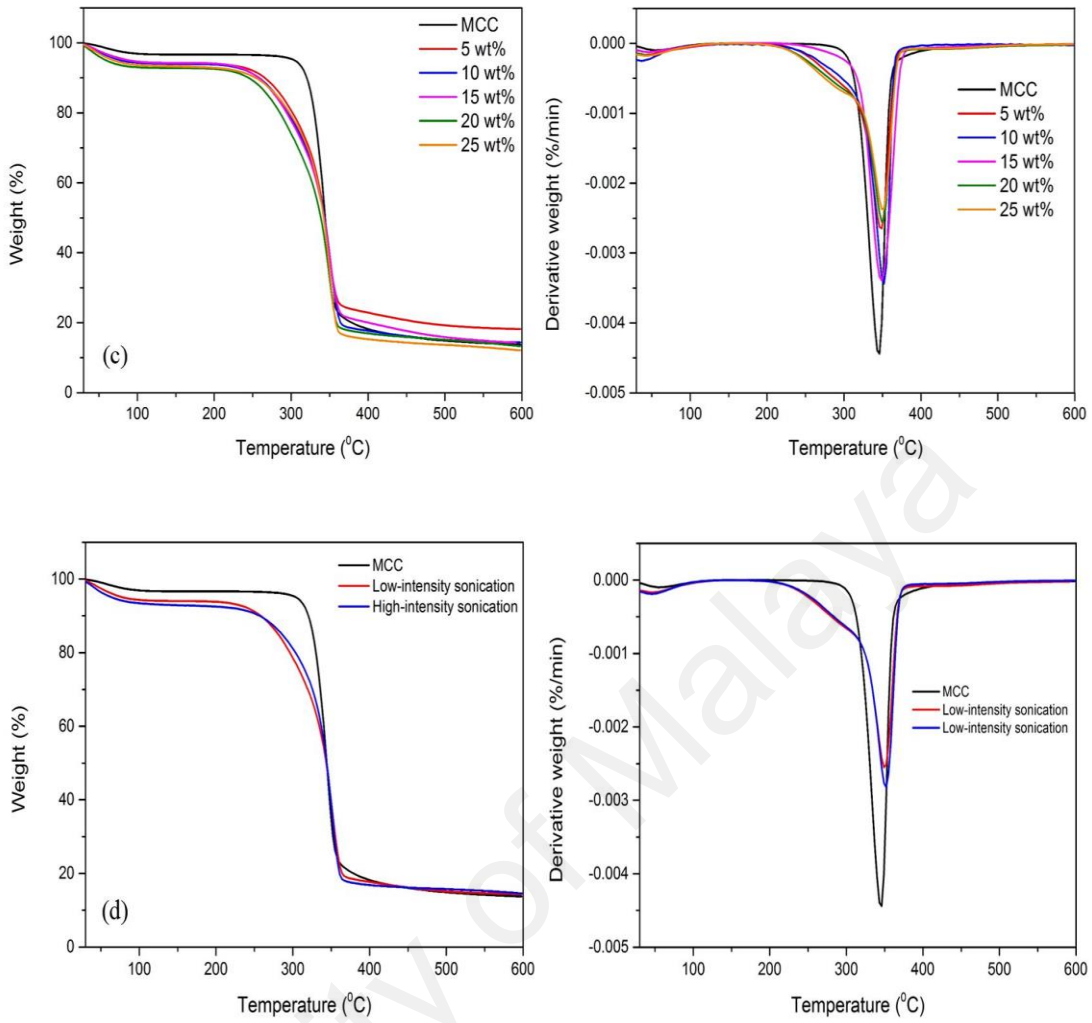

Figure 4.22, continued.

Table 4.7 summarizes the onset decomposition temperature (T_o), maximum decomposition temperature (T_{max}) and char yield of CNPs synthesized with BmimOAc via solvolysis approach. Surprisingly, the major decomposition temperature of CNPs are shifted to slightly higher temperature as compared to the corresponding MCC. Thus, TG analysis reveals that CNPs have better thermal stability than MCC. Similar to MCC, thermal decomposition behaviour of CNPs showed only one pyrolysis process as depicted in DTG graphs. CNPs started to decompose at around 310 to 325 ºC which are slightly higher than that of MCC (300 ºC). Moreover, T_{max} of CNPs are at around 350 ºC which are relatively higher than the decomposition temperature of MCC (345 ºC), as illustrated from DTG peaks. CNPs lost about 75 to 80 % of their relative mass during pyrolysis

process, which are comparably smaller than that of MCC (82 %). The char yield residue of CNPs are within the range of 13 to 20 %, which are comparable to MCC. The higher amorphous content in the material or the lower crystallinity of CNPs leads to higher production of char yield residue (Zhao et al., 2012).

Table 4.7: Onset decomposition temperature, maximum decomposition temperature and char yield of CNPs.

Sample	Onset decomposition temperature, T_0 (ºC)	Maximum decomposition temperature, T_{max} (ºC)	Char Yield (%)
a) Temperature (ºC)			
70	315	350	15.2
80	320	350	14.6
90	320	350	17.6
100	320	350	18.2
110	320	350	18.4
b) Time (hour)			
0.5	320	350	13.0
1.0	320	350	14.6
1.5	320	350	15.6
2.0	320	350	18.9
2.5	315	350	20.3
c) Percent mass loading of MCC (wt%)			
5	320	350	18.2
10	320	350	14.6
15	320	350	14.3
20	315	350	13.2
25	320	350	12.1
d) Sonication treatment			
Low-intensity sonication	320	350	14.3
High-intensity sonication	320	350	14.5

Interestingly, CNPs regenerated from BmimOAc via solvolysis approach are more thermally stable than NCC obtained from the hydrolysis process in $BmimHSO_4$. CNPs onset to decompose at around 310-330 ºC while NCC begin to decompose at around 230-280 ºC. The T_{max} for CNPs and NCC are 350 ºC and 330 ºC, respectively. The higher decomposition temperature of CNPs signifies the higher thermal stability of CNPs than NCC and MCC. It is suggested that the high thermal stability of CNPs is mainly ascribed

to the cellulose *II* crystalline structure as there are rearrangement of hydrogen bonding within CNPs during regeneration process. As a matter of fact, cellulose *II* nanoparticles have improved thermal stability than cellulose *I* nanocrystals because the chains in cellulose *II* are in antiparallel arrangement. In contrast to cellulose *I*, this arrangement yields more hydrogen bonds and thus, leads to a more stable structure (Lu et al., 2015; Moon et al., 2011).

Moreover, the high thermal stability of CNPs is also due to higher flexibility and hence, the higher possibility of entanglements of cellulose nanofibrils that consequently results in more thermodynamically stable structure (Maiti et al., 2013). Furthermore, the absence of sulfate groups in BmimOAc caused no sulfation to take place on the cellulose chains. Therefore, activation energy required for the thermal decomposition of cellulose will not been significantly lowered. The high thermal stability of cellulose *II* nanoparticles has large potential applications in composite materials which demand for thermal stability.

Char yield residue indicates the residual mass of non-volatile carbonaceous material produced at the end of pyrolysis process, usually at high temperature. CNPs produced about 13-20 % char yield on pyrolysis. Parameters such as temperature, time as well as cellulose concentration are influenced the char yield production. Char yield of CNPs increased gradually when temperature is increased from 80 to 110 ºC. Besides that, increase in char yield is also obvious with increasing dissolution time from 0.5 to 2.5 hours. This is likely due to substantially crystallinity reduction and increase in the amorphous content of CNPs. On the other hand, it is worth noting that CNPs synthesized at higher cellulose concentration are responsible for the lower char yield content. The variations in thermal decomposition temperature and char yield of CNPs are qualitatively dependent on the crystal structure as well as quantitative crystallinity of CNPs.

CHAPTER 5: CONCLUSION AND RECOMMENDATIONS

5.1 Conclusion

The present study was mainly focus to investigate the methodology for the synthesis of nanocellulose from cellulose aided by the catalytic and solvation properties of ILs. 1-butyl-3-methylimidazolium hydrogen sulfate ($BmimHSO_4$) and 1-butyl-3-methylimidazolium acetate (BmimOAc) ILs were adopted to perform dual functions as catalyst and solvent for the effective conversion of cellulose into nanocellulose. Despite having the same alkylmethylimidazolium cations, it is suggested that hydrogen sulfate anions exhibit higher acidic properties to induce hydrolysis reaction. On the other hand, higher electronegativity of acetate anions much prone to cause solvolysis of cellulose to produce nanocellulose. In summary, the target objectives for this thesis have been achieved. Synthesis parameters including reaction temperature, time, cellulose concentration (mass loading of MCC) and sonication treatments have been optimized in order to acquire controllable specific architecture and properties of nanocellulose.

In the first stage of research study, improved crystallinity of nanocellulose with the preservation of crystalline cellulose *I* structure has been accomplished with acidic $BmimHSO_4$. The intrinsic acidic character of $BmimHSO_4$ (pH 1) is attributed to the acidity from the hydrogen of $[HSO_4]^-$ which has a pKa value of about 2 in water. Nanocrystalline cellulose with essentially high crystallinity (CrI 92.2) and small size (15 nm) was successfully synthesized via $BmimHSO_4$-mediated hydrolysis at a temperature of 90 ºC for 1.5 hours. It was found that increasing the temperature and time of the hydrolytic reaction predominantly increased the crystallinity and produced smaller size nanocellulose. However, crystallinity dropped gradually with further increased in the temperature and time beyond the optimum conditions. The crystallinity improved is due to the preferential hydrolysis of amorphous regions. While crystallinity reduction is attributed to the uncontrollable hydrolysis of crystalline domains after exposure to higher

temperature and prolonged hydrolysis. Hydrolytic cleavage of glycosidic linkages and selectively removal of amorphous regions in the cellulose chains catalyzed by acidic $BmimHSO_4$ render the release of crystalline domains in nanocellulose which resulted in the higher crystallinity and smaller dimension size. Apart from that, cellulose concentration (in wt%) also has significant impact on the crystallinity as well as size of nanocellulose. Interestingly, the size of nanocellulose increase proportionally with increasing cellulose concentration, reasonably attributed to ineffective hydrolysis reaction at viscous environment.

On the other hand, regenerated cellulose nanoparticles from BmimOAc experienced structural transformation from native cellulose *I* into cellulose *II*. Solvolysis is suggested to take place in BmimOAc where it caused significant disruption to the hydrogen bonding network. Meanwhile, the IL also attacked the glycosidic bonds for fragmentation of cellulose chains. Cellulose nanoparticles with a crystallinity of 78.8 was acquired at 80 °C with 1 hour of solvolysis and cellulose was found to swell in BmimOAc. It is noteworthy the crystallinity of cellulose nanoparticles decreased apparently with increasing temperature and time of dissolution. Disruption caused to the original crystalline structure and breakage of hydrogen bonding between cellulose chains during solvolysis presumably lower the crystallinity of cellulose nanoparticles. Consequently, reconstruction of antiparallel mode hydrogen bonding during regeneration leads to the formation of more thermally and structurally stable structure of cellulose *II*. Moreover, the swelling of cellulose was evidenced by the proportional increase in sizes of cellulose nanoparticles with increasing temperature and time, as illustrated by AFM and TEM analysis.

The application of high-intensity ultrasonication aided the formation of higher crystallinity and smaller size nanocellulose in both hydrolysis and solvolysis approach.

Ultrasonication treatment was important because it is responsible for the defibrillation, defragmentation of fibers while extensively degraded the cellulose amorphous regions. It is important to essentially enhance the crystallinity and disintegrate the cellulose molecules into smaller particles in order to yield smaller size nanocellulose with improved dispersion stability. Suspension of nanocellulose prepared with $BmimHSO_4$ and BmimOAc were considered rather stable with their high absolute zeta potential values of -37.5 mV and -22.3 mV, respectively.

FTIR analysis have revealed the weakened intramolecular hydrogen bonding for nanocellulose due to the interaction and coordination of charged species of ILs with the hydroxyl groups of cellulose. Besides that, FTIR further confirmed the crystallinity of nanocellulose as obtained from the XRD analysis. Moreover, AFM and TEM observations demonstrated that nanoscale cellulose can be obtained after hydrolysis reaction in $BmimHSO_4$ and solvolysis in BmimOAc respectively. The size measurements revealed that the dimension (length or width) of nanocellulose is actually less than 100 nm, though some agglomeration can be observed. Rod-like nanocrystalline cellulose was obtained after hydrolysis with $BmimHSO_4$ whereas spherical cellulose nanoparticles were acquired after solvolysis with BmimOAc, as illustrated from TEM and AFM observations. Furthermore, nanocrystalline cellulose exhibit lower thermal stability although they have remarkable crystallinity due to the presence of sulfate groups from $BmimHSO_4$. The sulfate groups lowered the thermal stability of nanocrystalline cellulose by accelerated thermal degradation of cellulose and promote the dehydration reaction to be occurred at lower temperature. On the other hand, enhanced thermal stability of cellulose nanoparticles is attributed to the antiparallel arrangement and higher number of hydrogen bonding in cellulose *II* which makes it more thermally stable.

In summary, determination of optimum synthesis conditions is of critical importance to avoid uncontrollable depolymerisation of cellulose into monomer units. The formation of nanocellulose has been eased by the application of ILs as both the solvent and catalyst. The advantageous properties of ILs such as recyclability and reusability have been manifested by their high recovery yield (86-90 %). The method adopted in this study is a green and environmental friendly approach because it did not produce any toxic and hazardous waste products. The ILs solution that collected after the reaction were able to recover and regenerate by evaporated the water content and re-concentrated in a vacuum freeze dryer. Meanwhile, it is an economical feasible process because the retrieval of ionic liquids is high, so as they are recyclable and reusable.

5.2 Recommendations for Future Work

An ideal method of production of nanocellulose should encompass green and environmentally benign character to conform with the principle of green chemistry emphasized in governmental regulations and policies. ILs are generally known as green solvents for cellulose processing because they are recyclable and reusable. In the present work, ILs have been utilized as the solvent and catalyst for the manufacture of nanocellulose. The methodology has greatly contributed to the identification of optimum synthesis conditions on the production of highly crystalline structure of nano-dimensional cellulose. The successful formation of nanocellulose through hydrolysis and solvolysis approach with ILs evidenced effectiveness of methods employed which is suggested to replace the conventional acid hydrolysis as well as volatile cellulose solvents system.

Nonetheless, there are several recommendations and suggestions should be noteworthy for future work as proposed below:

i. To investigate the hydrolysis and solvolysis by using alternative cellulosic sources such as Avicel, biomass materials including hard and soft wood,

coconut husk, palm empty fruit bunch (EFB), cotton linter, sugarcane bagasse and wheat straw. However, factors such as availability and cost of raw materials need to be taken into consideration to select suitable materials for further investigation.

ii. The utilization of different anions-based ILs (e.g., phosphate, formate and sulfonate) and vary the cations (e.g., pyridinium) as well as different side chain (alkyl chain length) of alkylimidazolium cations (e.g., ethyl-, butyl- and hexyl-) for hydrolysis and solvolysis of cellulose and their influences on the properties of nanocellulose. Once again, the accessibility and price of ILs are important elements to be considered for their roles as catalyst and solvents, so that the process is economically feasible.

iii. To investigate the regeneration of nanocellulose from cellulose/IL mixture by using other types of anti-solvents such as ethanol, acetone or their combination and their influences on the specific architecture and properties of nanocellulose. The maximum yield and remarkable properties of regenerated nanocellulose such as crystallinity will decide upon the applicability of anti-solvents used.

iv. The nanocellulose can be characterized extensively for their degree of depolymerization (DP) by Gel Permeation Chromatography (GPC) technique with suitable column and dissolving medium to determine the changes in molecular weight after the reaction in future research.

REFERENCES

Abraham, E., Deepa, B., Pothen, L. A., Cintil, J., Thomas, S., John, M. J., ... & Narine, S. S. (2013). Environmental friendly method for the extraction of coir fibre and isolation of nanofibre. *Carbohydrate polymers*, *92*(2), 1477-1483.

Abushammala, H., Krossing, I., & Laborie, M.-P. (2015). Ionic liquid-mediated technology to produce cellulose nanocrystals directly from wood. *Carbohydrate polymers*, *134*, 609-616.

Adebajo, M. O., Frost, R. L., Kloprogge, J. T., & Kokot, S. (2006). Raman spectroscopic investigation of acetylation of raw cotton. *Spectrochimica Acta Part a: molecular and biomolecular spectroscopy*, *64*(2), 448-453.

Adsul, M., Soni, S. K., Bhargava, S. K., & Bansal, V. (2012). Facile approach for the dispersion of regenerated cellulose in aqueous system in the form of nanoparticles. *Biomacromolecules*, *13*(9), 2890-2895.

Ahmadi, M., Madadlou, A., & Sabouri, A. A. (2015). Isolation of micro-and nano-crystalline cellulose particles and fabrication of crystalline particles-loaded whey protein cold-set gel. *Food chemistry*, *174*, 97-103.

Amarasekara, A. S., & Owereh, O. S. (2009). Hydrolysis and decomposition of cellulose in Bronsted acidic ionic liquids under mild conditions. *Industrial & Engineering Chemistry Research*, *48*(22), 10152-10155.

Ang, T. N., Ngoh, G. C., Chua, A. S. M., & Lee, M. G. (2012). Elucidation of the effect of ionic liquid pretreatment on rice husk via structural analyses. *Biotechnology for biofuels*, *5*(1), 1.

Angles, M. N., & Dufresne, A. (2000). Plasticized starch/tunicin whiskers nanocomposites. 1. Structural analysis. *Macromolecules*, *33*(22), 8344-8353.

Angles, M. N., & Dufresne, A. (2001). Plasticized starch/tunicin whiskers nanocomposite materials. 2. Mechanical behavior. *Macromolecules*, *34*(9), 2921-2931.

Ashori, A., Harun, J., Raverty, W. D., & Yusoff, M. N. M. (2006). Chemical and morphological characteristics of Malaysian cultivated kenaf (Hibiscus cannabinus) fiber. *Polymer-Plastics Technology and Engineering*, *45*(1), 131-134.

Azizi Samir, M. A. S., Alloin, F., & Dufresne, A. (2005). Review of recent research into cellulosic whiskers, their properties and their application in nanocomposite field. *Biomacromolecules*, *6*(2), 612-626.

Belbekhouche, S., Bras, J., Siqueira, G., Chappey, C., Lebrun, L., Khelifi, B., Marais, S., & Dufresne, A. (2011). Water sorption behavior and gas barrier properties of cellulose whiskers and microfibrils films. *Carbohydrate Polymers*, *83*(4), 1740-1748.

Bittmann, B., Haupert, F., & Schlarb, A. K. (2009). Ultrasonic dispersion of inorganic nanoparticles in epoxy resin. *Ultrasonics sonochemistry*, *16*(5), 622-628.

Blackley, D. C. (2012). *Polymer Latices: Science and Technology Volume 3: Applications of Latices*. Springer Science & Business Media.

Bonhote, P., Dias, A. P., Papageorgiou, N., Kalyanasundaram, K., & Grätzel, M. (1996). Hydrophobic, highly conductive ambient-temperature molten salts. *Inorganic chemistry*, *35*(5), 1168-1178.

Broido, A., & Nelson, M. A. (1975). Char yield on pyrolysis of cellulose. *Combustion and Flame*, *24*, 263-268.

Brandt, A., Hallett, J. P., Leak, D. J., Murphy, R. J., & Welton, T. (2010). The effect of the ionic liquid anion in the pretreatment of pine wood chips. *Green Chemistry*, *12*(4), 672-679.

Brinchi, L., Cotana, F., Fortunati, E., & Kenny, J. (2013). Production of nanocrystalline cellulose from lignocellulosic biomass: technology and applications. *Carbohydrate polymers*, *94*(1), 154-169.

Brodeur, G., Yau, E., Badal, K., Collier, J., Ramachandran, K. B., & Ramakrishnan, S. (2011). Chemical and physicochemical pretreatment of lignocellulosic biomass: a review. *Enzyme research*, *2011*.

Cammarata, L., Kazarian, S. G., Salter, P. A., & Welton, T. (2001). Molecular states of water in room temperature ionic liquids. *Physical Chemistry Chemical Physics*, *3*(23), 5192-5200.

Cao, X., Chen, Y., Chang, P. R., Stumborg, M., & Huneault, M. A. (2008). Green composites reinforced with hemp nanocrystals in plasticized starch. *Journal of Applied Polymer Science*, *109*(6), 3804-3810.

Cao, X., Chen, Y., Chang, P. R., Muir, A. D., & Falk, G. (2008). Starch-based nanocomposites reinforced with flax cellulose nanocrystals. *Express Polym Lett*, *2*(7), 502-510.

Cao, X., Ding, B., Yu, J., & Al-Deyab, S. S. (2012). Cellulose nanowhiskers extracted from TEMPO-oxidized jute fibers. *Carbohydrate polymers*, *90*(2), 1075-1080.

Cao, Y., Wu, J., Zhang, J., Li, H., Zhang, Y., & He, J. (2009). Room temperature ionic liquids (RTILs): a new and versatile platform for cellulose processing and derivatization. *Chemical Engineering Journal*, *147*(1), 13-21.

Chauhan, V. S., & Chakrabarti, S. K. (2012). Use of nanotechnology for high performance cellulosic and papermaking products. *Cellulose Chemistry and Technology*, *46*(5), 389.

Chen, H. Z., Wang, N., & Liu, L. Y. (2012). Regenerated cellulose membrane prepared with ionic liquid 1-butyl-3-methylimidazolium chloride as solvent using wheat straw. *Journal of Chemical Technology and Biotechnology*, *87*(12), 1634-1640.

Chen, W., Li, Q., Cao, J., Liu, Y., Li, J., Zhang, J., Luo, S. & Yu, H. (2015). Revealing the structures of cellulose nanofiber bundles obtained by mechanical nanofibrillation via TEM observation. *Carbohydrate polymers*, *117*, 950-956.

Chen, W., Yu, H., Liu, Y., Chen, P., Zhang, M., & Hai, Y. (2011). Individualization of cellulose nanofibers from wood using high-intensity ultrasonication combined with chemical pretreatments. *Carbohydrate Polymers*, *83*(4), 1804-1811.

Chen, W., Yu, H., Liu, Y., Hai, Y., Zhang, M., & Chen, P. (2011). Isolation and characterization of cellulose nanofibers from four plant cellulose fibers using a chemical-ultrasonic process. *Cellulose*, *18*(2), 433-442.

Cheng, G., Varanasi, P., Arora, R., Stavila, V., Simmons, B. A., Kent, M. S., & Singh, S. (2012). Impact of ionic liquid pretreatment conditions on cellulose crystalline structure using 1-ethyl-3-methylimidazolium acetate. *The Journal of Physical Chemistry B*, *116*(33), 10049-10054.

Cheng, Q., Wang, S., & Rials, T. G. (2009). Poly (vinyl alcohol) nanocomposites reinforced with cellulose fibrils isolated by high intensity ultrasonication. *Composites Part A: Applied Science and Manufacturing*, *40*(2), 218-224.

Cherian, B. M., Leão, A. L., de Souza, S. F., Thomas, S., Pothan, L. A., & Kottaisamy, M. (2010). Isolation of nanocellulose from pineapple leaf fibres by steam explosion. *Carbohydrate Polymers, 81*(3), 720-725.

Cherian, B. M., Pothan, L. A., Nguyen-Chung, T., Mennig, G., Kottaisamy, M., & Thomas, S. (2008). A novel method for the synthesis of cellulose nanofibril whiskers from banana fibers and characterization. *Journal of agricultural and food chemistry, 56*(14), 5617-5627.

Chirayil, C. J., Mathew, L., & Thomas, S. (2014). Review of recent research in nano cellulose preparation from different lignocellulosic fibers. *Rev Adv Mater Sci, 37*(1-2), 20-28.

Chowdhury, Z. Z., Zain, S. M., Hamid, S. B. A., & Khalid, K. (2014). Catalytic role of ionic liquids for dissolution and degradation of biomacromolecules. *BioResources, 9*(1), 1787-1823.

Cintas, P., & Luche, J.-L. (1999). Green chemistry. The sonochemical approach. *Green Chem., 1*(3), 115-125.

da Costa Lopes, A. M., João, K. G., Morais, A. R. C., Bogel-Łukasik, E., & Bogel-Łukasik, R. (2013). Ionic liquids as a tool for lignocellulosic biomass fractionation. *Sustain Chem Process, 1*(1), 3.

Dadi, A. P., Schall, C. A., & Varanasi, S. (2007). Mitigation of cellulose recalcitrance to enzymatic hydrolysis by ionic liquid pretreatment *Applied Biochemistry and Biotecnology* (pp. 407-421): Springer.

Damodaran, S., Parkin, K. L., & Fennema, O. R. (Eds.). (2007). *Fennema's food chemistry*. CRC press.

de Morais Teixeira, E., Corrêa, A. C., Manzoli, A., de Lima Leite, F., de Oliveira, C. R., & Mattoso, L. H. C. (2010). Cellulose nanofibers from white and naturally colored cotton fibers. *Cellulose, 17*(3), 595-606.

de Olyveira, G. M., Costa, L. M. M., Basmaji, P., & Xavier Filho, L. (2011). Bacterial nanocellulose for medicine regenerative. *Journal of Nanotechnology in Engineering and Medicine, 2*(3), 034001.

Dharaskar, S. A., Varma, M. N., Shende, D. Z., Yoo, C. K., & Wasewar, K. L. (2013). Synthesis, characterization and application of 1-butyl-3 methylimidazolium

chloride as green material for extractive desulfurization of liquid fuel. *The Scientific World Journal*, *2013*.

Dharaskar, S. A., Wasewar, K. L., Varma, M. N., Shende, D. Z., & Yoo, C. (2013). Synthesis, characterization and application of 1-butyl-3-methylimidazolium tetrafluoroborate for extractive desulfurization of liquid fuel. *Arabian Journal of Chemistry*.

Ding, Z.-D., Chi, Z., Gu, W.-X., Gu, S.-M., Liu, J.-H., & Wang, H.-J. (2012). Theoretical and experimental investigation on dissolution and regeneration of cellulose in ionic liquid. *Carbohydrate polymers*, *89*(1), 7-16.

Dong, Y., Holm, J., & Lassi, U. (2015). Dissolution and Hydrolysis of Lignocellulosic Biomass using Tailored Ionic Liquids.

Dufresne, A. (2013). Nanocellulose: a new ageless bionanomaterial. *Materials Today*, *16*(6), 220-227.

Dufresne, A., & Belgacem, M. N. (2013). Cellulose-reinforced composites: from micro-to nanoscale. *Polímeros*, *23*(3), 277-286.

Duran, N., Lemes, A. P., Duran, M., Freer, J., & Baeza, J. (2011). A minireview of cellulose nanocrystals and its potential integration as co-product in bioethanol production. *Journal of the Chilean Chemical Society*, *56*(2), 672-677.

Elazzouzi-Hafraoui, S., Nishiyama, Y., Putaux, J.-L., Heux, L., Dubreuil, F., & Rochas, C. (2007). The shape and size distribution of crystalline nanoparticles prepared by acid hydrolysis of native cellulose. *Biomacromolecules*, *9*(1), 57-65.

Fan, J. S., & Li, Y. H. (2012). Maximizing the yield of nanocrystalline cellulose from cotton pulp fiber. *Carbohydrate Polymers*, *88*(4), 1184-1188.

Fan, M., Dai, D., & Huang, B. (2012). Fourier transform infrared spectroscopy for natural fibres. *Fourier transform–materials analysis. InTech*.

Fernandes, A. M., Rocha, M. A., Freire, M. G., Marrucho, I. M., Coutinho, J. A., & Santos, L. M. (2011). Evaluation of cation− anion interaction strength in ionic liquids. *The Journal of Physical Chemistry B*, *115*(14), 4033-4041.

Ferrer, A., Filpponen, I., Rodríguez, A., Laine, J., & Rojas, O. J. (2012). Valorization of residual Empty Palm Fruit Bunch Fibers (EPFBF) by microfluidization:

production of nanofibrillated cellulose and EPFBF nanopaper. *Bioresource technology*, *125*, 249-255.

Filson, P. B., & Dawson-Andoh, B. E. (2009). Sono-chemical preparation of cellulose nanocrystals from lignocellulose derived materials. *Bioresource Technology*, *100*(7), 2259-2264.

Frone, A. N., Panaitescu, D. M., Donescu, D., Spataru, C. I., Radovici, C., Trusca, R., & Somoghi, R. (2011). Preparation and characterization of PVA composites with cellulose nanofibers obtained by ultrasonication. *BioResources*, *6*(1), 487-512.

Gao, K., Shao, Z., Li, J., Wang, X., Peng, X., Wang, W., & Wang, F. (2013). Cellulose nanofiber–graphene all solid-state flexible supercapacitors. *Journal of Materials Chemistry A*, *1*(1), 63-67.

George, J., & Sabapathi, S. N. (2015). Cellulose nanocrystals: synthesis, functional properties, and applications. *Nanotechnology, science and applications*, *8*, 45.

Gericke, M., Fardim, P., & Heinze, T. (2012). Ionic liquids—promising but challenging solvents for homogeneous derivatization of cellulose. *Molecules*, *17*(6), 7458-7502.

Goetz, J. L., Keltner, D., & Simon-Thomas, E. (2010). Compassion: an evolutionary analysis and empirical review. *Psychological bulletin*, *136*(3), 351.

Guo, J., Guo, X., Wang, S., & Yin, Y. (2016). Effects of ultrasonic treatment during acid hydrolysis on the yield, particle size and structure of cellulose nanocrystals. *Carbohydrate polymers*, *135*, 248-255.

Ha, S. H., Mai, N. L., An, G., & Koo, Y. M. (2011). Microwave-assisted pretreatment of cellulose in ionic liquid for accelerated enzymatic hydrolysis. *Bioresource technology*, *102*(2), 1214-1219.

Haafiz, M. M., Hassan, A., Zakaria, Z., & Inuwa, I. M. (2014). Isolation and characterization of cellulose nanowhiskers from oil palm biomass microcrystalline cellulose. *Carbohydrate polymers*, *103*, 119-125.

Habibi, Y., Lucia, L. A., & Rojas, O. J. (2010). Cellulose nanocrystals: chemistry, self-assembly, and applications. *Chemical reviews*, *110*(6), 3479-3500.

Habibi, Y., Mahrouz, M., & Vignon, M. R. (2009). Microfibrillated cellulose from the peel of prickly pear fruits. *Food Chemistry, 115*(2), 423-429.

Hamelinck, C. N., Van Hooijdonk, G., & Faaij, A. P. (2005). Ethanol from lignocellulosic biomass: techno-economic performance in short-, middle-and long-term. *Biomass and bioenergy, 28*(4), 384-410.

Hamid, S. B. A., Zain, S. K., Das, R., & Centi, G. (2016). Synergic effect of tungstophosphoric acid and sonication for rapid synthesis of crystalline nanocellulose. *Carbohydrate Polymers, 138*, 349-355.

Han, J., Zhou, C., French, A. D., Han, G., & Wu, Q. (2013). Characterization of cellulose II nanoparticles regenerated from 1-butyl-3-methylimidazolium chloride. *Carbohydrate polymers, 94*(2), 773-781.

Harmsen, P., Huijgen, W., Bermudez, L., & Bakker, R. (2010). Literature review of physical and chemical pretreatment processes for lignocellulosic biomass. *Energy Research Centre of the Netherlands*, 10-13.

Herrmann, S. (2015). *New Synthetic Routes to Polyoxometalate Containing Ionic Liquids: An Investigation of Their Properties*: Springer.

Hidaka, H., Kim, U. J., & Wada, M. (2010). Synchrotron X-ray fiber diffraction study on the thermal expansion behavior of cellulose crystals in tension wood of Japanese poplar in the low-temperature region. *Holzforschung, 64*(2), 167-171.

Hu, X., Xiao, Y., Niu, K., Zhao, Y., Zhang, B., & Hu, B. (2013). Functional ionic liquids for hydrolysis of lignocellulose. *Carbohydrate polymers, 97*(1), 172-176.

Ibrahim, M. M., El-Zawawy, W. K., Jüttke, Y., Koschella, A., & Heinze, T. (2013). Cellulose and microcrystalline cellulose from rice straw and banana plant waste: preparation and characterization. *Cellulose, 20*(5), 2403-2416.

Igarashi, K., Uchihashi, T., Koivula, A., Wada, M., Kimura, S., Okamoto, T., . . . Samejima, M. (2011). Traffic jams reduce hydrolytic efficiency of cellulase on cellulose surface. *Science, 333*(6047), 1279-1282.

Ioelovich, M (2016). Study of thermodynamic properties of various allomorphs of cellulose. *ChemXpress,* 9(3), 259-265.

Isik, M., Sardon, H., & Mecerreyes, D. (2014). Ionic liquids and cellulose: Dissolution, chemical modification and preparation of new cellulosic materials. *International journal of molecular sciences, 15*(7), 11922-11940.

Itoh, T. (2014). Design of Ionic Liquids for Cellulose Dissolution *Production of Biofuels and Chemicals with Ionic Liquids* (pp. 91-106): Springer.

Jackson, J. K., Letchford, K., Wasserman, B. Z., Ye, L., Hamad, W. Y., & Burt, H. M. (2011). The use of nanocrystalline cellulose for the binding and controlled release of drugs. *International journal of nanomedicine, 6*, 321.

Janardhnan, S., & Sain, M. M. (2007). Isolation of cellulose microfibrils–an enzymatic approach. *Bioresources, 1*(2), 176-188.

Jiang, F., & Hsieh, Y. L. (2013). Chemically and mechanically isolated nanocellulose and their self-assembled structures. *Carbohydrate Polymers, 95*(1), 32-40.

Jiang, G., Huang, W., Wang, B., Zhang, Y., & Wang, H. (2012). The changes of crystalline structure of cellulose during dissolution in 1-butyl-3-methylimidazolium chloride. *Cellulose, 19*(3), 679-685.

Jin, Z., Wang, S., Wang, J., & Zhao, M. (2012). Effects of plasticization conditions on the structures and properties of cellulose packaging films from ionic liquid [BMIM] Cl. *Journal of Applied Polymer Science, 125*(1), 704-709.

Johar, N., Ahmad, I., & Dufresne, A. (2012). Extraction, preparation and characterization of cellulose fibres and nanocrystals from rice husk. *Industrial Crops and Products, 37*(1), 93-99.

John, M. J., & Thomas, S. (2008). Biofibres and biocomposites. *Carbohydrate polymers, 71*(3), 343-364.

Johnson, R. K., Zink-Sharp, A., & Glasser, W. G. (2011). Preparation and characterization of hydrophobic derivatives of TEMPO-oxidized nanocelluloses. *Cellulose, 18*(6), 1599-1609.

Jonoobi, M., Khazaeian, A., Tahir, P. M., Azry, S. S., & Oksman, K. (2011). Characteristics of cellulose nanofibers isolated from rubberwood and empty fruit bunches of oil palm using chemo-mechanical process. *Cellulose, 18*(4), 1085-1095.

Jonoobi, M., Niska, K. O., Harun, J., & Misra, M. (2009). Chemical composition, crystallinity, and thermal degradation of bleached and unbleached kenaf bast (Hibiscus cannabinus) pulp and nanofibers. *BioResources, 4*(2), 626-639.

Kalia, S., Dufresne, A., Cherian, B. M., Kaith, B. S., Avérous, L., Njuguna, J., & Nassiopoulos, E. (2011). Cellulose-based bio-and nanocomposites: a review. *International Journal of Polymer Science, 2011*.

Karande, V., Bharimalla, A., Hadge, G., Mhaske, S., & Vigneshwaran, N. (2011). Nanofibrillation of cotton fibers by disc refiner and its characterization. *Fibers and Polymers, 12*(3), 399-404.

Karatzos, S. K., Edye, L. A., & Doherty, W. O. S. (2012). Sugarcane bagasse pretreatment using three imidazolium-based ionic liquids; mass balances and enzyme kinetics. *Biotechnology for biofuels, 5*(1), 1.

Khalil, H. A., Bhat, A., & Yusra, A. I. (2012). Green composites from sustainable cellulose nanofibrils: a review. *Carbohydrate Polymers, 87*(2), 963-979.

Khalil, H. A., Davoudpour, Y., Islam, M. N., Mustapha, A., Sudesh, K., Dungani, R., & Jawaid, M. (2014). Production and modification of nanofibrillated cellulose using various mechanical processes: a review. *Carbohydrate polymers, 99*, 649-665.

Kilpeläinen, I., Xie, H., King, A., Granstrom, M., Heikkinen, S., & Argyropoulos, D. S. (2007). Dissolution of wood in ionic liquids. *Journal of agricultural and food chemistry, 55*(22), 9142-9148.

Kim, H. S., Kim, S., Kim, H. J., & Yang, H. S. (2006). Thermal properties of bio-flour-filled polyolefin composites with different compatibilizing agent type and content. *Thermochimica Acta, 451*(1), 181-188.

Kim, U. J., Eom, S. H., & Wada, M. (2010). Thermal decomposition of native cellulose: influence on crystallite size. *Polymer Degradation and Stability, 95*(5), 778-781.

Klemm, D., Kramer, F., Moritz, S., Lindström, T., Ankerfors, M., Gray, D., & Dorris, A. (2011). Nanocelluloses: A New Family of Nature-Based Materials. *Angewandte Chemie International Edition, 50*(24), 5438-5466.

Klemm, D., Schmauder, H. P., & Heinze, T. (2005). Cellulose. *Biopolymers online*.

Kokol, V., Božič, M., Vogrinčič, R., & Mathew, A. P. (2015). Characterisation and properties of homo-and heterogenously phosphorylated nanocellulose. *Carbohydrate polymers, 125*, 301-313.

Kosan, B., Michels, C., & Meister, F. (2008). Dissolution and forming of cellulose with ionic liquids. *Cellulose, 15*(1), 59-66.

Kumar, P., Barrett, D. M., Delwiche, M. J., & Stroeve, P. (2009). Methods for pretreatment of lignocellulosic biomass for efficient hydrolysis and biofuel production. *Industrial & engineering chemistry research, 48*(8), 3713-3729.

Kümmerer, K., Menz, J., Schubert, T., & Thielemans, W. (2011). Biodegradability of organic nanoparticles in the aqueous environment. *Chemosphere, 82*(10), 1387-1392.

Kuo, C.-H., & Lee, C.-K. (2009). Enhancement of enzymatic saccharification of cellulose by cellulose dissolution pretreatments. *Carbohydrate Polymers, 77*(1), 41-46.

Lam, E., Male, K. B., Chong, J. H., Leung, A. C., & Luong, J. H. (2012). Applications of functionalized and nanoparticle-modified nanocrystalline cellulose. *Trends in biotechnology, 30*(5), 283-290.

Lan, W., Liu, C.-F., Yue, F.-X., Sun, R.-C., & Kennedy, J. F. (2011). Ultrasound-assisted dissolution of cellulose in ionic liquid. *Carbohydrate polymers, 86*(2), 672-677.

Lee, H., Hamid, S., & Zain, S. (2014). Conversion of lignocellulosic biomass to nanocellulose: structure and chemical process. *The Scientific World Journal, 2014*.

Lee, K.-Y., Aitomäki, Y., Berglund, L. A., Oksman, K., & Bismarck, A. (2014). On the use of nanocellulose as reinforcement in polymer matrix composites. *Composites Science and Technology, 105*, 15-27.

Legnani, C., Vilani, C., Calil, V. L., Barud, H. S., Quirino, W. G., Achete, C. A., Ribeiro, S.J.L. & Cremona, M. (2008). Bacterial cellulose membrane as flexible substrate for organic light emitting devices. *Thin Solid Films, 517*(3), 1016-1020.

Lemaitre, J., Chaboche, J. L., Benallal, A., & Desmorat, R. (2009). *Mécanique des matériaux solides-3eme édition*. Dunod.

Leung, A. C., Lam, E., Chong, J., Hrapovic, S., & Luong, J. H. (2013). Reinforced plastics and aerogels by nanocrystalline cellulose. *Journal of nanoparticle research*, *15*(5), 1-24.

Li, F., Biagioni, P., Bollani, M., Maccagnan, A., & Piergiovanni, L. (2013). Multi-functional coating of cellulose nanocrystals for flexible packaging applications. *Cellulose*, *20*(5), 2491-2504.

Li, J., Wei, X., Wang, Q., Chen, J., Chang, G., Kong, L., . . . Liu, Y. (2012). Homogeneous isolation of nanocellulose from sugarcane bagasse by high pressure homogenization. *Carbohydrate polymers*, *90*(4), 1609-1613.

Li, J., Zhang, X., Zhang, M., Xiu, H., & He, H. (2015). Ultrasonic enhance acid hydrolysis selectivity of cellulose with HCl–$FeCl_3$ as catalyst. *Carbohydrate polymers*, *117*, 917-922.

Li, M. C., Wu, Q., Song, K., Lee, S., Qing, Y., & Wu, Y. (2015). Cellulose nanoparticles: structure–morphology–rheology relationships. *ACS Sustainable Chemistry & Engineering*, *3*(5), 821-832.

Li, W., Yue, J., & Liu, S. (2012). Preparation of nanocrystalline cellulose via ultrasound and its reinforcement capability for poly (vinyl alcohol) composites. *Ultrasonics sonochemistry*, *19*(3), 479-485.

Lin, J., Yu, L., Tian, F., Zhao, N., Li, X., Bian, F., & Wang, J. (2014). Cellulose nanofibrils aerogels generated from jute fibers. *Carbohydrate polymers*, *109*, 35-43.

Liu, D., Zhong, T., Chang, P. R., Li, K., & Wu, Q. (2010). Starch composites reinforced by bamboo cellulosic crystals. *Bioresource Technology*, *101*(7), 2529-2536.

Liu, H., Sale, K. L., Holmes, B. M., Simmons, B. A., & Singh, S. (2010). Understanding the interactions of cellulose with ionic liquids: a molecular dynamics study. *The Journal of Physical Chemistry B*, *114*(12), 4293-4301.

Liu, Y., Xiao, W., Xia, S., & Ma, P. (2013). SO_3H-functionalized acidic ionic liquids as catalysts for the hydrolysis of cellulose. *Carbohydrate polymers*, *92*(1), 218-222.

Lu, H., Gui, Y., Zheng, L., & Liu, X. (2013). Morphological, crystalline, thermal and physicochemical properties of cellulose nanocrystals obtained from sweet potato residue. *Food research international*, *50*(1), 121-128.

Lu, P., & Hsieh, Y.-L. (2010). Preparation and properties of cellulose nanocrystals: rods, spheres, and network. *Carbohydrate Polymers*, *82*(2), 329-336.

Lu, Q. L., Tang, L. R., Wang, S., Huang, B., Chen, Y. D., & Chen, X. R. (2014). An investigation on the characteristics of cellulose nanocrystals from Pennisetum sinese. *Biomass and Bioenergy*, *70*, 267-272.

Lu, Q., Lin, W., Tang, L., Wang, S., Chen, X., & Huang, B. (2015). A mechanochemical approach to manufacturing bamboo cellulose nanocrystals. *Journal of Materials Science*, *50*(2), 611-619.

Lu, Q., Tang, L., Lin, F., Wang, S., Chen, Y., Chen, X., & Huang, B. (2014). Preparation and characterization of cellulose nanocrystals via ultrasonication-assisted $FeCl_3$-catalyzed hydrolysis. *Cellulose*, *21*(5), 3497-3506.

Lu, Q.-l., Tang, L.-r., Wang, S., Huang, B., Chen, Y.-d., & Chen, X.-r. (2014). An investigation on the characteristics of cellulose nanocrystals from Pennisetum sinese. *Biomass and Bioenergy*, *70*, 267-272.

Lu, Z., Fan, L., Zheng, H., Lu, Q., Liao, Y., & Huang, B. (2013). Preparation, characterization and optimization of nanocellulose whiskers by simultaneously ultrasonic wave and microwave assisted. *Bioresource technology*, *146*, 82-88.

Luo, W., Schardt, J., Bommier, C., Wang, B., Razink, J., Simonsen, J., & Ji, X. (2013). Carbon nanofibers derived from cellulose nanofibers as a long-life anode material for rechargeable sodium-ion batteries. *Journal of Materials Chemistry A*, *1*(36), 10662-10666.

MacFarlane, D. R., Pringle, J. M., Johansson, K. M., Forsyth, S. A., & Forsyth, M. (2006). Lewis base ionic liquids. *Chemical communications*, (18), 1905-1917.

Mai, N. L., Ahn, K., & Koo, Y.-M. (2014). Methods for recovery of ionic liquids—A review. *Process Biochemistry*, *49*(5), 872-881.

Maiti, S., Jayaramudu, J., Das, K., Reddy, S. M., Sadiku, R., Ray, S. S., & Liu, D. (2013). Preparation and characterization of nano-cellulose with new shape from different precursor. *Carbohydrate polymers*, *98*(1), 562-567.

Man, Z., Muhammad, N., Sarwono, A., Bustam, M. A., Kumar, M. V., & Rafiq, S. (2011). Preparation of cellulose nanocrystals using an ionic liquid. *Journal of Polymers and the Environment*, *19*(3), 726-731.

Mandal, A., & Chakrabarty, D. (2011). Isolation of nanocellulose from waste sugarcane bagasse (SCB) and its characterization. *Carbohydrate Polymers*, *86*(3), 1291-1299.

Mao, J., Heck, B., Reiter, G., & Laborie, M.-P. (2015). Cellulose nanocrystals' production in near theoretical yields by 1-butyl-3-methylimidazolium hydrogen sulfate ([Bmim]HSO_4)–mediated hydrolysis. *Carbohydrate polymers, 117*, 443-451.

Mao, J., Osorio-Madrazo, A., & Laborie, M.-P. (2013). Preparation of cellulose I nanowhiskers with a mildly acidic aqueous ionic liquid: reaction efficiency and whiskers attributes. *Cellulose, 20*(4), 1829-1840.

Marchessault, R., Morehead, F., & Koch, M. J. (1961). Some hydrodynamic properties of neutral suspensions of cellulose crystallites as related to size and shape. *Journal of Colloid Science, 16*(4), 327-344.

Masruchin, N., Park, B. D., Causin, V., & Um, I. C. (2015). Characteristics of TEMPO-oxidized cellulose fibril-based hydrogels induced by cationic ions and their properties. *Cellulose*, *22*(3), 1993-2010.

Mehmood, N., Husson, E., Jacquard, C., Wewetzer, S., Büchs, J., Sarazin, C., & Gosselin, I. (2015). Impact of two ionic liquids, 1-ethyl-3-methylimidazolium acetate and 1-ethyl-3-methylimidazolium methylphosphonate, on Saccharomyces cerevisiae: metabolic, physiologic, and morphological investigations. *Biotechnology for biofuels, 8*(1), 1.

Millet, M. A., Moore, W. E., & Saeman, J. E. (1954). Preparation and properties of hydrocelluloses. *Industrial & Engineering Chemistry, 46*(7), 1493-1497.

Minelli, M., Baschetti, M. G., Doghieri, F., Ankerfors, M., Lindström, T., Siró, I., & Plackett, D. (2010). Investigation of mass transport properties of microfibrillated cellulose (MFC) films. *Journal of Membrane Science*, *358*(1), 67-75.

Mishra, S. P., Manent, A.-S., Chabot, B., & Daneault, C. (2012). The use of sodium chlorite in post-oxidation of TEMPO-oxidized pulp: Effect on pulp characteristics and nanocellulose yield. *Journal of Wood Chemistry and Technology, 32*(2), 137-148.

Mohkami, M., & Talaeipour, M. (2011). Investigation of the chemical structure of carboxylated and carboxymethylated fibers from waste paper via XRD and FTIR analysis. *BioResources*, *6*(2), 1988-2003.

Moon, R. J., Martini, A., Nairn, J., Simonsen, J., & Youngblood, J. (2011). Cellulose nanomaterials review: structure, properties and nanocomposites. *Chemical Society Reviews, 40*(7), 3941-3994.

Morais, J. P. S., de Freitas Rosa, M., Nascimento, L. D., do Nascimento, D. M., & Cassales, A. R. (2013). Extraction and characterization of nanocellulose structures from raw cotton linter. *Carbohydrate polymers*, *91*(1), 229-235.

Nakagaito, A., & Yano, H. (2004). The effect of morphological changes from pulp fiber towards nano-scale fibrillated cellulose on the mechanical properties of high-strength plant fiber based composites. *Applied Physics A, 78*(4), 547-552.

Nascimento, D. M., Almeida, J. S., Dias, A. F., Figueirêdo, M. C. B., Morais, J. P. S., Feitosa, J. P., & Rosa, M. D. F. (2014). A novel green approach for the preparation of cellulose nanowhiskers from white coir. *Carbohydrate polymers*, *110*, 456-463.

Nelson, M. L., & O'Connor, R. T. (1964). Relation of certain infrared bands to cellulose crystallinity and crystal lattice type. Part II. A new infrared ratio for estimation of crystallinity in celluloses I and II. *Journal of Applied Polymer Science, 8*(3), 1325-1341.

Novoselov, N., Sashina, E., Petrenko, V., & Zaborsky, M. (2007). Study of dissolution of cellulose in ionic liquids by computer modeling. *Fibre Chemistry, 39*(2), 153-158.

Nyström, G., Mihranyan, A., Razaq, A., Lindström, T., Nyholm, L., & Strømme, M. (2010). A nanocellulose polypyrrole composite based on microfibrillated cellulose from wood. *The Journal of Physical Chemistry B, 114*(12), 4178-4182.

Ohno, H., & Fukaya, Y. (2009). Task specific ionic liquids for cellulose technology. *Chemistry letters*, *38*(1), 2-7.

Oliveri, A. F., Elliott, E. W., Carnes, M. E., Hutchison, J. E., & Johnson, D. W. (2013). Elucidating inorganic nanoscale species in solution: complementary and corroborative approaches. *ChemPhysChem, 14*(12), 2655-2661.

Olivier-Bourbigou, H., Magna, L., & Morvan, D. (2010). Ionic liquids and catalysis: recent progress from knowledge to applications. *Applied Catalysis A: General*, *373*(1), 1-56.

Otulugbu, K. (2012). Production of ethanol from cellulose (sawdust).

Pääkkö, M., Ankerfors, M., Kosonen, H., Nykänen, A., Ahola, S., Österberg, M., . . . Ikkala, O. (2007). Enzymatic hydrolysis combined with mechanical shearing and high-pressure homogenization for nanoscale cellulose fibrils and strong gels. *Biomacromolecules, 8*(6), 1934-1941.

Palme, A., Theliander, H., & Brelid, H. (2016). Acid hydrolysis of cellulosic fibres: Comparison of bleached kraft pulp, dissolving pulps and cotton textile cellulose. *Carbohydrate polymers, 136*, 1281-1287.

Pang, J. H., Liu, X., Wu, M., Wu, Y. Y., Zhang, X. M., & Sun, R. C. (2014). Fabrication and characterization of regenerated cellulose films using different ionic liquids. *Journal of Spectroscopy, 2014*.

Pang, J., Wu, M., Zhang, Q., Tan, X., Xu, F., Zhang, X., & Sun, R. (2015). Comparison of physical properties of regenerated cellulose films fabricated with different cellulose feedstocks in ionic liquid. *Carbohydrate polymers, 121*, 71-78.

Pengfei, Y., Kobayashi, H., & Fukuoka, A. (2011). Recent developments in the catalytic conversion of cellulose into valuable chemicals. *Chinese Journal of Catalysis, 32*(5), 716-722.

Pielesz, A., & Biniaś, W. (2010). Cellulose acetate membrane electrophoresis and FTIR spectroscopy as methods of identifying a fucoidan in Fucusvesiculosus Linnaeus. *Carbohydrate research, 345*(18), 2676-2682.

Pinkert, A., Marsh, K. N., Pang, S., & Staiger, M. P. (2009). Ionic liquids and their interaction with cellulose. *Chemical Reviews, 109*(12), 6712-6728.

Poletto, M., Ornaghi, H. L., & Zattera, A. J. (2014). Native cellulose: structure, characterization and thermal properties. *Materials, 7*(9), 6105-6119.

Puls, J., Wilson, S. A., & Hölter, D. (2011). Degradation of cellulose acetate-based materials: a review. *Journal of Polymers and the Environment, 19*(1), 152-165.

Qing, Y., Sabo, R., Zhu, J., Agarwal, U., Cai, Z., & Wu, Y. (2013). A comparative study of cellulose nanofibrils disintegrated via multiple processing approaches. *Carbohydrate polymers, 97*(1), 226-234.

Qua, E., Hornsby, P., Sharma, H., & Lyons, G. (2011). Preparation and characterisation of cellulose nanofibres. *Journal of materials science, 46*(18), 6029-6045.

Rattaz, A., Mishra, S. P., Chabot, B., & Daneault, C. (2011). Cellulose nanofibres by sonocatalysed-TEMPO-oxidation. *Cellulose*, *18*(3), 585-593.

Rinaldi, N., & Dwiatmoko, A. A. (2012). Hydrolysis process of cellulose and palm stem into total reducing sugars (TRS) over solid acid in 1-n-butyl-3-methylimidazolium chloride: a preliminary study. *International Journal of Engineering & Technology, 12*, 26-29.

Rojas, J., Bedoya, M., & Ciro, Y. (2015). Current Trends in the Production of Cellulose Nanoparticles and Nanocomposites for Biomedical Applications.

Saito, T., Kimura, S., Nishiyama, Y., & Isogai, A. (2007). Cellulose nanofibers prepared by TEMPO-mediated oxidation of native cellulose. *Biomacromolecules, 8*(8), 2485-2491.

Salas, C., Nypelö, T., Rodriguez-Abreu, C., Carrillo, C., & Rojas, O. J. (2014). Nanocellulose properties and applications in colloids and interfaces. *Current Opinion in Colloid & Interface Science, 19*(5), 383-396.

Saraswathy, M., & Gong, S. (2014). Recent developments in the co-delivery of siRNA and small molecule anticancer drugs for cancer treatment. *Materials Today, 17*(6), 298-306.

Satyamurthy, P., & Vigneshwaran, N. (2013). A novel process for synthesis of spherical nanocellulose by controlled hydrolysis of microcrystalline cellulose using anaerobic microbial consortium. *Enzyme and microbial technology, 52*(1), 20-25.

Shafizadeh, F. (Ed.). (2012). *Thermal uses and properties of carbohydrates and lignins*. Elsevier.

Shankar, S., & Rhim, J. W. (2016). Preparation of nanocellulose from micro-crystalline cellulose: The effect on the performance and properties of agar-based composite films. *Carbohydrate polymers*, *135*, 18-26.

Shimada, M., Takahashi, M., Hon, D., & Shiraishi, N. (1991). Wood and cellulosic chemistry (pp. 621): Marcel. Dekker, New York.

Siddiqui, N., Mills, R. H., Gardner, D. J., & Bousfield, D. (2011). Production and characterization of cellulose nanofibers from wood pulp. *Journal of Adhesion Science and Technology*, *25*(6-7), 709-721.

Siró, I., & Plackett, D. (2010). Microfibrillated cellulose and new nanocomposite materials: a review. *Cellulose, 17*(3), 459-494.

Socrates, G. (2004). *Infrared and Raman characteristic group frequencies: tables and charts*. John Wiley & Sons.

Soni, B., Hayes, T., & Srivastava, V. (2004). *U.S. Patent Application No. 11/011,837*.

Spagnol, C., Rodrigues, F. H., Neto, A. G., Pereira, A. G., Fajardo, A. R., Radovanovic, E., ... & Muniz, E. C. (2012). Nanocomposites based on poly (acrylamide-co-acrylate) and cellulose nanowhiskers. *European Polymer Journal*, *48*(3), 454-463.

Spence, K. L., Venditti, R. A., Rojas, O. J., Pawlak, J. J., & Hubbe, M. A. (2011). Water vapor barrier properties of coated and filled microfibrillated cellulose composite films. *Bioresources, 6*(4), 4370-4388.

Stelte, W., & Sanadi, A. R. (2009). Preparation and characterization of cellulose nanofibers from two commercial hardwood and softwood pulps. *Industrial & engineering chemistry research*, *48*(24), 11211-11219.

Sun, L., Chen, J. Y., Jiang, W., & Lynch, V. (2015). Crystalline characteristics of cellulose fiber and film regenerated from ionic liquid solution. *Carbohydrate polymers*, *118*, 150-155.

Sun, Y., & Cheng, J. (2002). Hydrolysis of lignocellulosic materials for ethanol production: a review. *Bioresource technology*, *83*(1), 1-11.

Suslick, K. S., Choe, S. B., Cichowlas, A. A., & Grinstaff, M. W. (1991). Sonochemical synthesis of amorphous iron. *nature*, *353*(6343), 414-416.

Swatloski, R. P., Spear, S. K., Holbrey, J. D., & Rogers, R. D. (2002). Dissolution of cellose with ionic liquids. *Journal of the American Chemical Society*, *124*(18), 4974-4975.

Szczęsna-Antczak, M., Kazimierczak, J., & Antczak, T. (2012). Nanotechnology-Methods of Manufacturing Cellulose Nanofibres. *Fibres & Textiles in Eastern Europe*, 8-12.

Tadesse, H., & Luque, R. (2011). Advances on biomass pretreatment using ionic liquids: an overview. *Energy & Environmental Science*, *4*(10), 3913-3929.

Tang, L., Huang, B., Lu, Q., Wang, S., Ou, W., Lin, W., & Chen, X. (2013). Ultrasonication-assisted manufacture of cellulose nanocrystals esterified with acetic acid. *Bioresource technology*, *127*, 100-105.

Tang, L.-r., Huang, B., Ou, W., Chen, X.-r., & Chen, Y.-d. (2011). Manufacture of cellulose nanocrystals by cation exchange resin-catalyzed hydrolysis of cellulose. *Bioresource technology*, *102*(23), 10973-10977.

Tao, F., Song, H., & Chou, L. (2011a). Dehydration of fructose into 5-hydroxymethylfurfural in acidic ionic liquids. *RSC Advances*, *1*(4), 672-676.

Tao, F., Song, H., & Chou, L. (2011b). Hydrolysis of cellulose in SO 3 H-functionalized ionic liquids. *Bioresource technology*, *102*(19), 9000-9006.

Tian, D., Han, Y., Lu, C., Zhang, X., & Yuan, G. (2014). Acidic ionic liquid as "quasi-homogeneous" catalyst for controllable synthesis of cellulose acetate. *Carbohydrate polymers*, *113*, 83-90.

Tibolla, H., Pelissari, F. M., & Menegalli, F. C. (2014). Cellulose nanofibers produced from banana peel by chemical and enzymatic treatment. *LWT-Food Science and Technology*, *59*(2), 1311-1318.

Tischer, P. C. F., Sierakowski, M. R., Westfahl Jr, H., & Tischer, C. A. (2010). Nanostructural reorganization of bacterial cellulose by ultrasonic treatment. *Biomacromolecules*, *11*(5), 1217-1224.

To, T. Q. (2012). *Investigation of the acidity and nucleophilicity of ionic liquid mixtures and their effects on reaction rates.* Imperial College London.

Tolonen, L. K., Bergenstråhle-Wohlert, M., Sixta, H., & Wohlert, J. (2015). Solubility of cellulose in supercritical water studied by molecular dynamics simulations. *The Journal of Physical Chemistry B*, *119*(13), 4739-4748.

Walden, P. (1914). Ueber die Molekulargrösse und elektrische Leitfähigkeit einiger geschmolzenen Salze. *Известия Российской академии наук. Серия математическая, 8*(6), 405-422.

Wang, H., Gurau, G., & Rogers, R. D. (2012). Ionic liquid processing of cellulose. *Chemical Society Reviews, 41*(4), 1519-1537.

Wang, N., Ding, E., & Cheng, R. (2007). Thermal degradation behaviors of spherical cellulose nanocrystals with sulfate groups. *Polymer, 48*(12), 3486-3493.

Wang, X., Li, H., Cao, Y., & Tang, Q. (2011). Cellulose extraction from wood chip in an ionic liquid 1-allyl-3-methylimidazolium chloride (AmimCl). *Bioresource technology, 102*(17), 7959-7965.

Xiong, R., Zhang, X., Tian, D., Zhou, Z., & Lu, C. (2012). Comparing microcrystalline with spherical nanocrystalline cellulose from waste cotton fabrics. *Cellulose, 19*(4), 1189-1198.

Xu, A., Wang, J., & Wang, H. (2010). Effects of anionic structure and lithium salts addition on the dissolution of cellulose in 1-butyl-3-methylimidazolium-based ionic liquid solvent systems. *Green chemistry, 12*(2), 268-275.

Xu, A., Zhang, Y., Zhao, Y., & Wang, J. (2013). Cellulose dissolution at ambient temperature: role of preferential solvation of cations of ionic liquids by a cosolvent. *Carbohydrate polymers, 92*(1), 540-544.

Yang, H., Yan, R., Chen, H., Lee, D. H., & Zheng, C. (2007). Characteristics of hemicellulose, cellulose and lignin pyrolysis. *Fuel, 86*(12), 1781-1788.

Yuan, Z., Zhang, J., Jiang, A., Lv, W., Wang, Y., Geng, H., . . . Qin, M. (2015). Fabrication of cellulose self-assemblies and high-strength ordered cellulose films. *Carbohydrate polymers, 117*, 414-421.

Zavrel, M., Schmidt, T., Michalik, C., Ansorge-Schumacher, M., Marquardt, W., Büchs, J., & Spiess, A. C. (2008). Mechanistic kinetic model for symmetric carboligations using benzaldehyde lyase. *Biotechnology and bioengineering, 101*(1), 27-38.

Zhang, J., Zhang, H., Wu, J., Zhang, J., He, J., & Xiang, J. (2010). NMR spectroscopic studies of cellobiose solvation in EmimAc aimed to understand the dissolution mechanism of cellulose in ionic liquids. *Physical Chemistry Chemical Physics, 12*(8), 1941-1947.

Zhang, S., Li, F.-X., Yu, J.-y., & Hsieh, Y.-L. (2010). Dissolution behaviour and solubility of cellulose in NaOH complex solution. *Carbohydrate polymers, 81*(3), 668-674.

Zhang, Z. C. (2013). Catalytic transformation of carbohydrates and lignin in ionic liquids. *Wiley Interdisciplinary Reviews: Energy and Environment*, *2*(6), 655-672.

Zhao, D., Li, H., Zhang, J., Fu, L., Liu, M., Fu, J., & Ren, P. (2012). Dissolution of cellulose in phosphate-based ionic liquids. *Carbohydrate Polymers*, *87*(2), 1490-1494.

Zhao, H., Kwak, J. H., Zhang, Z. C., Brown, H. M., Arey, B. W., & Holladay, J. E. (2007). Studying cellulose fiber structure by SEM, XRD, NMR and acid hydrolysis. *Carbohydrate polymers*, *68*(2), 235-241.

LIST OF PUBLICATIONS AND PAPERS PRESENTED

ISI-Cited Publications:

1. **Xiao Yun Tan**, Sharifah Bee Abd Hamid, Chin Wei Lai (2015). Preparation of high crystallinity cellulose nanocrystals (CNCs) by ionic liquid solvolysis. *Biomass and Bioenergy, 81,* 584-591.

2. **Xiao Yun Tan**, Chin Wei Lai, Sharifah Bee Abd Hamid (2015). Facile Preparation of Highly Crystalline Nanocellulose by using Ionic Liquid. *Advanced Materials Research, 1087*, 106-110.

Conference Proceedings:

1. **Xiao Yun Tan**, Chin Wei Lai, Sharifah Bee Abd Hamid (2015). Facile Preparation of Highly Crystalline Nanocellulose by using Ionic Liquid. *Proceeding of International Conference on X-Rays and Related Technique in Research & Industry 2014 (ICXRI 14)*, 11-13th August 2014, KSL Resort Hotel, Johor Bahru, Malaysia.

2. **Xiao Yun Tan**, Chin Wei Lai, Sharifah Bee Abd Hamid (2014). Preliminary Study on Preparation and Characterization of Nanosize Cellulose. *Proceeding of 6th International Conference on Postgraduate Education 2014 (ICPE-6)*, 17-18th December 2014, Main Hall, Universiti Teknikal Malaysia Melaka (UTeM), Malacca, Malaysia.

APPENDIX

APPENDIX A: Published Paper (Biomass and Bioenergy)

Biomass and Bioenergy 81 (2015) 584–591

Contents lists available at ScienceDirect

Biomass and Bioenergy

journal homepage: http://www.elsevier.com/locate/biombioe

Research paper

Preparation of high crystallinity cellulose nanocrystals (CNCs) by ionic liquid solvolysis

Xiao Yun Tan, Sharifah Bee Abd Hamid*, Chin Wei Lai

Nanotechnology & Catalysis Research Centre (NANOCAT), Block A, Institute of Postgraduate Studies (IPS), University of Malaya, 50603 Kuala Lumpur, Malaysia

ARTICLE INFO

Article history:
Received 19 March 2015
Received in revised form
11 August 2015
Accepted 12 August 2015
Available online xxx

Keywords:
Cellulose nanocrystals
Ionic liquid
Catalyst
Crystallinity
Regeneration

ABSTRACT

High crystallinity cellulose nanocrystals (CNCs) were successfully prepared from microcrystalline cellulose (MCC) by utilization of 1-butyl-3-methylimidazolium hydrogen sulfate ($BmimHSO_4$) as both catalyst and solvent. Interestingly, it was found that crystallinity of CNCs was improved with increase in temperature which attributed to selective removal of the amorphous phase of cellulose performed at a higher rate with higher temperature. The successful conversion of MCC to CNCs was supported by HRTEM in which the uniform rod-like shape of CNCs was obtained. CNCs with diameter range from 15 to 20 nm and length range from 70 to 80 nm were successfully produced at 90 °C with $BmimHSO_4$. In the present work, CNCs synthesized at different temperatures from 70 °C to 100 °C were investigated. The application of $BmimHSO_4$ as both catalyst and solvent introduced a green chemistry approach as it does not produce any hazardous waste products and is an economical process because the recovery of ionic liquid is high (>90%).

1. Introduction

Cellulose is a promising feedstock from lignocellulosic biomass because it is a prospective carbon-neutral as well as a renewable energy resource which has attracted considerable attention from researchers during the past decade [1–4]. Cellulose nanocrystals (CNCs) are endowed with several characteristics which make them unique. They are high surface area to volume ratio, light weight, high aspect ratio, exceptional mechanical properties with high stiffness and Young's modulus up to 134 GPa as well as high tensile strength (up to 7.5 GPa), low coefficient of thermal expansion [5], modifiable surface properties, and environmental benefits which include biodegradability and biocompatibility [6,7]. CNCs have the potential to be applied in optical and electronic devices, reinforcement and fillers in composite materials [8], automotive applications, molecular biology, and regenerative medicine [7,9,10].

To date, a new type of green solvent known as ionic liquids (ILs) has become popular because of the unique physiochemical properties and potential to be environmentally friendly. ILs are generally defined as salts that melt below 100 °C and are composed entirely of ions [2,11,12]. Interestingly, ILs have many attractive properties such as chemical and thermal stability, low melting point, non-volatility and -flammability, negligible vapor pressure, recyclable and able to dissolve cellulose easily [13–16]. According to Rogers and his coworkers, ILs could be nonderivatizing solvents for cellulose such that cellulose can dissolve in ILs without any derivatization and pretreatments [17]. ILs can be eco-friendly solvents because they can be easily recovered and reused after the regeneration of cellulose by simple methods such as evaporation, salting out and reverse osmosis. Gutowski and his coworkers revealed that the recovery rate of IL (BmimCl) can be up to 99.5% by evaporating the anti-solvents. Therefore, ILs can be promising solvents as well as catalysts with high recovery rate, and recyclable and reusable properties [11,18]. However, there are limited publications regarding the catalytic behavior of ILs. In the present study, we introduced a relatively new green chemistry approach for the preparation of CNCs by using 1-butyl-3-methylimidazolium hydrogen sulfate ($BmimHSO_4$) as both catalyst and solvent. The influence of $BmimHSO_4$ treatment with temperature on the preparation of CNCs was investigated. Moreover, the properties of CNCs and the starting material, MCC were evaluated and compared. To the best of our knowledge, the literature regarding the formation of CNCs through the use of ILs as catalyst is still lacking. Therefore, this study aims to investigate the effect of heating temperatures on the

* Corresponding author.
E-mail addresses: xyun_90@hotmail.com (X.Y. Tan), sharifahbee@um.edu.my (S.B. Abd Hamid), cwlai@um.edu.my (C.W. Lai).

http://dx.doi.org/10.1016/j.biombioe.2015.08.016
0961-9534/